CHALMERS

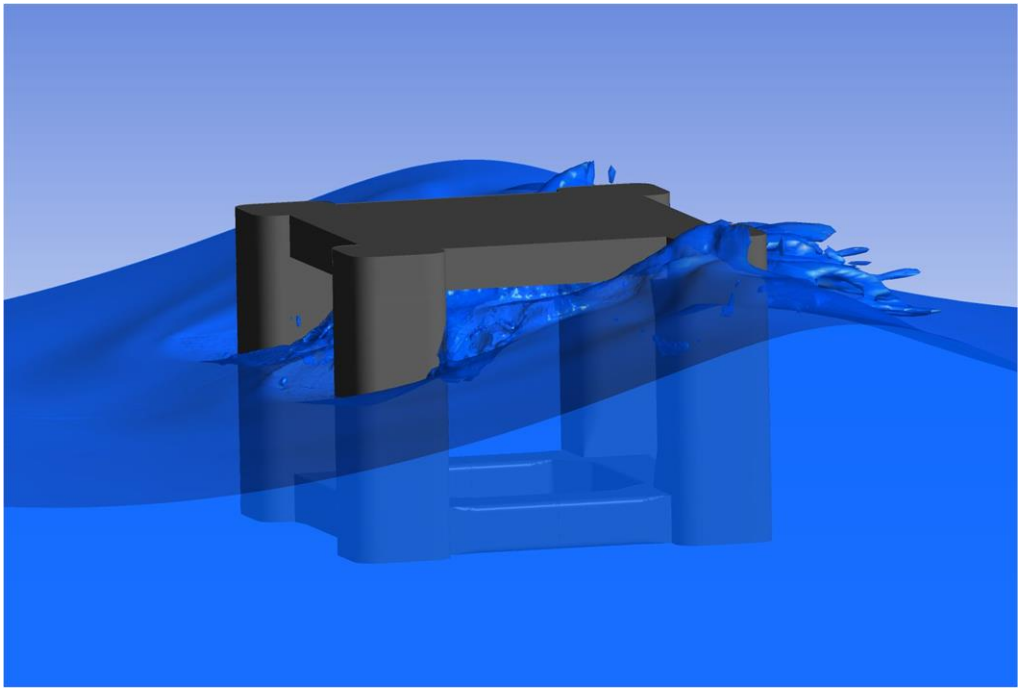

CFD simulation of wave-in-deck loads on offshore structures

Master of Science Thesis in Naval Architecture and Ocean Engineering

ADAM OLSSON

MARTIN TUNLID

Department of Shipping and Marine Technology
Division of Marine Structures and Hydrodynamics
CHALMERS UNIVERSITY OF TECHNOLOGY
Gothenburg, Sweden 2015
Master's Thesis 2015:332

MASTER'S THESIS IN NAVAL ARCHITECTURE AND OCEAN ENGINEERING

CFD simulation of wave-in-deck loads on offshore structures

ADAM OLSSON

MARTIN TUNLID

Department of Shipping and Marine Technology
Division of Marine Structures and Hydrodynamics
CHALMERS UNIVERSITY OF TECHNOLOGY
Gothenburg, Sweden 2015

CFD simulation of wave-in-deck loads on offshore structures

ADAM OLSSON
MARTIN TUNLID

Master's Thesis 2015:332
Department of Shipping and Marine Technology
Division of Marine Structures and Hydrodynamics
Chalmers University of Technology
SE-412 96 Gothenburg
Sweden
Telephone: + 46 (0)31-772 1000

Cover:
CFD scene of a three-dimensional platform exposed to a wave-in-deck impact.

Printed by Chalmers Reproservice
Gothenburg, Sweden 2015

CFD simulation of wave-in-deck loads on offshore structures

Master's Thesis in the International Master's Programme in Naval Architecture and Ocean Engineering

ADAM OLSSON AND MARTIN TUNLID
Department of Shipping and Marine Technology
Division of Marine Structures and Hydrodynamics
Chalmers University of Technology

ABSTRACT

In the offshore industry, physical model tests are common to predict slamming loads and wave impacts, but also to investigate platform motions and structural responses. Unfortunately, creating models and performing experimental tests can be time-consuming and relatively expensive. Problems with scaling effects emerges and reliability of measurement equipment can be questioned. This makes other alternatives interesting and there is a growing need for numerical tools capable of predicting hydrodynamic loads in detail, such as Computational Fluid Dynamics (CFD) programs. A numerical model has the advantage that a simulation can quickly be adapted to changes in geometry or wave conditions, but also it has the possibility to measure physical properties at any location in the computational domain. This motivates the use of CFD solvers to predict wave loads and the objective of this thesis is to use CFD to estimate wave-in-deck loads in simplified situations.

A two-dimensional platform deck with a specified air-gap to the free water surface is modelled and in order to verify the feasibility of the CFD software, the deck is subjected to regular incident waves and the vertical lifting force is compared to experimental data. Simulations are performed with four different settings, two wave heights and two wave periods, respectively. A three-dimensional platform is also modelled as an illustrative example to further explore and demonstrate the possibilities of the CFD software. In this case, wave run-up is observed and pressure impulses around the columns of the platform are estimated.

When a wave hits the deck, the structure experiences a positive slamming dominated lifting force during the initial water entry phase, followed by a negative force during the water exit phase. The force in the latter phase is dominated by a negative added mass force due to negative fluid particle accelerations and its magnitude may be larger than the positive force peak. The water exit phase is important for global structural effects, while the initial impact yields the highest pressures and is critical for local structural responses. The force magnitude is highly dependent on wave amplitude and wave period. Simulations are performed in ANSYS Fluent and input parameters, modelling approach and assumptions are thoroughly described in the report.

Ultimately, the results from the CFD simulations agree well with the empirical model tests and ANSYS Fluent is proved to be a powerful tool predicting wave-in-deck loads. It yields very satisfactory results for water entry, but slightly less for water exit. Conclusions drawn from the study are that quality of the mesh and time step size clearly influence the results and it can be difficult to model turbulence correctly, due to numerical diffusion of the waves.

Key words: CFD, Fluent, semi-submersible, slamming, wave-in-deck, wave loads

CFD simulering av våglaster på offshore-konstruktioner

Examensarbete inom Naval Architecture and Ocean Engineering

ADAM OLSSON OCH MARTIN TUNLID
Institutionen för Sjöfart och Marin Teknik
Avdelningen för Marina Konstruktioner och Hydrodynamik
Chalmers Tekniska Högskola

SAMMANFATTNING

Inom offshore-branschen genomförs vanligtvis fysiska modellförsök för att uppskatta våglaster, men också för att utvärdera rörelser och strukturbelastningar på plattformar. Tyvärr kan det vara tidskrävande och kostsamt att ta fram modeller och genomföra dessa fysiska tester. Problem med skalningseffekter uppstår och mätutrustningens tillförlitlighet kan ifrågasättas. Detta motiverar andra alternativ och det finns ett ökat intresse för numeriska lösare som kan beskriva hydrodynamiska laster mer i detalj, såsom CFD-program (Computational Fluid Dynamics). CFD erbjuder många fördelar, exempelvis möjligheten att modifiera geometrin och vågförhållandena, undvika skalningseffekter, men också förmågan att kunna mäta fysikaliska variabler vid valfri position i beräkningsdomänen. Detta motiverar användandet av CFD lösare för att förutse våglaster och syftet med detta arbete är att använda dessa program för att uppskatta våglaster på strukturer till havs.

Detta arbete har fokuserat på ett tvådimensionellt däck med ett bestämt avstånd till den fria vattenytan. För att verifiera möjligheten att använda CFD för beräkning av våglaster har reguljära vågor modellerats och den vertikala lyftkraften jämförts med experimentdata. Simuleringar utfördes med fyra olika inställningar, två våghöjder respektive två våglängder. En tredimensionell plattform har också modellerats för att mer illustrativt visa möjligheterna med CFD. I den simuleringen uppskattas tryckimpulserna från en vågsammanstötning kring plattformens bakre pontoner.

När en våg slår i däcket under den inledande fasen upplever plattformen en positiv stötdominerande lyftkraft, följt av en negativ kraft när vågen lämnar däcket. Kraften i det senare skedet består huvudsakligen av en negativ tröghetskraft på grund av negativa partikelaccelerationer och dess storlek kan vara större än den maximala positiva kraften. Slutfasen på tillslaget är väldigt viktig för globala strukturella effekter medan första stöten medför de största medeltrycken och är kritisk för lokala strukturella komponenter. Storleken på kraften är mycket beroende av vågamplitud, vågperiod och avstånd till vattenytan. Simuleringar utfördes i ANSYS Fluent och invariabler, modelleringsteknik och antaganden är utförligt förklarade i rapporten.

Slutligen kan nämnas att resultaten från CFD simuleringarna stämmer väldigt väl överens med resultaten från de empiriska modellförsöken. ANSYS Fluent har visat sig vara ett kraftfullt verktyg för att modellera våglaster. Lyftkraften under vågens inledningsfas har ett mycket bra överensstämmande, medan slutfasen på tillslaget är något sämre. Slutsatser från studien är att kvalitén på beräkningsnätet samt storleken på tidssteget tydligt påverkar resultaten och det kan vara svårt att modellera turbulens korrekt, på grund av numerisk diffusion av vågorna.

Nyckelord: ANSYS, CFD, Fluent, offshore, semi-submersible, slamming, våglaster

Contents

Acknowledgements

This report is submitted to fulfil the requirement to the Master's degree at Chalmers University of Technology, Gothenburg, and has been carried out in collaboration with the hydrodynamics department of GVA Consultants AB in Gothenburg, Sweden. The main objective of the thesis is to study water impact loads underneath decks of offshore structures due to propagating waves, using commercial CFD tools, i.e. ANSYS Fluent. The project should result in an engineering CFD practice, making CFD useful to estimate slamming loads in simplified situations. This working procedure for estimating wave loads should correspond and be verified to earlier empirical results from model tests executed by the business segment.

The work was done during the spring semester of 2015 and was examined by the department of Shipping and Marine Technology at Chalmers University of Technology (30 higher educational credits).

It is with immense gratitude that we acknowledge the support and help from our supervisor Claes Eskilsson from Chalmers University of Technology for his resourceful comments and involvement during the project. We are also grateful and owe our deepest appreciation to our supervisors from GVA, Vahik Khodagolian and Johan Lennblad, whose contributions, continuous guidance and admirable efforts have been highly appreciated. We would also like to thank Tomas Jarneholt and the other employees of ANSYS Sweden for their technical support and education of the CFD software used throughout the thesis work. During hard times with complex obstacles, Tomas selfless guidance and persistent support helped us a lot to accomplish this work.

Gothenburg June 2015

Adam Olsson & Martin Tunlid

Abbreviations

2D	Two-dimensional
3D	Three-dimensional
ABC	Absorbing Boundary Conditions
BEM	Boundary Element Method
CFD	Computational Fluid Dynamics
CPU	Central Processing Unit
DNS	Direct Numerical Simulation
DNV	Det Norske Veritas
GBS	Gravity-Based Structure
LES	Large Eddy Simulation
MPS	Moving Particles Semi-implicit
NITA	Non-Iterative Time Advancement
NTNU	Norwegian University of Science and Technology
PB	Port
PDE	Partial Differential Equation
PISO	Pressure Implicit with Splitting of Operators
RANS	Reynolds Averaged Navier-Stokes
SB	Starboard
SIMPLE	Semi-Implicit Method for Pressure Linked Equations
SIMPLEC	Semi-Implicit Method for Pressure Linked Equations-Consistent
TS	Time Step
UDF	User Defined Function (ANSYS)
VOF	Volume of Fluid

Notations

Roman letters

A	Area [m^2]
c	Deck clearance (air-gap) [m]
c_g	Group velocity waves [m/s]
d	Water depth [m]
F	Force [N]
g	Gravitational acceleration [m/s^2]
H	Wave height [m]

H_s	Significant wave height [m]
k	Kinetic energy [J]
l_m	Turbulent length scale
M_a	Mach number
n	Normal vector
p	Pressure [N/m^2]
$S_\emptyset$	Source term of property $\emptyset$
$s_{i,j}$	Rate of deformation tensor
T	Wave period [s]
T_{im}	Time duration of impact event [s]
T_p	Spectral peak period [s]
t	Time [s]
u	Velocity in x-direction [m/s]
$\hat{u}$	Internal energy [J]
V	Volume [m^3]
v	Velocity in y-direction [m/s]
v	Velocity vector, (u,v,w) [m/s]
w	Velocity in z-direction [m/s]
y^+	Wall coordinate, dimensionless distance to the wall

Greek letters

α	Under-relaxation factor / Weighing parameter
Γ	Diffusion coefficient
γ	JONSWAP Peak enhancement factor
δ_{ij}	Kronecker's delta
ε	Rate of dissipation [J/s]
θ	Local deformation (Shear strain)
λ	Wave length [m]
μ	Dynamic viscosity [kg/(s·m)]
ν	Kinematic viscosity [m^2/s]
ρ	Density [kg/m^3]
σ	Standard deviation
τ	Shear stress (Viscous stress) [N/ m^2]
$\emptyset$	General property
ω	Turbulence frequency (Specific dissipation rate) [1/s]

Introduction

Focus in this Master's thesis is CFD simulation on wave impact loads acting on offshore structures. Simplified situations are studied and can be used as a guideline for more advanced analysis. As an introduction to the thesis work a short background on slamming loads on offshore structures is presented as a motivation for the study and attempts to emphasize the relevance of computational fluid dynamics in the field. Also the objective, delimitations and outline of the thesis are presented.

This thesis has been carried out in collaboration with GVA Consultants, which is a consultancy company specializing in marine and offshore design related to the oil and gas industry. They are world-leading designers for a wide variety of semi-submersibles such as drilling, production, accommodation and heavy lift units. They have produced a series of break-through designs in 30 countries over the last 20 years with well-known projects as Atlantis, Thunder Horse and Åsgard (GVA, 2013). Figure 1.1 shows a CAD model of the GVA 7600 drilling unit.

Figure 1.1 - GVA 7600 drilling unit from (GVA, 2013).

1.1 Background

When designing offshore platforms, it is common practice to design the lower deck of the superstructure to have a positive clearance for all its structures to the predicted water level, called an air-gap. Global loads from large masses of water occasionally impacting the main constructions have for a long time been of concern to designers. These water impact loads could propagate along the deck and be of such magnitude they could be critical for the global strength and overall stability of the platform. Despite the potential risk of water impacts causing severe damage, knowledge regarding the variability of environmental conditions and sea loads over time have been restricted, at least when the first generation of bottom-fixed platforms began to operate. Furthermore, initial safe deck clearance to the water level could also be reduced over time. For bottom-fixed platforms the altered clearance could be caused either by settlement of the platform due to its own weight or by foundation subsidence into the seabed and reservoir compaction (Baarholm & Stansberg, 2004).

As offshore exploration is progressing towards deeper waters, there is an increasing demand for floaters such as semi-submersibles. They are widely used for different offshore operations with water depth capabilities ranging from 600 m to 3600 m and designed to withstand harsh environmental conditions. If the platform is designed with

a sufficient safety margin from the surface level to the deck height, the probability of waves reaching the decks can be neglected. On the other hand, deck height also affects total weight of the platform and intact stability, which makes air-gap a substantial cost driver. In the design, one might allow some extreme waves to hit the deck structure to avoid conservative safety margins. This highlights the importance of considering wave loads early in the design work. For semi-submersibles a reduction in the clearance height may occur involuntarily in damaged condition or after failure in their ballast systems. If higher production volumes are desired, increased storage capacity and deck weight must be compensated by increased draft, thus smaller deck clearance. Evidently, changing the layout and topside weight implies a higher risk of wave impacts (Baarholm & Faltinsen, 2004). Owing to above mentioned uncertainties in the safety level, the deck may be subjected to wave-induced loads that may not have been accounted for in the original design.

The water loads may roughly be categorized into global and local loads. Large local effects could damage important safety functions and equipment, but generally the global loads, affecting the structural integrity of the whole platform, are of primary interest. The Facilities Regulations of the Petroleum Safety Authority states that accidental and environmental loads with an annual probability greater than 10^{-4} shall not result in loss of a main safety function (Petroluem Safety Authority Norway, 2014). In this context, the main safety function includes the main load-bearing structures, rooms with equipment for combatting accidents, facility's safe areas, living quarters and evacuation routes including life crafts. Common UK and US practices dictate a finite margin between the 100 year design wave crest and the deck to have an air-gap of at least 1.5 m (American Petroleum Institute, 2002). Figure 1.2 shows the Borgholm Dolphin installation unit in the North Sea east of Aberdeen, being subjected to extreme waves during a storm in January 2015.

Figure 1.2 – Borgholm Dolphin installation rig during storm in January 2015 from (Daily Mail, 2015).

It is important to obtain an accurate prediction of the hydrodynamic loads in the design work and common practice is to estimate air-gaps by potential theory and thereby estimating the relative motion between the structure and water surface. When this quantity is negative, slamming and wave-in-deck loads occur and the pressure could be estimated. For wave-in-deck loads, DNV considers a simple box-type deck and uses two approaches: a simplified approach and a momentum method (DNV, 2010). In the simplified approach, the vertical wave-in-deck force can be predicted from the vertical

velocity in the wave at the point of initial contact and the wetted deck area at the time instant of the maximum vertical impact force. The location of the initial contact is defined as when the lowest part of the deck encounters the wave. For the wetted deck length, an equivalent length between the point of initial contact and the top of the wave crest can be used instead. The vertical velocity in the wave is computed from general wave kinematics for a given wave height defined from a specified storm condition. The vertical wave-in-deck force is then: $F_v = \frac{1}{2}\,\rho\, C_v\, A\, v_z^2$, where C_v is 5 for head or broadside waves and 10 for 45^0 oblique waves. The vertical force should be distributed evenly over the wetted deck area. In the momentum method, the vertical impact force is given by the combined effect of the rate of change of momentum due to added mass and drag force. A time dependent function of vertical lifting force can be established with information of how the wetted area and vertical velocity varies with time.

In the industry, the use of model tests is also still a preferred method for predicting loads and the results are used for design rules. Such empirical tests are often expensive and time consuming, making other alternatives interesting. Generally, the phenomenon with slamming loads is very complex to analyse, which involves extreme sea states where the kinematics of the waves are uncertain and shows non-linear behaviour. The geometry and motion of the platform may change and interfere with the incoming wave, making the inflow even more complicated. It might also be difficult to know where to place the transducers in order to capture the maximum pressures.

Complementary to potential theory and model tests, development and use of more sophisticated numerical tools such as Navier-Stokes solvers is however increasing for these kind of problems. There is a growing need for a numerical simulation tool capable of predicting hydrodynamic loads due to waves, wind and current more in detail. CFD can be an ideal tool for such assessments, provided good physical models for both the free water surface and incoming waves together with models for the structure motions. A numerical model has the advantage that a simulation can quickly be adapted to small changes in geometry or environmental conditions, scaling effects can be avoided and detailed insight in the hydrodynamic processes can be obtained. The instantaneous availability of a numerical model is another important advantage. Numerical computations are less costly and time-consuming than model tests (in comparison with the operational costs of a model basin) and computational methods could provide far more information, since the forces and details of the flow can be obtained from any location in the computational domain (Veldman & Huijsmans, 2008). Therefore it can be used in an early stage of the design process.

However, CFD is relatively new and has only been useful to solve complex free-surface flow problems for about a decade. The industry still considers CFD software to be too inaccurate to base a complete assessment, but the results from such analysis are often proved to be highly relevant input and used to validate experiments (Vestbostad, 2009). The development of better software, together with the decreasing costs for CPU capacity, will make the use of CFD and numerical tools even more favourable in the future. Simulation results today compare well with model tests and this practice gives a better understanding of the phenomenon behind slamming loads, than either of the two provides separately. It is important to remember that both experiments and numerical computations have error sources and represent only a simplified model of the reality.

In addition to slamming loads due to water impact underneath platform decks, incoming waves that break on the vertical columns of the platform and run along the legs to eventually hit the deck structure, called 'wave run-up', can also cause structural problems. The latter case is crucial to local structural responses and to the comfort of the platform crew, but less important in terms of global effects (Baarholm, 2001). Wave run-up is briefly investigated in the three-dimensional study in this thesis.

1.2 Objective

The objective of this thesis is to investigate the use of CFD for estimating wave-in-deck loads in a simplified situation where regular incoming waves are modelled. To be able to use CFD simulations as a complimentary to empirical data and model tests, one has to make sure that the simulations are performed in the right way, generating correct results. A working procedure to make the simulations in ANSYS Fluent reliable is therefore of interest. The results from the CFD simulations in this project shall therefore be verified with reference experiments, and hopefully in the future be used for more advanced cases.

The task can be further specified:

- Comparison of the wave-in-deck forces between computational simulations and empirical experiments.
- A parametric analysis of wave input parameters (e.g. wave height and wave period).
- Comparison of maximum and minimum vertical slamming forces on tested models.
- Special attention should be given to modelling the free water surface and wave reflections on model boundaries.
- Study of error sources and set-up details of previous experiments.
- A simplified 2D structure will be investigated in the majority of the project. A 3D simulation is performed in the end to illustrate the possibilities of using CFD in more advanced cases.

1.3 Delimitations

The purpose of this project is to come up with an initial working procedure for the load cases, previously described in Section 1.2. In the future more advanced simulations could be performed when the designer is more familiar with the software and knowledge about various input parameters and physical models are increased. To stay within the timeframe of this master thesis and avoid unnecessary complexity, following delimitations have been specified:

- The project will only focus on commercial software ANSYS Fluent.

- Only wave-in-deck forces are considered. Local effects from wave run-up will briefly be treated in the 3D study. Air-gap prediction will not be conducted.

- Regular fully developed waves are going to be modeled in all simulations with no heading.

- Shallow water regions and related effects are excluded, only deep-water simulations will be conducted.

- The models/geometries in the simulations are fixed, i.e. no motion responses.

- The fluids are assumed to be incompressible (constant ρ).

- No hydroelasticity, i.e. no elastic structural response of the platform.

1.4 Outline of thesis

The first part of this thesis is a literature study with the purpose of finding reference projects with test data in order to verify the CFD results from Fluent. The literature study also outlines what other researchers in the field has accomplished and what conclusions they have made from their experiments. Furthermore, the experimental set-up for the selected reference project is presented as well as assumptions made and key results.

Chapter 4 describes the basic theory behind CFD programs. The goal is to systematically go through how CFD programs use the conservation laws of fluid dynamics to array discretized equations that can be solved subject to proper boundary conditions. Turbulence models and differencing schemes are briefly explained as well as errors sources and uncertainties in numerical models.

Chapter 5 presents the case study for the 2D slamming event. ANSYS DesignModeler will be used to create the CAD geometry, ANSYS Meshing will be used as mesher and Fluent to perform the calculations. The results will be exported to CFD Post for further analysis, visualization and animation. The design methodology of this study is iterative, which involves dependency studies of turbulence models, mesh size and discretization schemes. Several iterations have been carried out in order to obtain satisfying results.

In Chapter 6 the results are presented and discussed with figures, velocity plots and slamming force graphs. Chapter 7 treats the 3D wave run-up event and presents the experimental set-up, simulation model and results of the study.

Conclusions drawn during this thesis is given in Chapter 8 and lastly, future work and recommendations for further research is presented in Chapter 9.

2 Literature study and relevant research in the field

In order to verify the wave-in-deck loads from Fluent and ensure the simulations are performed in the right way, a literature study has been conducted with the goal to find a reference project that could be used as a framework for the CFD investigation. To this day, no decent analytical solution exists that fully describes the non-linear behaviour of wave-in-deck loads. However, a few numerical studies have been performed in the industry, mostly with the second-order diffraction program WAMIT and the CFD software COMFLOW. Many different companies and institutions have also performed numerous model tests where scaled models are subjected to environmental loads in a wave basin.

Kisacik et al. executed small-scale experiments of breaking wave impact using a vertical wall with a horizontal cantilevering slab. Tests were conducted for a broad range of water depths, wave periods and wave heights. A parametric analysis of measured forces was executed, both on the vertical and horizontal part of the scaled model (Kisacik et al.). Vertical breakwaters and sea walls are frequently used structures to protect ports from sea actions like waves and high water levels. The results showed that the horizontal and vertical forces are very sensitive for the variation of water depth and wave height, while variation of wave period has a rather limited effect. Although the waves in each sample are nominally identical, their impact behaviour varies significantly between tests. The non-repeatability of the breaking wave pressures and forces on the vertical structures are a well-known phenomenon and the main reasons for the non-repeatability are:

• Turbulence left behind by a preceding wave

• Strong interaction with the reflection of the preceding wave

• Influence of trapped air

These parameters have a strong influence on the breaking wave kinematics and on the shape of the waves, which has a strong relation to the value of peak pressures.

Another topic that has been investigated in a few studies is wave loads from extreme weather events acting on bridges and other infrastructures. In coastal areas, it is essential to predict extreme loads on the road system in order to construct durable and safe bridges (Henry, 2011). Together with an increasing sea level and more extreme weather conditions, infrastructure near the shore is very vulnerable. Unfortunately, the data provided from these tests are not very useful since the geometry is not comparable with a platform deck and there are also shallow water effects.

Iwanowski et al. performed wave run-up experiments on a three-dimensional model of a semi-submersible and compared the results with a numerical solution from COMFLOW. An improved VOF method with a height function for better accuracy was used to simulate flow around the semi-submersible platform due to incoming regular waves. In particular, wave run-up on the columns and under-deck wave impact were investigated. The model experiments were performed by MARIN at their basin in The Netherlands. They concluded that the wave elevation was rather constant for the first and second column, but the pressures on the second column were higher for sensors placed near the top of a column due to higher run-up velocity. However, the averaged pressure was lower than for the bottom sensors, mainly due to higher hydrostatic pressure (Iwanowski et al., 2009). Huijs et al. performed similar experiments as Iwanowski et al., but with shallow draft (Huijs et al., 2011).

Matsumoto et. al. addresses the problem of estimating air-gap for a large semi-submersible production platform by performing simplified tests with the model both moored and fixed. The platform was subjected to regular waves of varying steepness. Wave elevation at different points were measured and compared to predictions obtained from two numerical methods, BEM (Boundary Element Method) code from WAMIT and COMFLOW. Results showed that a standard linear analysis may lead to significant errors concerning the air-gap evaluation. Extending the BEM model to second-order clearly improved the results and VOF simulations presented very good agreement to the experimental results (Matsumoto et al., 2013).

Wellens et. al. conducted a similar study, but instead of using numerical damping zones near the outflow boundary they employed so-called Absorbing Boundary Conditions (ABC) (Wellens et al., 2009). A numerical damping zone often require multiple wave lengths behind the modelled object to efficiently dissipate wave energy and avoid reflections. By implementing ABC, boundaries can be located relatively close to an object without influencing outgoing waves. Hence, with the ABC setting less mesh elements are required for the same accuracy, which reduces the computing time. In numerical simulations of irregular waves, the ABC gives less reflections with a reduction of the computational effort of roughly a factor four, than a traditional dissipation zone that is three times as long. Unfortunately, the ABC condition is not available in ANSYS Fluent.

Bellezi and Cheng presented in 2014 a study on wave impacts onto a semi-submersible by using Moving Particles Semi-implicit (MPS) method. The MPS method is a fully Lagrangian particle-based method and is promising in highly non-linear phenomena analysis, such as hydrodynamic impacts. Wave-in-deck loads and wave run-up were considered in two different types of semi-submersibles; one with square columns and one with circular columns. In the same way as Iwanowski et al., they also noted a higher pressure on the second column than the first. They concluded that run-up at the first column last longer for a floating structure, while run-up at the second column had a shorter duration. Generally, longer run-up can be associated with smaller pressures (Bellezi & Cheng, 2014).

Kraskowski describes a proposal of a method for simulating the motion of freely floating and moored objects in waves, based on the RANS flow model. The paper includes the description of the proposed method, which consists of a mesh generation technique, efficient wave generation method and a mooring system module. Two samples of marine applications are considered, a fishing vessel in head waves and a moored semi-submersible drilling platform in quartering waves. The results are verified against towing tank experiments and the STAR CCM+ software is used for all numerical computations with a VOF model (Kraskowski, 2012).

2.1 Studies performed by R. Baarholm

Above mentioned projects have provided useful insights and inspiration, but have not been used as reference projects. The main reason is that the results from these papers are presented as small graphs, which are hard to interpret and extract reliable values from. Most of the tests are also performed on three-dimensional moored bodies with motions in six degrees of freedom. Since using CFD tools can be comprehensive and require a lot of computing capacity, the idea was to perform simulations on a two-dimensional fixed body as a start.

The choice of reference project and main source of inspiration has been the scaled wave-in-deck tests campaign accomplished by Rolf Baarholm in July 2009 at the Norwegian Marine Technology Research Institute (MARINTEK) (Baarholm, 2001). The main objective with his work was to study water impact underneath decks of offshore platforms due to incident propagating waves and validate the results against different theory models (Baarholm & Faltinsen, 2004). The platform deck had no substructure and the tests were performed with different wave and air-gap settings. More information about this experiment is provided in Chapter 3.

Baarholm did also develop the analysis and studied three-dimensional effects. The purpose was to better understand what effect transverse and longitudinal structural members have on the flow. The results showed that three-dimensional effects significantly reduce wave-in-deck loads, in particular for the water exit phase where the vertical lifting force is almost halved. Theoretically, two analytical methods are used, generalization of Wagner's impact theory and von Karman approach. Comparisons show that the Wagner based method yields good results in the water entry phase, but overestimates the water exit force and underestimates the duration of the wave event. The von Karman approach underestimates the water entry force, but gives significant improvements during the water exit phase. Three-dimensional effects reduce the magnitude of the upward directed force peak typically 15-30% and the magnitude of the downward directed force close to 50% for impacts were the entire underside of the deck is wetted (Baarholm, 2009).

Together with Carl T. Stansberg, the method for three-dimensional impact loads was implemented into the numerical simulation program WAMIT. The WAMIT results are validated against experiments from a scaled gravity-based structure (GBS) platform subjected to regular waves. For such structures, horizontal forces are usually considered to be most critical for platform safety, but vertical loads may also contribute to critical responses (Baarholm & Stansberg, 2004).

Stansberg et al. predicted air-gap and deck impact on column-based platforms in steep and high waves. Numerical models based on linear and second-order diffraction-radiation analysis (WAMIT) were validated against model test data, once again carried out at MARINTEK. The wave-in-deck loads are modelled by a simple formulation similar to Kaplan's approach and four different cases are included: a circular column, four circular columns, three column GBS (with a caisson) and a moored semi-submersible (Stansberg et al., 2005).

3 Experimental reference project of slamming event

In this section the experimental set-up for the reference project is presented as well as the key results from the study. The work that has been selected as reference project is the PhD thesis "Theoretical and Experimental Studies of Wave Impact underneath Decks of Offshore Platforms" by Rolf Jarle Baarholm (Baarholm, 2001). The purpose of the PhD thesis was to study the phenomenon of water impact underneath the deck of offshore platforms due to regular propagating waves. Two theoretical methods based on two-dimensional potential theory were developed, a Wagner based method and a nonlinear boundary element method (BEM). To validate the theories, experiments were carried out in the wave flume at the Department of Marine Hydrodynamics, NTNU. To isolate and study the important physical effects governing the impact process, a fixed horizontal platform deck in two-dimensional flow conditions was considered. Main parameters measured were vertical lifting force and the wetted length of the platform.

3.1.1 Experimental set-up

The wave basin at NTNU is a narrow flume designed with a length of 13.5 m, depth of 1.3 m (effective water depth 1.0 m) and breadth of 0.6 m. Three different parameters were presumed and changed during the experiments; wave amplitude, wave period and initial deck clearance to the free water surface. An electrically operated wave maker is installed in one end of the flume. It is a computer controlled single flap wave maker equipped with a system that enables the flap to damp out reflected waves. The flap is hinged 0.1 m above the bottom of the basin and a beach is installed to effectively damp out the waves at the other end of the flume. This is a conventional type of beach with a parabolic arc profile. Two-dimensional flow required the model to cover the entire breadth of the basin. A thin rubber membrane was placed between the model and the flume wall to prevent water from passing the deck. This membrane was assumed to transfer no vertical force to the walls. Three force transducers were installed in a triangular configuration above the deck to measure the vertical force during the impact event. The deck was designed in a way to eliminate structural responses, hence it could be assumed as rigid.

During the experiments three different wave periods were used; 1.11 s, 1.25 s and 1.43 s. These specific wave periods were chosen to represent realistic full scale waves, but also to minimize the risk of unwanted waves in the basin. The bottom side of the deck model, on which the force transducers were placed, had a length of 0.63 m and a breadth of 0.56 m. Since the model is scaled 1:150 the full length of the platform would be 94.5 m. Only regular incident waves were considered because it was easier to study the impact process in detail and get a better understanding of the physics involved. It was believed that if the theory could be validated for regular waves, the theory could also be applicable for more general sea states. Several wave heights were used, ranging from $H = 0.10$ m to $H = 0.14$ m (full-scale: 15 m to 22.5 m) and was limited by wave steepness. If the steepness becomes too large, time series with regular waves are difficult to produce since breaking may start to occur.

To ensure the entire impact event was captured, a sampling frequency of 100 Hz was used. The model was kept out of the waves until steady-state was reached and then quickly lowered between two wave crests in the middle of the flume. The location lengthwise was chosen so it was far enough away from the wave maker to allow the waves to get fully developed, but also far away from the beach to avoid reflections.

After the first wave had reached the deck, the water surface was disturbed and the following waves were not equally regular which influenced the measured lift force significantly. Baarholm decided therefore to only measure the forces from the first impact event and not from the following waves, even though they could exhibit much higher peak forces. Figure 3.1 shows sketches from six time instants of the impact process associated with the first wave hitting the structure.

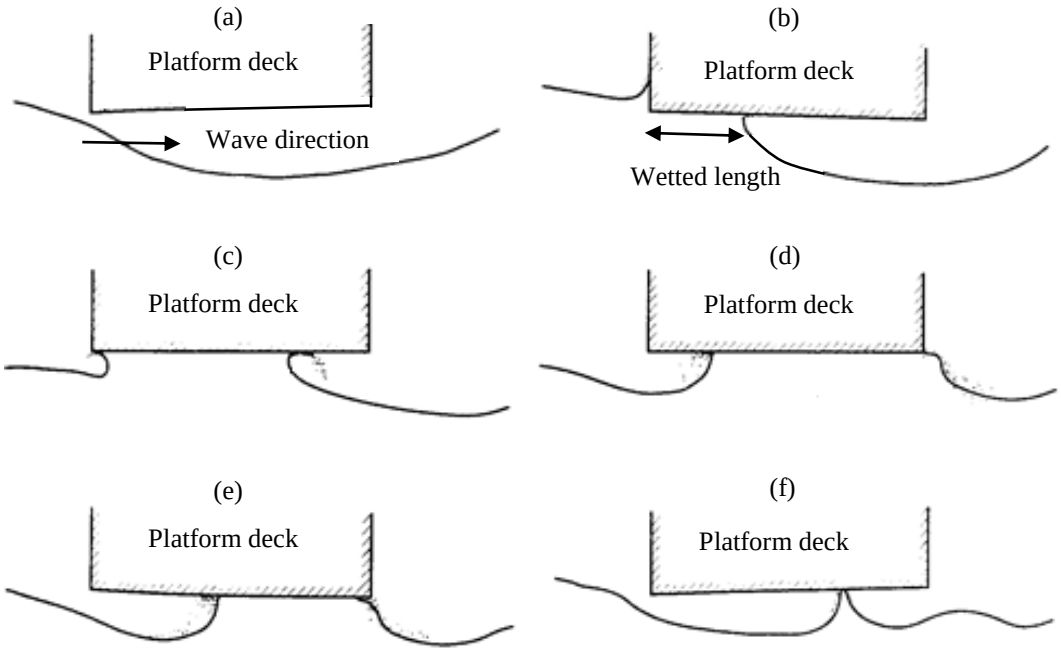

Figure 3.1 – Sketches of six time instants of a wave-in-deck load (Baarholm, 2001).

The first sketch (a) shows the platform deck and the undisturbed wave before impact occurs. As the wave hits the left corner (b), the wetted area increases smoothly and a pile-up of water and jet is formed at the front end of the platform. In sketch (c) the upstream body/water intersection has just moved around the left corner of the deck and the free surface near the intersection is characterized by high curvature. As the downstream intersection reaches the aft end of the deck (d), the fluid flow leaves the deck tangentially which indicates that fluid particles at the immediate neighbourhood of the body has no vertical velocity. Spray is observed on the free surface behind the body as well as breaking. These effects will dissipate energy from the system and the wave amplitude behind the body is reduced compared to the incident wave. The reduction is also caused by wave reflection from the front end and the bottom plate. The magnitude of this reduction depends on both wave condition and air-gap, where a large difference between wave elevation and deck clearance yields a more significant reflected wave, energy dissipation and spray. The water exit phase has a duration longer than if the wave would have propagated undisturbed and the water seems to "stick" to the bottom plate (e), which results in a wave profile with much higher curvature close to the body. After some time, the downstream intersection starts to move forward again and finally the water exits the deck in a manner shown in (f). The downstream intersection starts to propagate upstream towards the fore body and the location of the final water exit is dependent on impact condition, but generally located a distance around 1/3 from the aft corner. It is especially this last mentioned complex behaviour observed in the water exit phase that is troublesome for analytical solutions. There were in total eleven different combinations of wave period, wave height and deck clearance

during the experiments, and several experiments were performed with the same configuration to get reliable results. In this thesis, it was decided to only replicate the results from four different experiments and the reason for selecting fewer was because of time limitations and the fact that the four chosen experiments all had the same deck clearance of 0.04 m. In this way it was possible to analyse different combinations of wave lengths and wave heights without having to change the geometry of the CFD model between tests.

3.1.2 Results from the experiment

The results from the single impact experiments can be seen in Table 3.1. These are the averaged values from all successful experiments for each configuration. The table shows the maximum and minimum lifting force acting on the platform as well as the time duration for the whole impact event. σ denotes the standard deviation from the different tests. The cases selected to be replicated in Fluent are cases 1, 2, 5 and 6.

Case no:	Impact condition			Experimental results				
	T [s]	H [m]	c [m]	F_{max} [N]	σ_{max} [N]	F_{min} [N]	σ_{min} [N]	T_{im} [s]
1	**1,11**	**0,10**	**0,04**	**29,3**	**1,71**	**-67,8**	**1,68**	**0,76**
2	**1,11**	**0,12**	**0,04**	**49,1**	**2,58**	**-83,5**	**3,67**	**0,82**
3	1,11	0,12	0,06	7,1	1,12	-36,5	3,95	0,53
4	1,11	0,14	0,06	31,7	0,87	-70,2	2,70	0,78
5	**1,25**	**0,10**	**0,04**	**37,0**	**2,26**	**-67,8**	**4,63**	**0,78**
6	**1,25**	**0,12**	**0,04**	**65,2**	**2,18**	**-70,2**	**3,26**	**0,87**
7	1,25	0,12	0,06	11,2	1,33	-61,7	2,87	0,83
8	1,25	0,14	0,06	41,0	1,36	-88,7	2,40	0,77
9	1,43	0,10	0,038	53,0	3,10	-51,9	2,38	0,92
10	1,43	0,12	0,038	97,5	2,39	-54,2	2,75	0,95
11	1,43	0,12	0,06	14,5	0,25	-58,9	1,35	0,79

Table 3.1 – Experimental results from the single impact events.

3.1.3 Conclusions from the experiment

When a regular propagating wave hits the deck it experiences a positive lift force during the initial water entry phase, followed by a negative force during the water exit phase. The negative peak of the lift force in the latter phase occurs when the wetting of the deck is at its maximum and its magnitude may be larger than the positive force peak. Experiments show that the duration of the water exit phase is longer than the entry phase, where the fluid seems to "stick" to the deck. The main parameters governing the impact force is assumed to be wave amplitude, wave period and deck clearance. Additional effects such as cushioning due to entrapped air, compressibility of the fluid and surface roughness are assumed to be of minor importance and are left out of the discussion. Theoretically, the shape of the force time history could be explained by dividing the deck force into three components: slamming force, added mass force and incident wave force. Figure 3.2 shows their respective contributions.

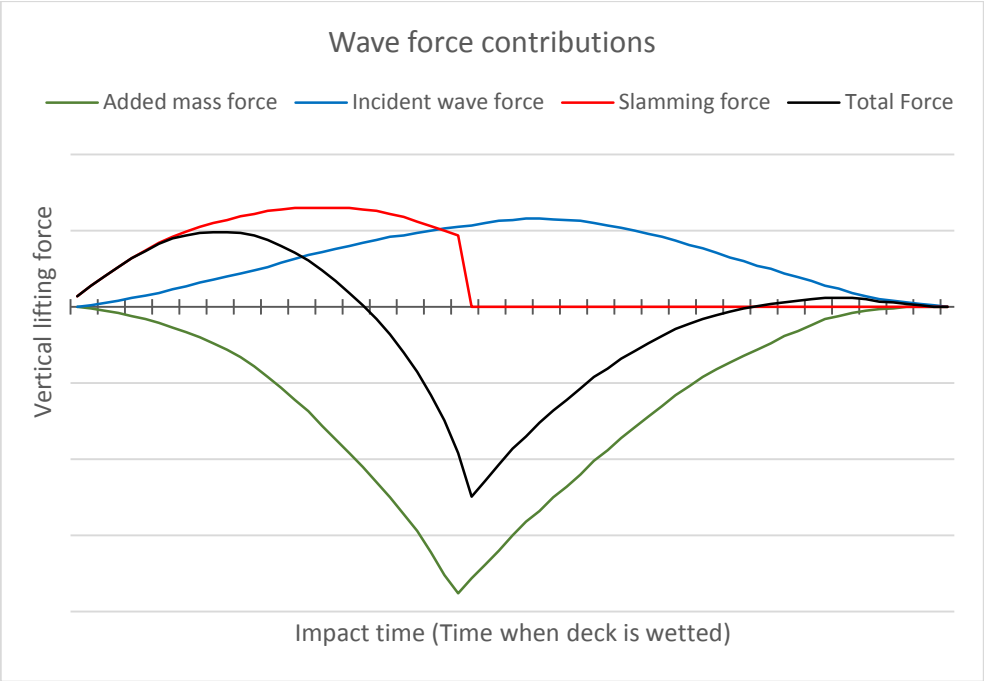

Figure 3.2 – Wave force contributions from a wave impact.

The positive water entry force is dominated by the slamming force. The wetted length of the deck at this time instant can differ, but is generally around half distance of the deck. The maximum peak also gets significant contribution from the incident wave force, while added mass force yields a negative contribution about the same magnitude. The slamming force is always positive, but equals zero when the wetted area starts decreasing. The added mass force is always negative throughout the entire impact process, since the fluid accelerations are negative in the wave crest. The added mass term has its peak when the wetted area is at its maximum, thus F_{min} occurs here as well. The water exit phase is therefore important for global structural effects, while the initial impact is crucial for local structural response in the deck. Even though the maximum force peak tends to be smaller, the pressure is often larger due to a smaller wetted area.

3.1.3.1 Wave amplitude dependency

If the wave period and deck clearance are kept constant, the wetted lengths are similar during the water entry phase for different wave amplitudes. Despite this, F_{max} is very dependent on the wave amplitude. Several reasons for this can be detected. Both the incident wave force and added mass force are affected by the increase in wave amplitude, but the main contribution comes from the change in slamming force. Wetting velocity remains quite unaffected, but due to larger impact velocities the slamming term increases significantly. The increase in impact velocity is caused by higher vertical fluid velocities in a wave with higher amplitude. Also, the first impact moves further downstream of the wave crest towards a location where the vertical fluid velocities are larger. Figure 3.3 shows the wave height dependency. However, F_{min} seems most of the time to be rather unaffected of the wave height. This can be described by increase in added mass due to higher averaged fluid accelerations is compensated by an increase in the incident wave force. Increase in wave amplitude leads to larger duration of the impact event. Below plot shows the dependency of the wave height in the experiments.

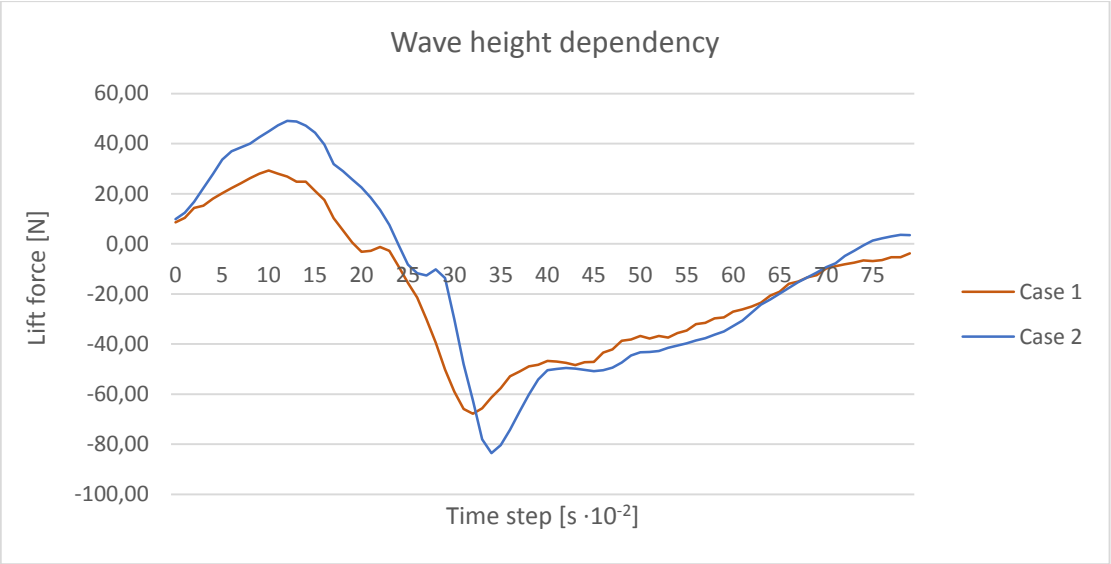

Figure 3.3 – Plot from case 1 and case 2 showing the wave height dependency.

3.1.3.2 Wave period dependency

The maximum vertical particle velocity in the wave crest decreases with increasing wave period and vertical particle velocities are crucial for the impact force. In spite of this fact, it can be noted that for a given wave amplitude and deck clearance, F_{max} increases as the wave period gets longer. This is mainly due to a more rapid wetting of the deck, where longer waves allow the deck to get wet faster because of lower wave steepness. So even if the average impact velocity is smaller at the time instant where F_{max} occurs, this is compensated by an increased wetting velocity and larger wetted area. A larger wetting velocity implies that the slamming force is dominant. Given that the maximum wetted area is equal for the two waves with different period, absolute value of F_{min} is smaller for the longer wave. This is mainly due to the negative particle acceleration and added mass force. Figure 3.4 shows the wave period dependency from the experiments.

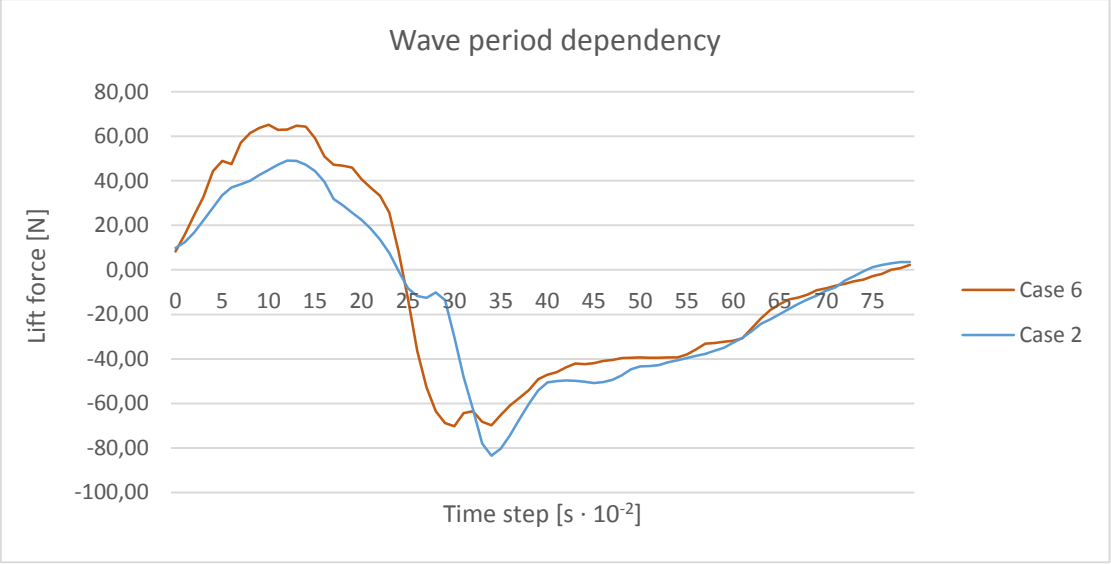

Figure 3.4 - Plot from case 2 and case 6 showing the wave period dependency.

3.1.3.3 Deck clearance dependency

The deck height for a fixed platform affects the water impact greatly, where a reduction in deck height implies larger incident wave force and a significant difference in impact velocity, hence a larger slamming force. F_{min} is affected too, mainly because of the differences in maximum wetting and the time rate of impact velocity. Because of smaller positive incident wave force, the larger of two different deck heights may give the largest magnitude of F_{min} if the wetted lengths are similar.

3.1.4 Error sources from the experiment

As with any physical experiment there are different errors sources that may affect the results and even the smallest deviation from reality could lead to invalid results. An essential component in the wave basin is the damping beach at the end of the flume. If some reflections may occur, they could travel and influence the wave elevation and particle kinematics of the waves near the platform. It is therefore important to observe the behaviour at the beach and know the time necessary for a reflected wave to travel to the deck area. If the model is placed in the middle of the flume, problems with reflections will not arise until the first wave in a wave train has travelled 1.5 times the length of the flume (20.25 m). The velocity of the wave train is characterized by the group velocity c_g which is the velocity in which the wave energy is transmitted. Since the longest waves propagate fastest they are most crucial. For the longest wave with $T = 1.43$ s, the phase velocity c_g is 1.12 m/s, thus it takes 18.1 s before the first reflected wave reaches the platform. Owing to above circumstances, measurements were conducted in a time window of 10 – 15 s after the wave maker was started.

Reflection and transient effects may also occur due to start-up of the wave maker, even though it is designed to minimize this unwanted behaviour. When the fluid inside the tank is set in motion by a disturbance, it will oscillate at the natural periods of the fluid motion. This could cause longitudinal sloshing in the tank. The control system of the wave maker is designed to damp out such oscillations.

Depending on the chosen wave period during the experiments, transverse waves can be unintentionally created in the narrow wave flume. The wave periods used in Baarholm's experiments were selected to guarantee that no transverse waves would be generated. Other sources of error are the measurement equipment such as the force transducers, wave gauge, electrodes and probes.

4 Theoretical background of the CFD method

Since the vast development of computers, numerical methods to solve and analyse fluid flow are increasingly important in the industry and are in constant development. This chapter gives a short background of the theory behind the governing equations used to solve fluid flow and then an overview of the numerical methods used by the CFD software to solve the governing equations. A short discussion about turbulence models and discretization schemes, will hopefully justify the use of numerical methods to solve fluid flow problems associated with wave induced loads. Lastly, some light are shed on errors and uncertainties related to numerical models which are important to be aware of in order to make complete assessments describing a complex reality. If not specified differently, the theory is based on (Versteeg & Malalasekera, 2007) and (White, 2011).

4.1 Governing equations

In fluid mechanics, the motions of liquids and gases are described using the approach of continuum mechanics, wherein the fluid is characterized by properties that aggregates over a large number of individual molecules. A fluid particle, or fluid element, is by continuum mechanics defined as an infinitesimally small region of fluid whose physical properties are independent of its actual size or the time over which they are measured. Hence the fluid element should be small enough to show independent properties, but much larger than the characteristic length of atomic spacing and time scales much larger than the characteristic time of atomic bond vibrations.

The governing equations of fluid flow represent mathematical statements of the conservation laws of physics. There are three conservation laws used in fluid dynamics that need to be fulfilled to accurately describe the flow;

- The mass of a fluid is conserved.
- The rate of change of momentum equals the sum of the forces acting on a fluid particle (Newton's second law).
- The rate of change of energy is equal to the sum of the rate of heat added and the rate of work done on a fluid particle (first law of thermodynamics).

A systematic account of changes in the mass, momentum and energy of a fluid element across its boundaries and due to action of sources inside the element, leads to the fluid flow equations used in CFD programs.

The mass conservation law states that the rate of increase of mass in a fluid element equals the net rate of flow of mass into that fluid element:

$$\frac{\partial \rho}{\partial t} + \frac{\partial(\rho u)}{\partial x} + \frac{\partial(\rho v)}{\partial y} + \frac{\partial(\rho w)}{\partial z} = 0 \qquad \text{or:} \quad \frac{\partial \rho}{\partial t} + \nabla \cdot (\rho \cdot \boldsymbol{v}) = 0$$

The conservation law of momentum states that the time rate of change of momentum in a fluid element equals the net rate of momentum flow out of the fluid element plus the sum of forces acting on the fluid element. The forces could either be surface forces due to pressure and viscosity or body forces due to gravity, centrifugal- or electromagnetic forces. However, in below equations gravity is considered to be the only body force acting on a fluid element. There are three momentum equations in total, one for x-, y-, z-direction respectively;

$$\rho\left(\frac{\partial u}{\partial t} + u\frac{\partial u}{\partial x} + v\frac{\partial u}{\partial y} + w\frac{\partial u}{\partial z}\right) = \rho g_x - \frac{\partial p}{\partial x} + \frac{\partial \tau_{xx}}{\partial x} + \frac{\partial \tau_{xy}}{\partial y} + \frac{\partial \tau_{xz}}{\partial z}$$

$$\rho\left(\frac{\partial v}{\partial t}+u\frac{\partial v}{\partial x}+v\frac{\partial v}{\partial y}+w\frac{\partial v}{\partial z}\right)=\rho g_y-\frac{\partial p}{\partial y}+\frac{\partial \tau_{xy}}{\partial x}+\frac{\partial \tau_{yy}}{\partial y}+\frac{\partial \tau_{yz}}{\partial z}$$

$$\rho\left(\frac{\partial w}{\partial t}+u\frac{\partial w}{\partial x}+v\frac{\partial w}{\partial y}+w\frac{\partial w}{\partial z}\right)=\rho g_x-\frac{\partial p}{\partial z}+\frac{\partial \tau_{xz}}{\partial x}+\frac{\partial \tau_{yz}}{\partial y}+\frac{\partial \tau_{zz}}{\partial z}$$

or: $\rho\frac{D\boldsymbol{v}}{Dt}=\rho\boldsymbol{g}-\nabla p+\nabla\cdot\tau$

The governing equations for momentum contain viscous stresses giving extra unknowns to the equation system. Another way to treat viscous stresses is by introducing a suitable model, where they can be expressed as functions of the local deformation rate or strain rate. Viscous stresses are proportional to the element strain rates and the coefficient of viscosity according to: $\tau=\mu\frac{d\theta}{dy}=\mu\frac{du}{dy}$. This relationship is called Newton's law for viscosity and is applicable for Newtonian fluids (i.e. $\mu=$ constant). Non-Newtonian materials show other characteristics such as shear-thinning or shear thickening behavior (cf. polymers). By applying Newton's law of viscosity to the momentum equations for incompressible flow, the differential equations can then be rewritten to form the so-called Navier –Stokes equations, which are the most important functions in fluid dynamics:

$$\rho\frac{Du}{Dt}=\rho g_x-\frac{\partial p}{\partial x}+\mu\left(\frac{\partial^2 u}{\partial x^2}+\frac{\partial^2 u}{\partial y^2}+\frac{\partial^2 u}{\partial z^2}\right)$$

$$\rho\frac{Dv}{Dt}=\rho g_y-\frac{\partial p}{\partial y}+\mu\left(\frac{\partial^2 v}{\partial x^2}+\frac{\partial^2 v}{\partial y^2}+\frac{\partial^2 v}{\partial z^2}\right)$$

$$\rho\frac{Dw}{Dt}=\rho g_z-\frac{\partial p}{\partial z}+\mu\left(\frac{\partial^2 w}{\partial x^2}+\frac{\partial^2 w}{\partial y^2}+\frac{\partial^2 w}{\partial z^2}\right)$$

or: $\rho\frac{D\boldsymbol{v}}{Dt}=\rho\boldsymbol{g}-\nabla p+\mu\nabla^2\boldsymbol{v}$

In energy conservation, the increase rate of energy of a fluid particle should equal net rate of heat added to the fluid particle plus net rate of work done on the fluid particle. The energy of a fluid is defined as the sum of internal (thermal) energy $\hat{u}$, kinetic energy k and gravitational potential energy. In total there are 5 equations (mass, x-, y-, z-momentum and energy) with 7 unknowns (density, pressure, velocity, internal energy, temperature).

However, liquids and gases flowing at low speed behave as incompressible fluids if $M_a<0.3$ and this approximation is applicable in most open-channel flows. Without density variations, there is no linkage between the energy equation, mass conservation and momentum equations and the flow field can be determined by considering the mass conservation and momentum equations solely. Therefore, the energy equation is not further described.

The continuity equation and the Navier-Stokes equations form a closed set of equation system containing four unknown variables (pressure and velocity) and can be solved, subject to proper boundary conditions.

4.2 Turbulence modelling

All flows encountered in engineering practice become unstable above a certain Reynolds number due to shear forces in the mean flow. At low Reynolds number the flow is laminar with no mixing or tangential component to the motion, but for high Reynolds numbers a chaotic and random state of motion develops in which the velocities and pressures change continuously. The transition to turbulence is strongly affected by factors such as pressure gradients, disturbances and wall roughness. For most engineering purposes it is unnecessary to resolve the details of the turbulent fluctuations as information concerning the time-averaged fluid properties is sufficient. Therefore, the vast majority of turbulent flow computations are carried out with procedures based on the RANS equations, by introducing Reynold's decomposition. Now, the fluid properties (velocity, pressure and temperature) are decomposed into a steady mean value and a fluctuating component. For instance, velocity in x-direction can be decomposed as: $u(t) = \bar{u} + u'(t)$, see Figure 4.1. By introducing Reynolds decomposition to the governing equations, below equations are obtained (in x-direction):

$$\nabla \cdot \bar{u} = 0$$

$$\rho \frac{D\bar{u}}{Dt} = -\frac{\partial p}{\partial x} + \mu \nabla^2 \bar{u} + \left[\frac{\partial\left(-\rho \overline{u'^2}\right)}{\partial x} + \frac{\partial(-\rho \overline{u'v'})}{\partial y} + \frac{\partial(-\rho \overline{u'w'})}{\partial z} \right]$$

It is important to note that above equations are the same as the originals except for new fluctuating terms inside the bracket and averaged velocities outside. The fluctuating terms are associated with convective momentum transfer due to turbulent eddies and result from six additional stresses called the Reynolds stresses:

$$\tau_{xx} = -\rho \overline{u'^2} \quad , \quad \tau_{yy} = -\rho \overline{v'^2} \quad , \quad \tau_{zz} = -\rho \overline{w'^2}$$

$$\tau_{xy} = \tau_{yx} = -\rho \overline{u'v'} \quad , \quad \tau_{xz} = \tau_{zx} = -\rho \overline{u'w'} \quad , \quad \tau_{yz} = \tau_{zy} = -\rho \overline{v'w'}$$

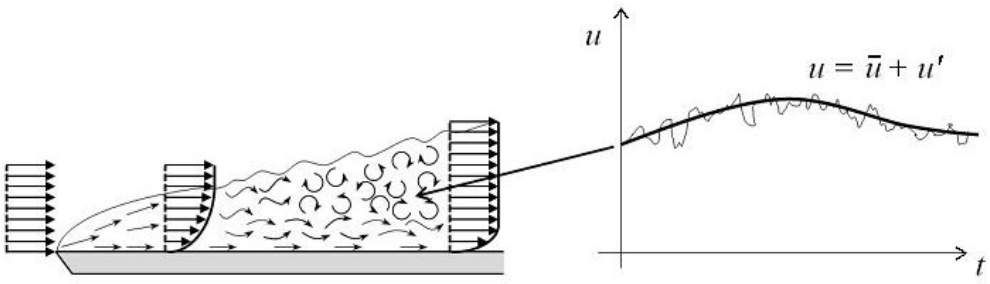

Figure 4.1 – Reynolds decomposition of a turbulent flow. The velocity can be decomposed into a steady mean value $\bar{u}$ and a fluctuating component u' (Frei, 2013).

4.2.1 Reynolds averaged Navier-Stokes (RANS) equations

The Reynolds stresses yield additional six unknowns in the equation system and in order to use RANS models and compute turbulent flow, it is necessary to develop models to describe and predict these stresses. The most widely used and validated turbulence models are the *mixing length model*, *k-ε model* and *k-ω model*. They are based on the presumption that there exists an analogy between the action of viscous stresses and Reynolds stresses. Boussinesq proposed that Reynolds stresses might be proportional to mean rates of deformation according to:

$$\tau_{ij} = -\rho\overline{\boldsymbol{v}_i{}'\boldsymbol{v}_j{}'} = \mu_t\left(\frac{\partial\overline{v_i}}{\partial x_i} + \frac{\partial\overline{v_j}}{\partial x_j}\right) - \frac{2}{3}\rho k\delta_{ij}$$

Where k is the turbulent kinetic energy, μ_t is turbulent or eddy viscosity and δ_{ij} is the Kronecker's delta (1 if $j = i$, otherwise 0).

4.2.1.1 Mixing length model

The mixing length model attempts to describe the Reynolds stresses by means of a simple equation of turbulent viscosity as a function of position. From dimensional analysis, it is assumed the kinematic turbulent viscosity (ν_t) is proportional to the product of a turbulent length scale (l_m) and velocity scale. This behaviour works very well for two-dimensional turbulent flows with slow changes in the flow direction, where the most significant Reynolds stress is τ_{xy} and the most significant mean velocity gradient is $\frac{\partial\overline{u}}{\partial y}$. For such flows, the turbulent Reynolds stress is approximated by:

$$\tau_{xy} = \rho l_m^2 \left|\frac{\partial\overline{u}}{\partial y}\right| \cdot \frac{\partial\overline{u}}{\partial y}$$

The mixing length model requires no extra transport equation, is easy to implement and cheap in terms of computing resources. It gives good predictions for thin shear layers and boundary layers. The main disadvantage is the incapability of describing flows with separation and recirculation, since only the mean flow properties and turbulent shear stress are computed.

4.2.1.2 The *k-ε* model

In flows where transport of turbulence properties by convection (transport due to density difference) and diffusion (net movement from high concentration to low concentration) cause significant differences between production and destruction of turbulence, e.g. recirculating flows, the mixing length model is no longer accurate. Instead the *k-ε* model is usually adopted which focuses on the mechanisms that affect the turbulent kinetic energy and the dynamics of the turbulence. It gives two extra transport equations (PDE's) for each Reynolds stress, one for the turbulent kinetic energy *k*, and another for the rate of dissipation *ε* (energy transformed to heat due to friction and turbulence). The dissipation of turbulent kinetic energy is caused by work done by the smallest eddies against viscous stresses. Below are the two transport equations forming the *standard k-ε model*, where $C_\mu, \sigma_k, \sigma_\varepsilon, C_{1\varepsilon}$ and $C_{2\varepsilon}$ are five adjustable constants that have been derived through comprehensive data fitting for a wide range of turbulent flows.

$$\mu_t = \rho C_\mu \frac{k^2}{\varepsilon}$$

$$\frac{\partial(\rho k)}{\partial t} + \nabla\cdot(\rho k\overline{\boldsymbol{v}}) = \nabla\cdot\left(\frac{\mu_t}{\sigma_k}\nabla k\right) + 2\mu_t\bar{s}_{ij}\cdot\bar{s}_{ij} - \rho\varepsilon$$

$$\frac{\partial(\rho\varepsilon)}{\partial t} + \nabla\cdot(\rho\varepsilon\overline{\boldsymbol{v}}) = \nabla\cdot\left(\frac{\mu_t}{\sigma_\varepsilon}\nabla\varepsilon\right) + C_{1\varepsilon}\frac{\varepsilon}{k}2\mu_t\bar{s}_{ij}\cdot\bar{s}_{ij} - C_{2\varepsilon}\rho\frac{\varepsilon^2}{k}$$

Here s_{ij} denotes the rate of deformation $\left(s_{ij} = \frac{\partial u_i}{\partial x_j} + \frac{\partial u_j}{\partial x_i}\right)$

In words the equations can be expressed as:

Rate of change of k or ε	+	Transport by convection of k or ε	=	Transport by diffusion of k or ε	+	Rate of production of k or ε	-	Rate of destruction of k or ε

The main advantage of the standard k-ε model is that it is the simplest model for which only initial conditions and boundary conditions are needed. The model is well established and the most widely validated turbulence model, making it suitable for many cases. Robustness, economy and reasonable accuracy for a wide range of turbulent flows explain its popularity. Disadvantages are poor performance in unconfined flows, flows with curved boundary layers, swirling flows and rotating flows. The model performs poorly near walls and use of special enhanced wall treatments is commonly adopted to increase the accuracy, see Section 4.2.2.

As the strengths and weaknesses of the standard model have become known, modifications have been introduced to improve its performance. In Fluent, other k-ε model variants are available and the most prominent is called *the realizable model*. The realizable model has shown substantial improvements over the standard model for complex separated flows, flows with strong streamline curvature, vortices and rotation (ANSYS Inc., 2013).

4.2.1.3 The k-ω model

The most prominent alternative to the k-ε model is *the k-ω model* which is an empirical model based on transport equations for the kinetic energy and the turbulence frequency ($\omega = \varepsilon/k$), also called specific dissipation rate. The Reynolds stresses are computed as usual with the Boussinesq equation. This method initially gained attention because integration to the wall does not require any wall-damping functions in low Reynolds number applications. The model performs better in the near-wall region compared to k-ε, but worse in the turbulent free stream region outside the shear layer. An improved version of the model is called *SST k-ω model* and is a hybrid that uses a transformation of the k-ε model into k-ω model in the near-wall region and the standard k-ε model in the fully turbulent region far away from the wall. The Reynolds stress computation and the k equation are the same as in the original *k-ω model*, but ε-equation is transformed into an ω-equation by substituting $\varepsilon = k\omega$. These features make the SST model more accurate and reliable for a wider class of flows than the standard k-ω model.

4.2.2 Wall functions and general comments on turbulence models

A turbulent flow is greatly affected by the walls where the gradients are large. Near the wall a turbulent boundary layer develops and in order to accurately predict and resolve this thin viscosity-affected layer, a very fine mesh would be needed. This resolution requirement is actually more important than achieving certain y^+ values and ANSYS recommends the minimum number of cells to cover a boundary layer to be at least 10-20 (ANSYS Inc., 2014). Sometimes it is not possible to model this region with a mesh all the way to the wall and another way is to use semi-empirical formulas called "wall functions" to bridge the viscosity-affected region between the wall and the fully turbulent region. Recommendation from ANSYS is to use the "enhanced wall treatment" for the k-ε model (default for k-ω model), which is a near-wall modeling method that is y^+ insensitive and will act like a wall function if the first grid point of the mesh is in the log-layer.

For a long time, efforts have been made to develop a general-purpose RANS model suitable for a wider range of practical applications. Unfortunately this has proved to be extremely difficult, mainly due to the differences in the behavior of large and small eddies. The smaller eddies are nearly isotropic, while larger eddies are more anisotropic and extract energy from the mean flow. When RANS equations are used, the collective behavior of all eddies should be described by a single method. A general approach accepts that larger eddies need to be computed for each problem with a time-dependent simulation. Smaller eddies should be easier to capture with a compact model, which is the essence of the Large Eddy Simulation (LES). Instead of time-averaging, LES uses a spatial filtering operation to separate larger and smaller eddies.

The continuity equation and Navier-Stokes equations for an incompressible flow form a closed set of four equations with four unknowns. Direct Numerical Simulation (DNS) is a method in which the entire set of equations is solved numerically without any turbulence model. This means that the whole range of spatial and temporal scales of the turbulence must be resolved. The downside is obviously the enormous computational resources for such simulations.

4.3 The finite volume method

One can note from the continuity equation and momentum equations that there are significant commonalities. To describe conservation of any kind, a general property variable $\emptyset$ can be introduced and used in the governing equations:

$$\frac{\partial(\rho\emptyset)}{\partial t} + \nabla \cdot (\rho\emptyset\boldsymbol{v}) = \nabla \cdot (\Gamma\nabla\emptyset) + S_{\emptyset}$$

It could easily be compared with the Navier-Stokes equations by substituting $\emptyset$ to velocity. In words, the transport equation can be expressed as:

Rate of increase of $\emptyset$	+	Net rate of flow of $\emptyset$ out of fluid element	=	Rate of increase of $\emptyset$ due to diffusion	+	Rate of increase of $\emptyset$ due to sources

The first term on the left side is linked to the steadiness of the flow and the second term is usually called the convective term. On the right side, there are a diffusive term with diffusion coefficient Γ and a source term. As an example, in conductive heat transfer the thermal conductivity, *k*, takes the place of Γ and the property variable $\emptyset$ is *T*. The source term can be heat generation from a source *q*. To explain the derivation of the transport equation into a discretized equation that can be solved numerically, above expression is simplified to be one-dimensional with pure diffusion in steady-state:

$$\frac{d}{dx}\left(\Gamma\frac{d\emptyset}{dx}\right) = 0$$

Integration of the transport equation forms the key step of the finite volume method and the first step is to divide the domain into discrete control volumes. Figure 4.2 shows three nodal points called W, P and E. The boundaries of control volumes are positioned mid-way between adjacent nodes, thus each node is surrounded by a control volume or a cell.

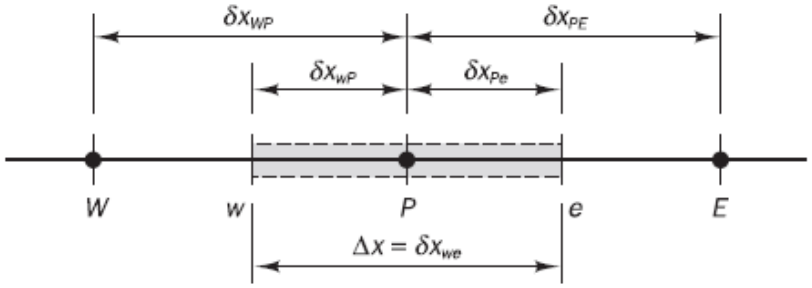

Figure 4.2 – Definition of nodal points and the distances between nodes (Versteeg & Malalasekera, 2007).

Now a discretized equation at a nodal point P can be expressed as:

$$\int_{\Delta V} \frac{d}{dx}\left(\Gamma \frac{d\emptyset}{dx}\right) dV = \left(\Gamma A \frac{d\emptyset}{dx}\right)_e - \left(\Gamma A \frac{d\emptyset}{dx}\right)_w$$

A is the cross-sectional area of the control volume face. Above equation states that the diffusive flux of $\emptyset$ leaving the east face minus the diffusive flux entering the west face is equal to the generation of $\emptyset$. To calculate gradients (and hence fluxes) at the control volume faces an approximate distribution of properties between nodal points must be used. Below is an example of linear approximation, called *central differencing*.

$$\Gamma_w = \frac{\Gamma_W + \Gamma_P}{2} \quad , \quad \Gamma_e = \frac{\Gamma_E + \Gamma_P}{2}$$

The diffusive flux terms are evaluated as:

$$\left(\Gamma A \frac{d\emptyset}{dx}\right)_e = \Gamma_e A_e \left(\frac{\emptyset_E - \emptyset_P}{\delta x_{PE}}\right) \quad , \quad \left(\Gamma A \frac{d\emptyset}{dx}\right)_w = \Gamma_w A_w \left(\frac{\emptyset_P - \emptyset_W}{\delta x_{WP}}\right)$$

After substitution and rearrangement:

$$\left(\frac{\Gamma_e}{\delta x_{PE}} A_e + \frac{\Gamma_w}{\delta x_{WP}} A_w\right) \emptyset_P = \left(\frac{\Gamma_w}{\delta x_{WP}} A_w\right) \emptyset_W + \left(\frac{\Gamma_e}{\delta x_{PE}} A_e\right) \emptyset_E$$

All discretized equations could be expressed in this general form, even problems with convection and source terms, by expanding the equation with a few extra terms inside the brackets. Discretized equations must be set up at all nodal points of the domain to create a closed equation system and control volumes adjacent to domain boundaries are modified to incorporate boundary conditions. Note that the expression can be simplified for most cases since most of the time $\Gamma_e = \Gamma_w = \Gamma$, $A_e = A_w = A$ and node spacing δ_x are constants.

4.3.1 Differencing schemes

Differencing schemes are used when partial differential equations are solved to numerically simulate the direction of propagation of information in a flow field (i.e. how the central node value should be determined between adjacent nodes). In derivations from above, the central differencing approximation was used, which uses linear interpolation to compute the cell face values of property $\emptyset$ between two adjacent nodes. This scheme faces some problems for certain convection problems were the velocity is high or the mesh is coarse. For a flow from left to right, the value of property $\emptyset$ at the west cell face is influenced by both $\emptyset_P$ and $\emptyset_W$, even though for some convective flows the west cell face should receive much stronger influence from node W. Owing to these circumstances, central differencing is not a suitable discretization practice for general purpose flow calculations.

In contrast to the central differencing scheme, the *upwind scheme* takes the flow direction into account when determining the value of a cell face. The value of $\emptyset$ is assumed to be equal to the value at the upstream node according to:

$\emptyset_w = \emptyset_W$ and $\emptyset_e = \emptyset_P$ for flows from west to east

$\emptyset_w = \emptyset_P$ and $\emptyset_e = \emptyset_E$ for flows from east to west

When the flow is aligned with the mesh on quadrilateral or hexahedral elements, the first-order upwind discretization is adequately accurate. A drawback of the scheme is that it produces erroneous results when the flow is very complex or not aligned with the grid lines. The upwind scheme causes the distributions of the transported properties to become smeared in such problems. The resulting error has a diffusion-like appearance and is referred to as false diffusion. For triangular and tetrahedral meshes, since the flow is then not aligned with the mesh, more accurate results are generally obtained by using the second-order upwind discretization (ANSYS Inc., 2013).

The oldest and most used high-order scheme for improved accuracy is called the *QUICK* scheme, which is a quadratic upstream interpolation. It uses a three-point upstream-weighted interpolation for the cell face values, see Figure 4.3.

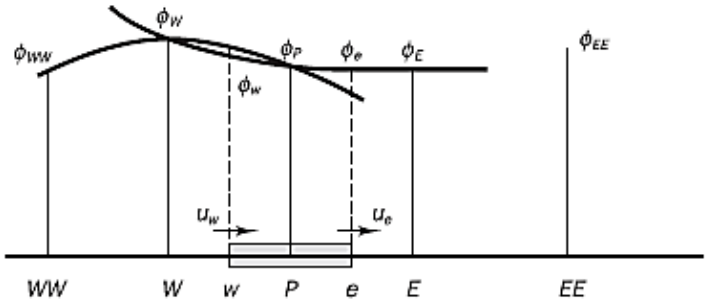

Figure 4.3 - Three-point upstream-weighted quadratic interpolation in QUICK scheme (Versteeg & Malalasekera, 2007).

For instance a quadratic fit through WW, W and P is used to determine the value of $\emptyset_w$ and a another quadratic fit through W, P and E to calculate $\emptyset_e$. The QUICK differencing scheme has greater formal accuracy then above schemes, the resultant false diffusion is small and solutions achieved with coarse grids are often considerably more accurate. On the downside, the discretized equations involve not only immediate-neighbor nodes but also nodes further away, which is unfavorable for very skewed/distorted meshes.

Fluent offers three choices for spatial discretization for gradients; Green-Gauss node based, Green-Gauss cell based and Least square cell based. The Green-Gauss node based gradient is known to be more accurate than the Green-Gauss cell based gradient, particularly on irregular (skewed and distorted) unstructured meshes. However, it is relatively more expensive to compute than the cell based gradient scheme. Least square cell based gradient is similar to node based gradient on irregular unstructured meshes, and therefore also more superior compared to the cell based gradient. It is less expensive to compute than node based gradient, thus this scheme is the default choice in the Fluent (ANSYS Inc., 2013).

4.3.2 Coupling between pressure and velocity

The main problem when solving the Navier-Stokes equations is that the convective terms and the continuity equation are coupled, as velocity terms appear in all equations. Another complex issue is the pressure which appear in the momentum equation, but not in the continuity equation. If the pressure gradient is known, discretization is rather straight-forward and for compressible flow, the pressure may be obtained from density and temperature by using the equation of state $p = p(\rho, T)$. However, if the fluid is incompressible the density is constant and hence not linked to pressure. In this case coupling between velocity and pressure introduces a constraint in the solution, where correct pressure must be applied in order to receive velocities satisfying the continuity equation. To overcome this dilemma, different iterative solution algorithms are used where fluxes are evaluated from guessed initial values and iterated until convergence is achieved. The differences between left and right sides of the discretized momentum equations are called the momentum residuals and they are monitored as an indication of satisfying convergence progress. For pressure and velocity coupling, Fluent provides three segregated types of algorithms (SIMPLE, SIMPLEC and PISO) and a pressure-based coupled algorithm, called Coupled. The segregated solvers solve the governing equations sequentially, while the coupled algorithm solves a coupled system of equations (ANSYS Inc., 2014).

SIMPLE algorithm is essentially a guess-and-correct procedure and to initiate the calculation a pressure field p^* is guessed. Discretized momentum equations are solved to yield velocity components $u^*, v^*$and w^*. The next step is to define *correction terms* as the difference between the correct value and the guessed value according to: $p = p^* + p'$. This formulation is substituted into the momentum equations once again. Without going into details, the equations for the correction terms are simplified by neglecting a few terms, which is the main approximation of the SIMPLE algorithm. By solving this equation, the pressure correction field p' can be obtained and once it is known, a new value for the correct pressure and velocity can be computed. Generally, SIMPLE algorithm is relatively straight-forward and has been successfully implemented in numerous CFD procedures. A version of the SIMPLE algorithm is SIMPLEC which follows the same routine, but with the difference that the momentum equations are manipulated so that the velocity correction factors neglect terms that are less significant. SIMPLEC can produce computational savings due to improved convergence. Both methods are generally used for steady-state (time independent) calculations (ANSYS Inc., 2013).

The PISO algorithm is developed originally for non-iterative computation of unsteady compressible flows, but has been adopted successfully for iterative steady-state problems as well. PISO may be seen as an extension of SIMPLE that uses a second correction step for pressure and velocities. Since the PISO algorithm solves the pressure correction equation twice, the method requires additional storage capacity. Despite this, the method has been found to be efficient and fast. The non-iterative transient calculation procedure relies on the temporal accuracy gained by the discretization practice. With sufficiently small time step, the pressure and velocity field obtained at the end of the process is accurate enough to proceed to the next time step immediately. PISO algorithm is recommended for transient calculations and may also be useful for steady-state calculations on highly skewed meshes. The main advantage with PISO is that it can maintain a stable calculation with larger time step and under-relaxation factors for both momentum and pressure compared to other segregated schemes (ANSYS Inc., 2013).

While the segregated solvers solve the governing equations sequentially, the pressure-based *coupled* algorithm solves a coupled system of equations. The coupled scheme offers some advantages over the other algorithms and a higher degree of implicitness. It obtains a more robust and efficient single-phase implementation for steady-state flows. For transient flows the coupled algorithm is proved to be very useful when the quality of the mesh is poor or if large time steps are needed. The main disadvantage is that it requires more computational memory.

4.3.3 Under-relaxation

In the iterative process, fluid variables can be sensitive to divergence unless some under-relaxation factors are used. Many times, the correction term of a variable from previous iteration is too large for stable computations when the guessed value is far away from the final solution. To overcome this problem, under-relaxed factors for a variable $\emptyset$, can be introduced as:

$$\emptyset^{new} = \emptyset^{*} + \alpha_p \emptyset'$$

α_p is the under-relaxation factor and is ranging between 0 and 1. Assigning α_p a value between 0 and 1 will add a fraction of the correction field $\emptyset'$ that is large enough to move the iterative improvement process forward, but small enough to ensure stable computations. A correct choice of under-relaxation factors is essential for cost-effective simulations. Too large values may lead to oscillatory or even divergent solutions, while too small factors will cause extremely slow convergence. Unfortunately optimal values of under-relaxation factors are flow dependent and must be sought on a case-by-case basis.

4.3.4 Implicit and explicit solution

When evaluating terms in the discretized equations for unsteady flow, there must be an assumption about the variation of a certain property since the property is varying with time. One could choose to use property values at time *t* or at time $t + \Delta t$ to calculate the time integral, or alternatively a combination of the two. A weighting parameter α is introduced which takes a value between 0 and 1 to decide which property value to use in the equations. Below formula shows how the time integral can be discretized with the weighing parameter:

$$\int_t^{t+\Delta t} (\emptyset_P)\, dt = \left[\alpha \cdot \emptyset_P + (1-\alpha) \cdot \emptyset_P^0\right] \cdot \Delta t$$

$\emptyset_P^0$ refers to the initial value of the property at time *t*. If α is zero, only property values at old time level *t* is used and the resulting scheme is called explicit. In the explicit scheme the right hand side of the discretized equations only contains values at the old time step so that left hand side can be calculated by forward marching in time. The error accuracy is first-order with respect to time and there is a maximum limit to the time step size, which gives a serious limitation to the scheme. It becomes very expensive to improve spatial accuracy and the method is generally not recommended for general transient problems.

If α is 1, the property at the new time $t + \Delta t$ is used instead. If α equals 1 or is ranging between 0 and 1, the resulting scheme is called implicit. In the implicit method both sides of the discretized equations contain properties at the new time step and a system

of algebraic equations needs to be solved at each time level. If $\alpha < 1$ it is second-order accurate and if $\alpha = 1$ the implicit method is unconditionally stable for any size of time step. It is recommended for general purpose transient problems because of it robustness and with sufficiently small time steps it is possible to achieve considerably greater accuracy than the explicit method.

4.4 Open Channel Settings

4.4.1 Boundary conditions

If the flow is unsteady, there must be an initial condition or initial spatial distribution known for each variable. Thereafter, variables at each boundary enclosing the flow must be known. Below are the most common boundary conditions encountered in fluid flow analysis:

- Solid wall – no slip and no temperature jump between wall and fluid.
- Inlet or Outlet – variables known as a function of position.
- Symmetry – Normal velocities are set to zero.
- Free surface – Equality of vertical velocity across the interface of the liquid and gas. Also, pressure must balance at the interface except surface tension effects.

4.4.2 Numerical beach

In open-channel flows, it is desirable to suppress numerical reflection caused by an outlet boundary for passing waves. To avoid wave reflection, a dampening sink term is added in the momentum equation (ANSYS Inc., 2014). This can be done in Fluent by enabling Numerical Beach Treatment and selecting start point and end point for the damping region. Damping type allows the user to choose between two-dimensional and one-dimensional, where the former is damping treatment in the flow and gravity direction, while the latter is damping treatment in the flow direction solely. Linear damping resistance is defined as the resistance per unit time and quadratic damping resistance is the resistance per unit length. Numerical beach in Fluent uses linear damping in the gravity direction and quadratic damping in the propagating wave direction. Damping resistance should be chosen carefully as too much or too little damping could affect the wave profiles in a no-damping zone. It is recommended to use an increasingly coarse mesh in the damping zone to create extra numerical diffusion (ANSYS Inc., 2013).

4.4.3 Volume of Fluid (VOF)

To create a free surface in CFD programs, the domain must somehow be divided into two or more phases of a fluid. Fluent can model the effects of open-channel flow using a Volume of Fluid (VOF) formulation. These flows are generally characterized by the dimensionless Froude number and governed by the forces of gravity and inertia. VOF model treats different phases mathematically as interpenetrating continua and is a surface-tracking technique applied to a fixed Eulerian mesh. A function F(x,y,t) is introduced, with values between 0 and 1, to indicate fractional volume of a cell occupied by a certain phase of a fluid. It is designed for two or more immiscible fluids by solving a single set of momentum equations and tracking the volume fraction of each of the fluids throughout the domain (Hirt & Nichols, 1981).

4.5 Errors and uncertainties

CFD is used in design and development across a wide range of industries because of time savings in the design work and product improvement through enhanced understanding of the engineering problem. Though, the application of CFD modelling as an engineering tool can only be justified on the basis of its accuracy and the level of confidence in its results. Valid results are crucial as the consequences of inaccurate CFD results are at best wasted time and money, but in worst cases it can result in catastrophic failures of components, structures or machines. Errors and uncertainties are usually distinguished as:

- Error – a recognizable deficiency in a CFD model that is not caused by lack of knowledge.
    - Round-off error: the result computational representation of real numbers (a finite number of significant digits).
    - Iterative convergence error: time and the available resources of computing power dictate when the iteration sequence should be truncated, which generates residuals.
    - Discretization error: temporal and spatial derivatives of the flow variables (fluxes and rate of change) are approximated in the finite volume method on the chosen time and space mesh.
    - Coding errors: bugs in the software.
- Uncertainty – a potential deficiency in a CFD model that is caused by lack of knowledge.

Limited information about geometry, boundary conditions, material properties and physics give rise to uncertainties in the CFD model. Concerning domain geometry, it is impossible to replicate a product perfectly and tolerances in the design will lead to discrepancies. It can also be difficult to specify the boundary conditions and initial conditions for all flow variables to a high degree of accuracy. Simple assumptions, such as constant temperature and fluxes, are often made and some parameters are very hard to specify, e.g. turbulence parameters and surface roughness. Fluid properties (e.g. density and viscosity) depend more or less on the local value of flow parameters and are often assumed to be constant. Physical model uncertainty is discrepancies between real flows and CFD due to simplifying assumptions and inadequate representation of the physical processes. Common assumptions in fluid flow are steady-state, two-dimensional, incompressibility and the use of various turbulence models. Modelling of complex flow phenomenon involves semi-empirical sub-models that contain adjustable constants derived from high-quality measurements (c.f. the k-ε model in Section 4.2.1.2). When extrapolating beyond the range of these data it is assumed that the physics do not change much so the model still applies.

Since errors and uncertainties are unavoidable aspects of CFD modelling, it becomes necessary to develop methods to quantify the level of confidence in its results. In this context, it is common to distinguish between verification and validation of a model:

- Verification – the numerical solution is proved to be consistent with the theoretical basis of the method ("Solving the equations right"). This process quantifies the errors.
- Validation – the process of determining the degree to which the model is an accurate representation of the physical reality ("Solving the right equations"). This process quantifies the uncertainties.

5 Case study of two-dimensional slamming event

Working with CFD using ANSYS is a straight-forward and logical practice with pre-processing, calculation and post-processing cleverly unified through ANSYS Workbench. Workbench is a drag-and-drop project schematic, featuring other programs such as DesignModeler, Meshing, Fluent and CFD-Post. DesignModeler is a geometry handling software which provides powerful tools for creating and manipulating geometry files, meshing is a mesh generating program and Fluent is the CFD solver. Lastly, CFD Post is the post-processing program used for visualization and further analysis of the results. This chapter describes how the case study of the two-dimensional slamming event has been implemented into the CFD software. Recommendations for different settings come from (ANSYS Inc., 2014) and (ANSYS Inc., 2013) if not stated differently.

5.1 Simulation model

The geometry file for the simulations is created with the same dimensions as the small-scale model test done at NTNU's wave flume by Baarholm, cf. Section 3.1.1. Four different cases are studied with two different wave amplitudes and wave periods, respectively. The reason why these four cases are selected is that the deck clearance is kept constant, hence the same geometry can be used for all simulations and only parameter changes in Fluent are necessary. The platform deck is represented by a rectangular block with outer dimensions of 0.63 m x 0.30 m. The fluid domain is 2 m high and the water depth is 1 m. The domain of air is then deemed to be sufficiently large to contain the waves and the block, without having to generate too many cells. Prior to the final simulations, a mesh dependency and turbulence study were performed on a coarser mesh with water depth of 2 m to compare the results. There is no good reason for this other water depth, but the results are considered to be unaffected since the waves are in both cases in the deep water range.

The wave flume length of 13.5 m is kept for the fluid domain, with the deck positioned in the middle, mainly to avoid wave reflections at the outlet. Figure 5.1 shows the main dimensions of the 2D geometry.

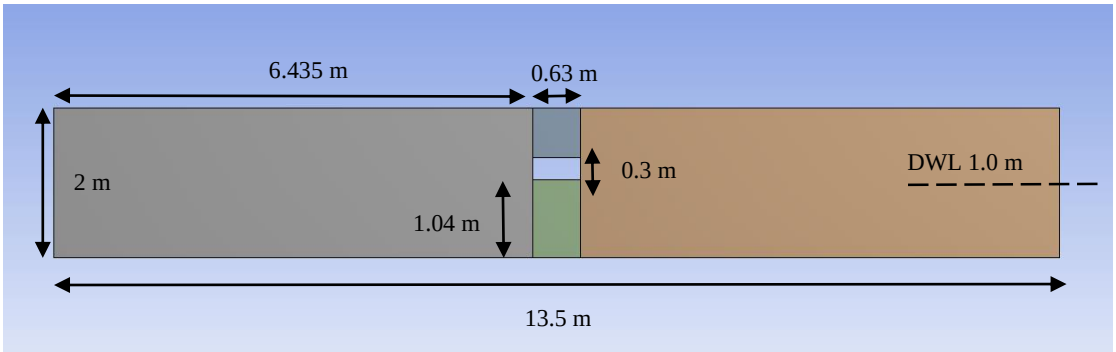

Figure 5.1 – Geometry file of the computational domain with dimensions.

5.2 Mesh

Before any computations can be done, a mesh has to be generated onto the specific geometry. In this case, it is the first step where the CFD engineer has the opportunity to influence the resolution and accuracy of the results. The meshing is performed using the automatic mesh tool in ANSYS Meshing, which features "face meshing" to create a controlled quadrilateral structured mesh by choosing element face size. In order to create a structured mesh the domain is divided into four rectangular blocks in DesignModeler, one block adjoining the west, north, east and south face of the platform deck respectively, see Figure 5.1. A quadrilateral mesh gives an easy geometric framework in which the position and slope of the water surface can be accurately described. On unstructured meshes, some kind of smearing of the surface is often necessary to describe the position of the free surface. This creates a 'spongy' surface, which will reduce peak pressures during impact (Veldman & Huijsmans, 2008).

In Fluent, a command called "Adapt – Region" is used to refine the mesh in critical areas. This feature splits selected quadrilateral elements into four new equally sized elements with "hanging nodes", which means the nodes are not connected to an adjacent cell and the node values are interpolated. As briefly mentioned before, a mesh dependency study was conducted where simulations were performed on two different meshes, a coarse mesh and a finer mesh computed on the Chalmers Beda cluster. The coarse mesh had an initial mesh edge size of 20 mm. The mesh was refined between 1.0 m and 2.5 m from the bottom, to an edge size of 10 mm and once again from 1.5 m to 2.2 m. Smallest mesh size was then 5 mm near the waterline and this refinement was done through the whole length of the domain. The higher resolution was made in order to maintain the shape of the propagating waves and to minimize numerical diffusion. Total number of elements were 532 428 and there were 535 537 computing nodes.

The finer mesh (from now on referred to as the Beda simulation) had an initial mesh edge size of 4 mm. The mesh was refined in a region near the waterline between 0.8 m and 1.1 m, to an edge size of 2 mm and once again underneath the deck between the block and the water surface (1.0 m to 1.04 m) to a size of 1 mm. The reason was to better describe turbulence effects and the boundary layer, by having the wall distance sufficiently small. Also, the measurement of the vertical lifting force and impact process could be captured more correctly. Based on the highest particle velocity in an undisturbed wave crest, y^+ would in this case be around 3. Because of water jets and other effects from a slamming wave, the fluid velocities could be higher and thus increasing the y^+ value. However, since a wall treatment is applied in Fluent, the wall distance is considered to be on the conservative side. Figure 5.2 displays the quadrilateral structured mesh from the Beda simulation. In the end, the mesh ended up with a total of 2 447 000 elements and 2 455 511 computing nodes in the entire domain.

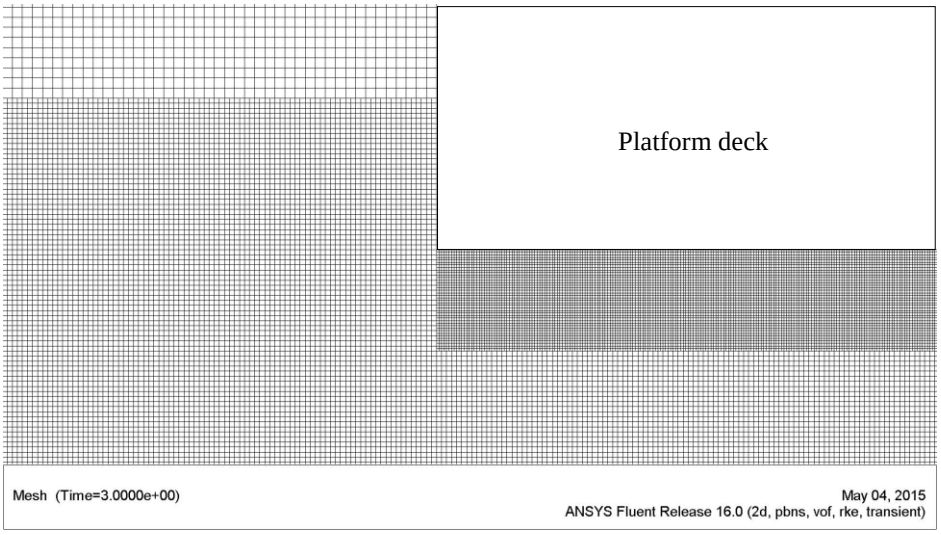

Figure 5.2 – Mesh refinement around the upstream corner of the platform for the Beda simulations.

5.3 Case setup

In this section, the major steps and settings for the 2D case are further elaborated and discussed, such as fluid properties, boundary conditions, initial conditions and discretization schemes. For a full detailed list of input parameters, see Appendix A and Appendix B.

Fluent is launched with a transient and pressure-based solver. Double precision is enabled, which is recommended for multi-phase flow. Volume fraction parameters are set to be implicit, with implicit body force formulation and interfacial anti-diffusion option activated. The default setting for open channel flow problems is implicit, which allows the usage of larger time step sizes. Gravity is activated in the negative y-direction.

A viscous model is adopted to describe the turbulence. *The realizable k-ε model* together with *Enhanced Wall Treatment* are chosen for this purpose.

5.3.1 Initial conditions

Two phases, air and water from the Fluent Database Library are used as materials for the simulation. In operating conditions, the operating density is set to the density of the lightest phase. This excludes the build-up of hydrostatic pressure within the lighter phase, improving the round-off accuracy for the momentum balance. It is also important to enter a reference pressure location, which is a location that corresponds to a region where the fluid will always be 100% of one of the phases. If this is not possible, it is recommended to select a region where the pressure value does not change much over time. This condition is essential for smooth and rapid convergence and will result in less round-off in the pressure calculation. The position should also be in a region that contains the least dense of phases, because variations in the static pressure are larger in a more dense fluid than in a less dense fluid, given the same velocity distribution. Thus, the reference pressure location is selected to be in the upper left corner of the domain, filled with air.

During the 2D slamming simulation, no numerical beach is activated. The reason is that the size of the domain, together with a relative short simulation time, ensure that no wave reflections from the outlet can influence the undisturbed waves near the block. A numerical beach would be superfluous in terms of computational effort.

5.3.2 Boundary conditions

The inlet boundary is chosen to be a velocity inlet, but since there is no current or wind influencing the deck, the averaged flow velocity magnitude is set to 0 m/s. When the flow enters the domain at an inlet, Fluent requires turbulence quantities to be specified. This can be done by assuming constants for turbulent intensity, viscosity ratio, length scale, hydraulic diameter or k and ε constants. In this project, values for both k and ε are set to 10^{-5}.

Wave theory for this simulation is chosen to be fifth order Stokes waves, with wave heights and wave length as the corresponding case from the reference experiment. In contrast to Airy waves, Stokes waves are nonlinear and often applied to finite amplitude waves in intermediate to deep water ranges, while Airy waves are linear and have small amplitudes. In order to see if the waves are in the deep water range or if any risk of wave breaking exists, it is common to check the wave steepness and relative depth. Wave steepness is defined as the ratio of wave height, H, to wave length, λ, and relative depth as the ratio of wave height to the water depth, d. Table 5.1 shows a few guideline values and ratios from this case. Table 5.1 concludes that almost all the waves propagating in this domain are in the deep water range. For case 5 and 6 the last criteria states that the simulations are performed in the intermediate depth regime, but these configurations were used anyway to fully replicate the experiments. No observations could be seen that this limit in water depth affected the waves. The air-gap level is fixed to 0.04 m, which is 6 m in full-scale. The wave heights are ranging between 15 m and 18 m, while the wave lengths are 288 m and 361.5 m in full-scale.

Case number:	Impact condition						
	T [s]	H [m]	λ [m]	d [m]	$[H/d]$	$[H/\lambda]$	$[d/\lambda]$
1	1,11	0,10	1,92	1,00	0,10	0,052	0,52
2	1,11	0,12	1,92	1,00	0,12	0,063	0,52
5	1,25	0,10	2,41	1,00	0,10	0,041	0,41
6	1,25	0,12	2,41	1,00	0,12	0,050	0,41
Deep water		$[H/d] < 0{,}55$		$[H/\lambda] < 0{,}1$		$[d/\lambda] > 0{,}5$	

Table 5.1 – Guideline values for deep water requirement.

The downstream boundary is specified as a pressure outlet with backflow direction "Normal to Boundary" and density interpolation method selected as "From Neighboring Cell". The density used in the hydrostatic profile is then interpolated using the volume fraction calculated from the neighboring cell. Fluent internally calculates the volume fraction values by using the neighboring cell values, so this is done automatically. On the outlet boundary, turbulence parameters and free surface level has

to be specified once again. The outlet can only be a single outflow boundary, i.e. splitting is not permitted in open channel flows.

The platform and the bottom of the domain is modelled as a wall with no-slip criterion, while the top boundary of the domain is chosen to be a symmetry boundary. The reason is to avoid an unnecessary boundary layer for the air.

5.3.3 Solver settings

As discretization scheme, second-order upwind scheme is used for momentum and turbulent kinetic energy and first-order upwind is used for the dissipation rate. Least square cell based scheme is the default choice in Fluent and selected as the gradient scheme. ANSYS recommends "PRESTO!" to be used for pressure interpolation in VOF multiphase simulations and the volume fraction to be "Compressive". The transient formulation is set to "First Order Implicit" since convergence problems occurred when this was changed to second order.

Even though ANSYS recommends PISO with non-iterative time advancement (NITA), Coupled scheme is used for the 2D simulation in this project. The reason behind this choice is that divergence in x-momentum seemed to occur more frequently with PISO than the Coupled scheme.

The simulation is initialized by "computing from Inlet boundary" and the Hybrid initialization method is used. The surface is set to be wavy, which creates fully developed waves throughout the domain as a starting condition, see Figure 5.3. Since the block is quite small compared to the waves, it can fit right between two wave crests. Performing the simulations in this way saves a lot of computational time and also ensures that no boundary reflections have time to interfere with the undisturbed waves near the deck. Since the simulation time is short, the risk of numerical diffusion affecting the wave profile is smaller.

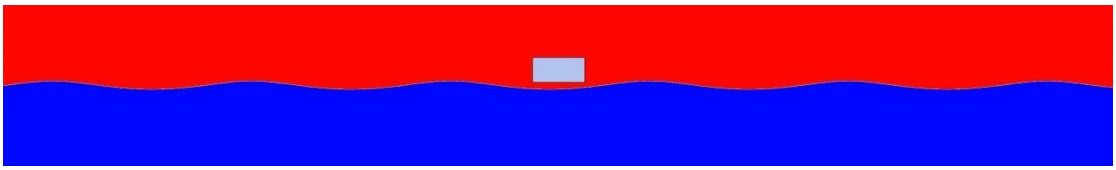

Figure 5.3 – Starting condition for the simulation.

The final step before starting the calculation is to specify the time step size, number of time steps and iterations per time step. For the four different 2D cases, the time step size is fixed to 0.001 s and the number of time steps set to 3000. Total simulation time then becomes 3.0 s which ensures that the entire impact event from the first wave is captured, but also with some safety margin afterwards.

6 Results from two-dimensional slamming event

The results from the simulations in Fluent are presented as contour plots over phases and velocities. The vertical lifting force is compared in graphs where the horizontal axis represent time step, but since each time step equals 0.001 seconds it can be interpreted as milliseconds. The graphs show the impact event from the first wave hitting the platform and the time has been truncated to fit the results from the empirical experiments. The vertical lifting force is given in Newton assuming a breadth of the platform of 0.56 m.

6.1 Effect of turbulence

Before final simulations were performed on the Chalmers Beda cluster, simulations with coarser mesh were executed with different turbulence settings. Figure 6.1 shows the result from case 1 with three different settings; inviscid, *k-ε* model with turbulence constants 10^{-5} and *k-ε* model with turbulence constants 10^{-1}. It can be noted that if the turbulence constants are extremely small, the lifting force curve obviously agrees very well with the inviscid model. However, in the water exit phase, the curve tends to go more towards experimental values, thus the negative force is maintained throughout the water exit. A mayor let-down was that when the turbulence constants (*k* and *ε*) are increased, the lifting force curve flattens out. Observations from animations demonstrated that this behavior was due to an extreme diffusion of the waves, where the wave amplitude decreased quickly. After the waves been travelling about a wave length's distance, the fluid domain was completely flat and the water surface undisturbed. No remedy for this effect was found, although performing more turbulence simulations on the Beda cluster with a finer mesh and smaller time step would be interesting. The *k-ε* model with constants 10^{-5} were used in all further simulations on the Beda cluster.

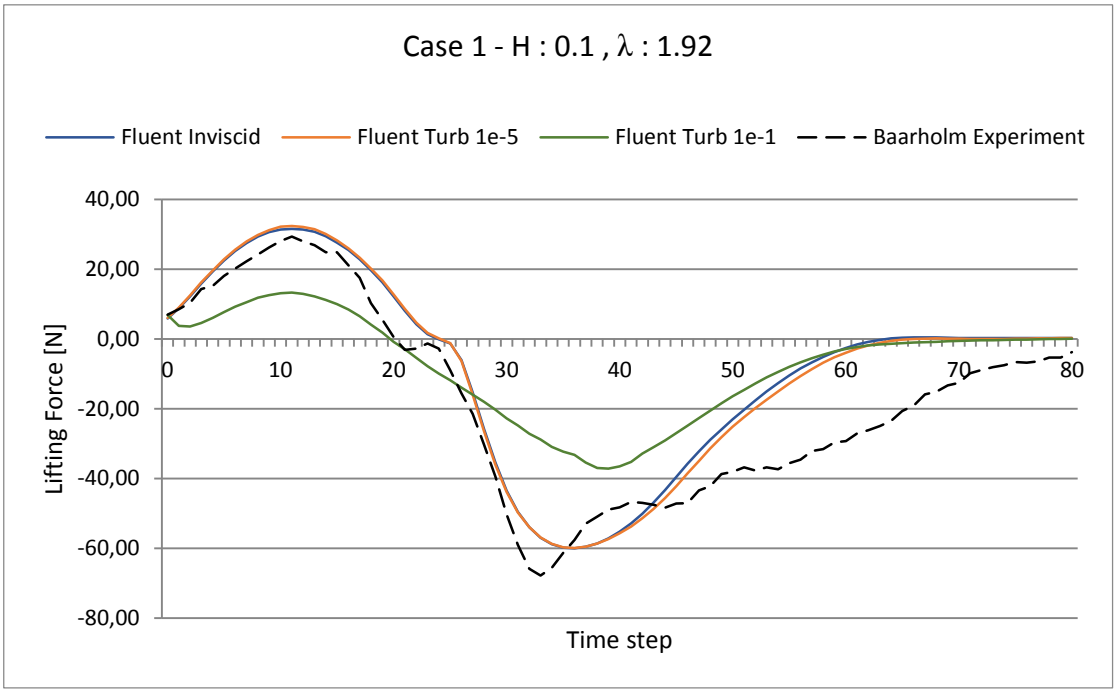

Figure 6.1 – Case 1. Effect of turbulence with different turbulence intensity constants.

6.2 Comparison of lifting force due to wave-in-deck loads

Figure 6.2 to Figure 6.5 show results for the four different cases. The black dashed line indicates the generated results from the empirical tests performed by Baarholm, the solid orange line represents the results from Fluent using a relatively coarse mesh and the solid blue line represents the results from Fluent using a higher resolution. The latter simulation was calculated on the Beda cluster on Chalmers with 48 cores. The coarser mesh had a larger time step (0.01 s instead of 0.001 s) and no turbulence model (inviscid). Previous chapter showed that applying a turbulence model with small turbulence constants on the coarse mesh only gave slight differences compared to the inviscid model. Since a turbulence study was not performed on all cases, the inviscid results are employed for the upcoming comparison.

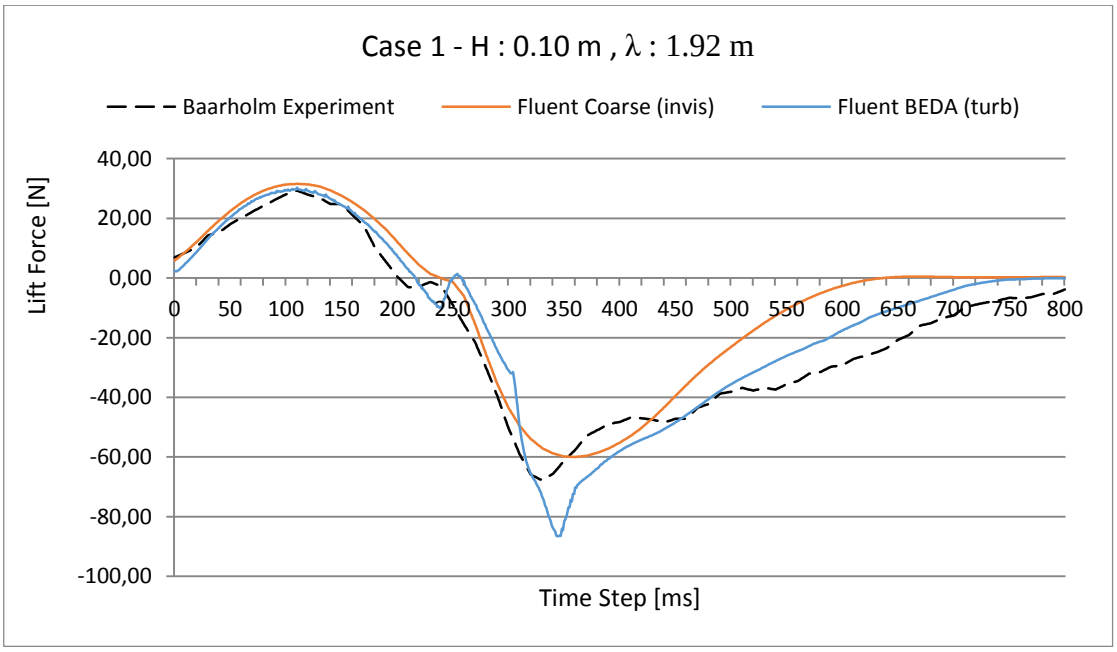

Figure 6.2 – Results from case 1. Wave height 0.10 m and wave length 1.92 m.

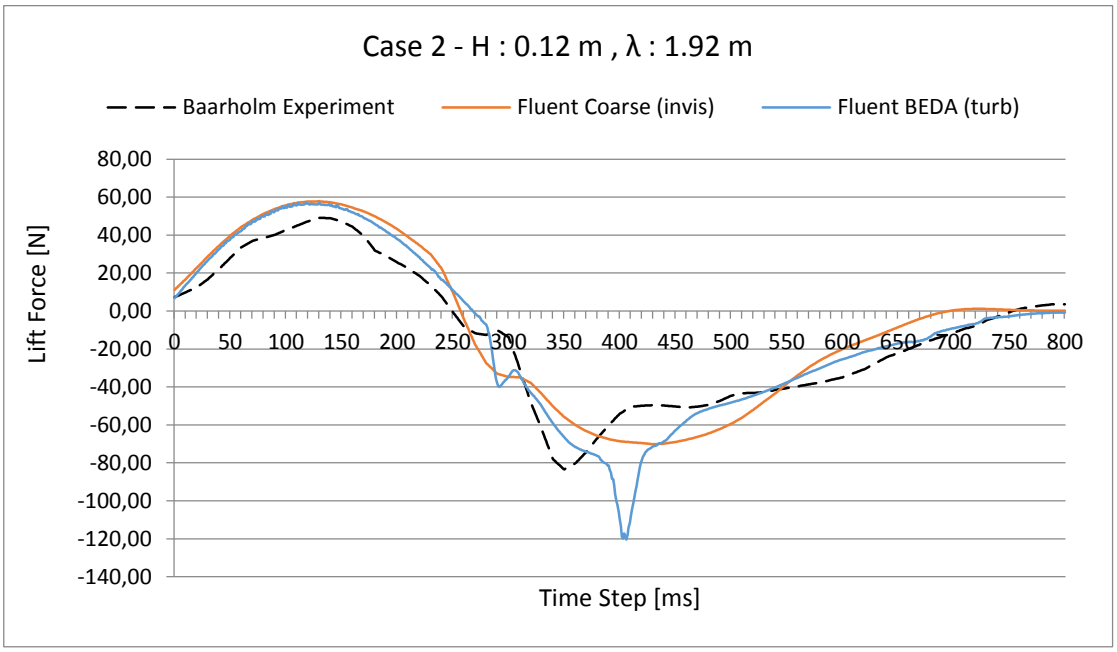

Figure 6.3 – Results from case 2. Wave height 0.12 m and wave length 1.92 m.

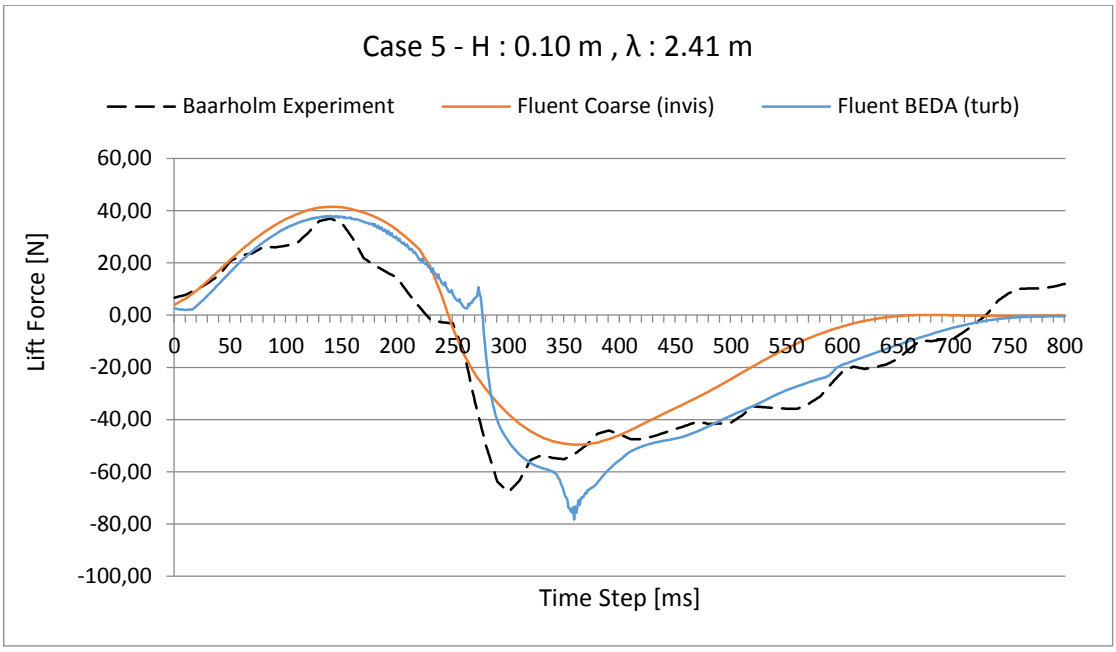

Figure 6.4 – Results from case 5. Wave height 0.10 m and wave length 2.41 m.

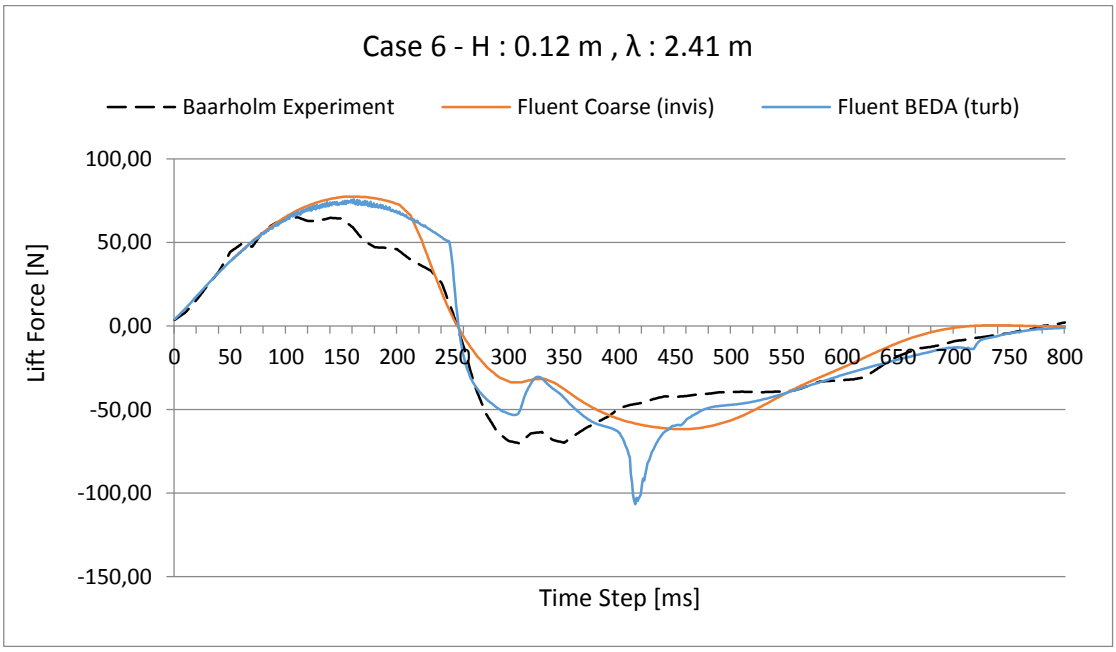

Figure 6.5 – Results from case 6. Wave height 0.12 m and wave length 2.41 m.

In case 1 and 2, where $T = 1.11$ s, wave entry phase (positive lifting force) is captured quite well for both the coarse and fine mesh, making resolution of the mesh and time step less important. The force magnitude in case 2 differs a bit compared to the empirical tests, but not significantly. When the force starts to become negative, the results from Beda seem to follow the empirical results better and details, such as the small force jump near the horizontal axis, is more accurately captured. Generally, the cluster simulations better describe small variations in the lifting force, even though the time instant were such effects occurs, may deviate a bit from the empirical tests.

During the water exit phase, it is clear that results from Beda are closer to the empirical results and maintain the negative added mass force during the water exit. Lifting forces

from coarser simulations tend to increase much faster to zero, which makes the impact duration for these simulations much smaller.

In case 5 and 6, where $T = 1.25$ s, the results from both simulations deviate more from the empirical results. Simulations seem to over predict the slamming force in the water entry phase and the time instant for the negative force peak is shifted to the right, i.e. occurs later. Beda simulations tend to conform better with the shape of the experimental test, compared to the coarse tests, but differences are larger than in case 1 and case 2.

Generally, the magnitude of the positive force peak is much larger for a larger wave height and a bit larger for an increased wave length as well. The negative force peak is harder to interpret since a very sudden and sharp force peak can be noticed in Beda simulations, but an increase in wave height seem to increase the magnitude of the negative force peak. On the contrary, a larger wave period decreases the absolute value of the negative force. Time duration between the force peaks appear to be larger for an increased wave height and as expected, a longer wave period gives a shorter duration since the wetting velocity increases. For all tests, the water exit phase is longer than the water entry phase and the magnitude of the negative force peak is larger than the positive lifting force. Above observations correspond fairly well to the conclusions done by Baarholm, see Chapter 3.1.3.

In all four Beda cases, a sharp and sudden negative peak can be noticed. The results from Baarholm do have similar tendency, but not as pronounced and significant. It appears this effect comes from some unphysical cause and therefore new simulations were performed in this region to see if some relationship could be seen based on the plots of volume fraction, velocity, pressure and turbulence. A theory was that the large negative force occurred when the water surface started to release from the upstream edge of the deck, but no such conclusions could be drawn from the second test.

Table 6.1 displays the maximum/minimum vertical force for both the experiments and the simulations as well as the percentage error. It can be noted that minimum force error is much larger than the maximum force prediction, which is mainly because of above mentioned unphysical "peak". However, it is interesting that the error is almost the same for a given wave amplitude for the maximum force. It can also be noticed that steeper waves generated larger errors.

	Maximum vertical force			Minimum vertical force		
No:	Experiment [N]	Simulation [N]	Error	Experiment [N]	Simulation [N]	Error
1	29.30	30.23	3.17 %	-67.80	-86.60	27.73 %
2	49.10	57.23	16.56 %	-83.50	-120.38	44.17 %
5	37.00	38.04	2.81 %	-67.80	-78,30	15.49 %
6	65.20	75.90	16.41 %	-70.20	-106.64	51.91 %

Table 6.1 – Maximum and minimum force comparison for the experiment and the simulation.

6.3 Time series of impact event

In this section, figures showing VOF distribution (the different phases) and velocity plots occurring from four different time instants are presented. The first time instant is when the maximum force peak is present. In this instant, the slamming pressure is at its maximum and since the wetted area is relatively small, the platform experiences the highest peak pressures locally. The second time instant is when the lifting force changes sign and goes from being positive to become negative. Now, the slamming force from the wave cease to influence the deck and therefore only the incident wave force and negative added mass force is present. Figures in the third time event show properties during the negative force peak. Lastly, the fourth time instant represents the time when the incident wave releases from the deck and the impact load heads towards zero once again. In order to be consistent, all figures are taken from case 5. The figures are named after the current time step they originate from, e.g. TS 520. These can be interpreted as milliseconds from the start of the simulation, but notice that this time is not the same as in above plots since they are truncated. Every 10^{th} time step was extracted from the simulation, which is why the lifting force does not coincide with the actual maximum and minimum values. The velocity plots show vectors in the direction of the flow and both its size and color are dependent on the velocity magnitude.

6.3.1 Maximum lifting force

When a regular propagating wave hits the deck it experiences a positive lifting force during the initial water entry phase dominated by slamming forces. As can be seen in Figure 6.6, the time instant when the maximum force peak occurs is when about half the deck's length is wetted. A pile-up of water is formed at the front end of the platform and at the downstream deck/water intersection, there is relatively low curvature. The velocity plot, Figure 6.7, shows high upward velocities where the water has not reached the deck yet and velocities near the upstream edge have started to become negative. The actual maximum force peak occurs at TS 518 and the lifting force is then 38.06 N.

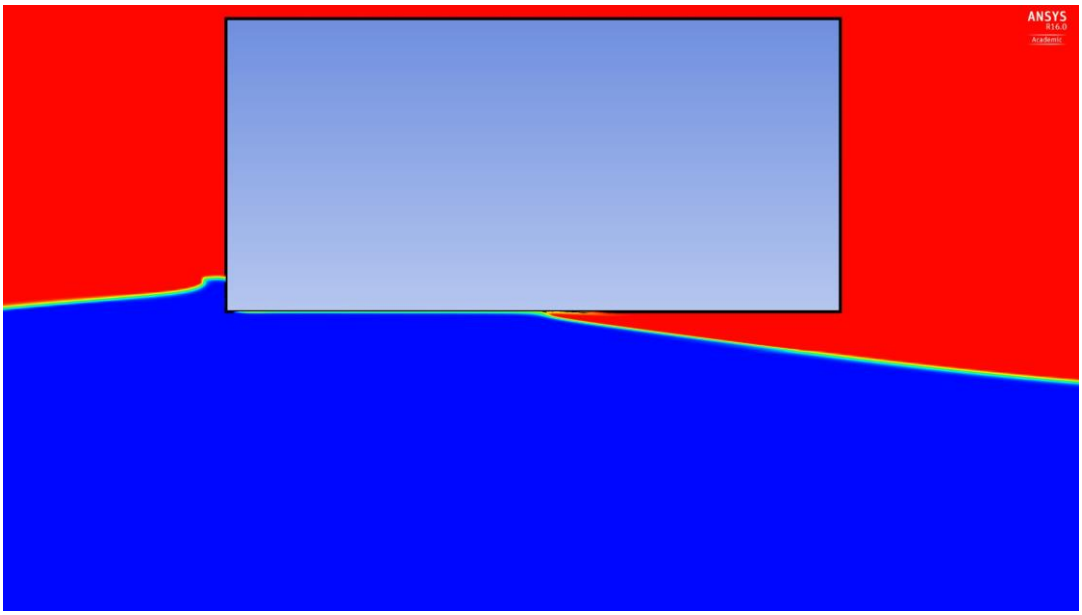

Figure 6.6 – VOF plot TS 520. 37.74 N.

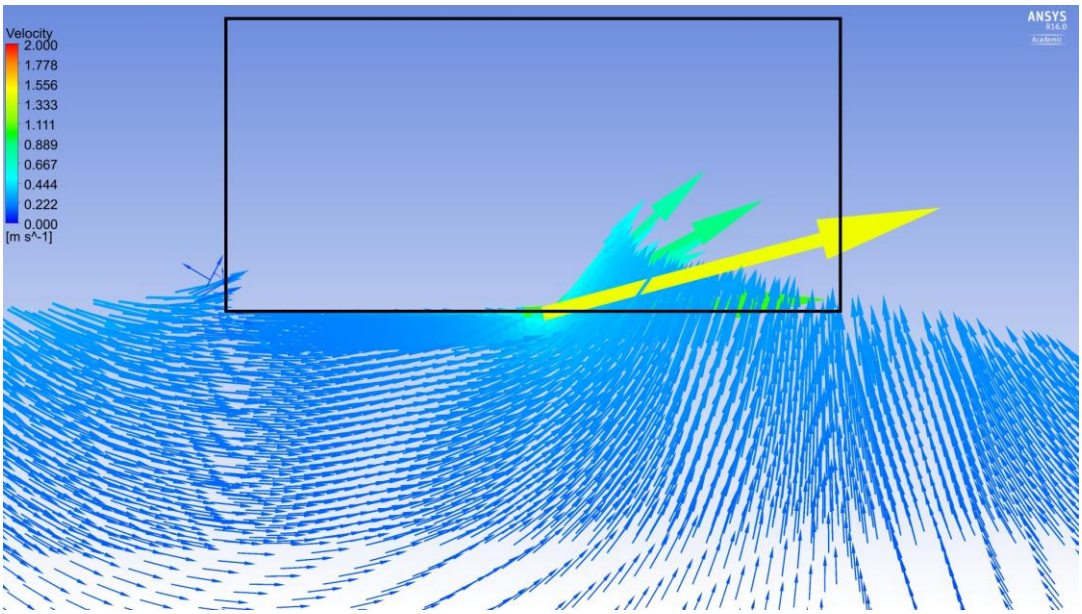

Figure 6.7 – Velocity plot TS 520. 37.74 N.

6.3.2 Lifting force is zero

At this time instant, the slamming force ceases to exist and the negative added mass force and incident wave force act solely on the platform, hence the lifting force decreases and starts to become negative (Baarholm, 2001). The actual time step for this occurrence is TS 655 and from Figure 6.8, a relationship can be noticed here. At this time, the water has just reached the downstream corner of the block and later starts to leave the corner tangentially in a jet. In figures from Appendix C one can also note that the uppermost point of the wave crest starts reaching the middle of the deck. At the upstream edge the water has now started to be sucked under the left corner. Here, the no-slip criterion of the plate can be seen clearly. The velocity plot, Figure 6.9, shows high downward velocities near the upstream edge and positive vertical velocities after the downstream edge, not influencing the platform substantially. Right underneath the platform the velocities are parallel with the propagating direction. Note that below plots are from TS 660 and the lifting force is -23.35 and not zero. This means that for each millisecond, the force decreases extremely fast. Especially compared to time series around the maximum peak where the time derivative of the force is much lower.

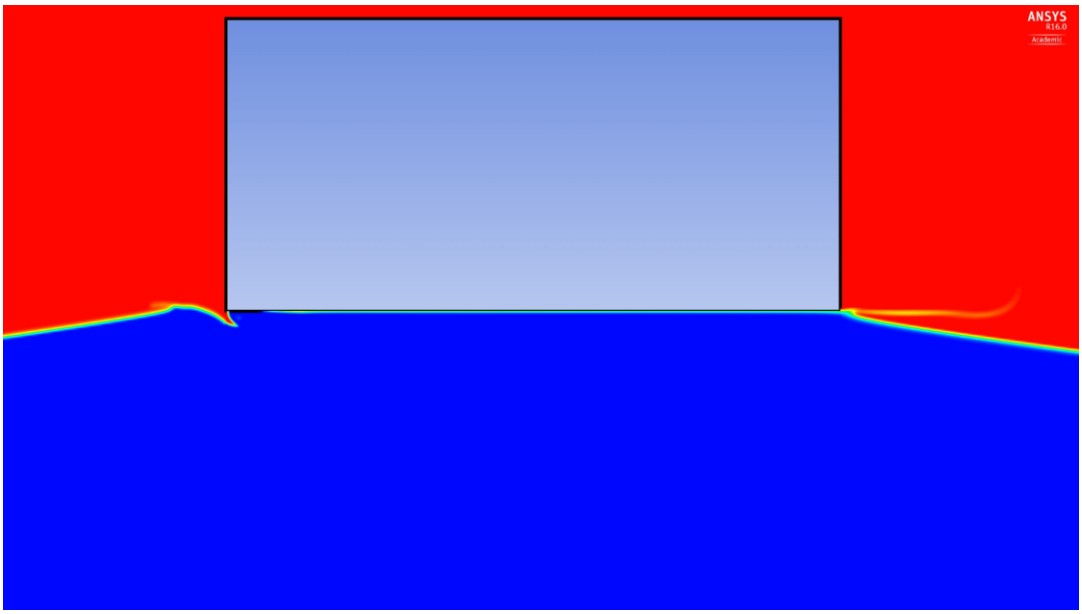

Figure 6.8 – VOF plot TS 660. -23.35 N.

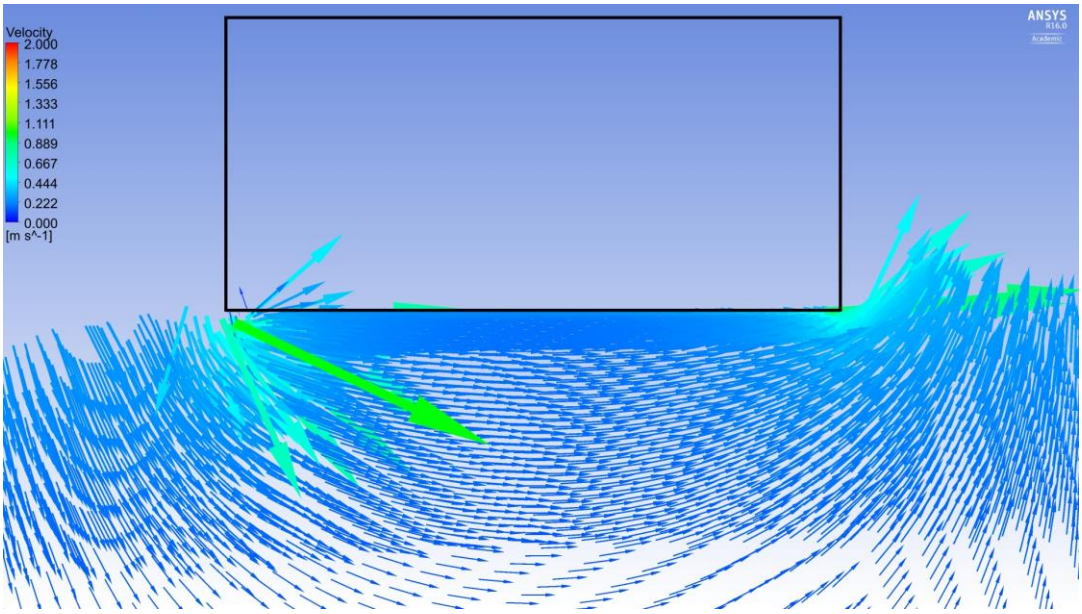

Figure 6.9 – Velocity plot TS 660. -23.35 N.

6.3.3 Negative force peak

According to the conclusions from Baarholm's experimental study, see Chapter 3.1.3, the negative force peak occurs when the wetting of the deck is at its maximum. However, in these simulations it can be seen that this has already happened, Figure 6.10. The uppermost point of the wave crest is around the latter quarter of the deck and the velocity plot, Figure 6.11, shows large negative velocities near the upstream corner. The water starts to release from the upstream edge and a whirl starts to develop. The minimum force peak occurs because the negative added mass term has its peak here. The actual time step is TS 737 and the negative force peak -78.3 N.

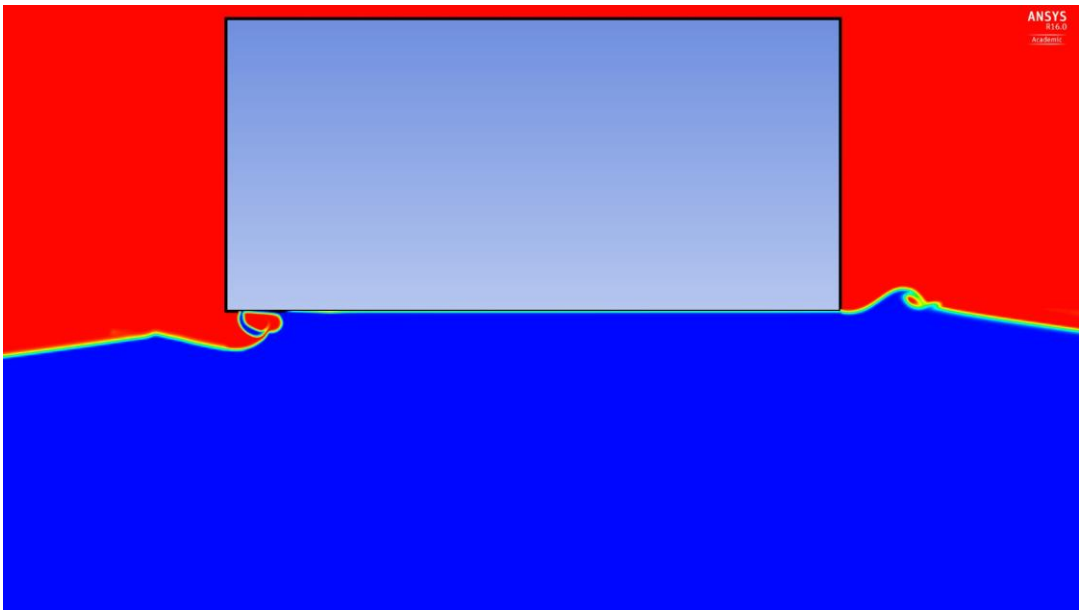

Figure 6.10 - VOF plot TS 740. -73.56 N.

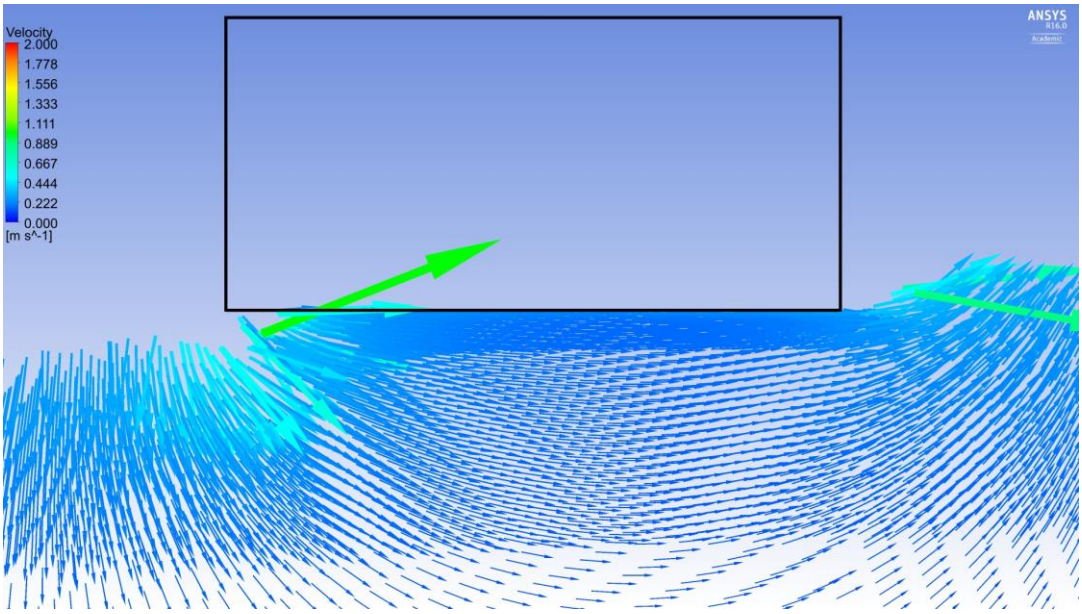

Figure 6.11 – Velocity plot TS 740. -73.56 N.

6.3.4 Lifting force is zero – after wave impact

Figure 6.12 shows the VOF plot right before the wave leaves the deck and the lifting force goes back to zero. The downstream water/body intersection has moved upstream and the water is released from the deck about a distance of $1/3$ from the downstream corner. In this project, no results from the second wave impact were analyzed, but it was observed that this last thread of water releasing from the deck was actually important. When the second wave reaches the deck, it interferes with this "water thread" and it is spurted back again causing an extremely high local peak pressure.

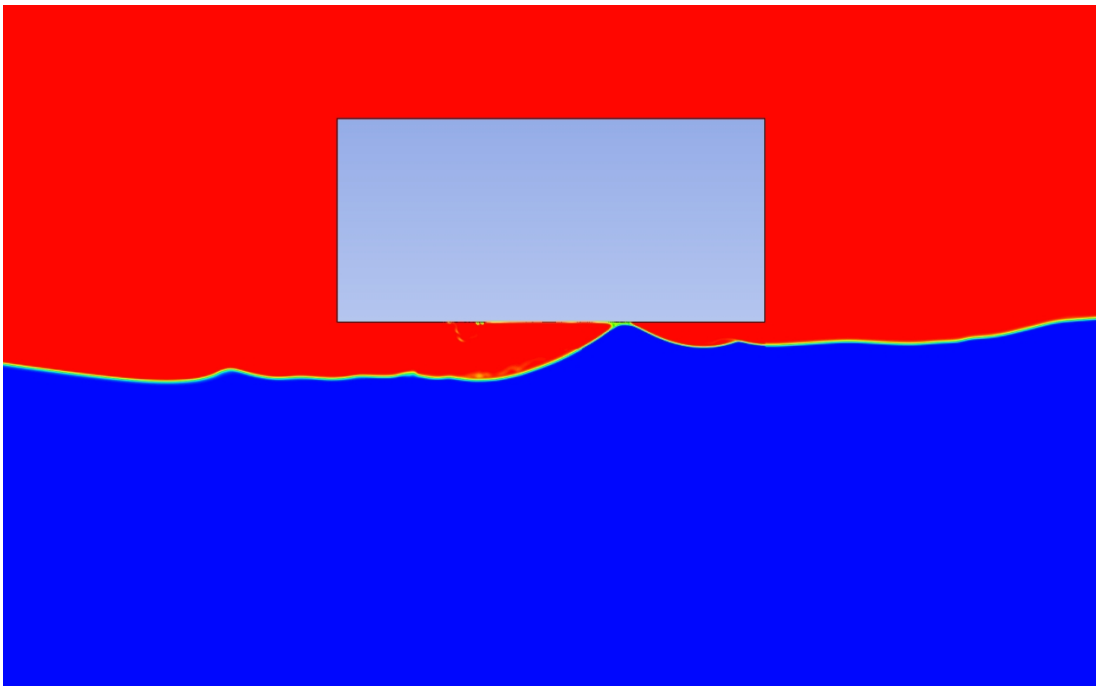

Figure 6.12 – VOF plot TS 1150. -0.56 N.

7 Three-dimensional wave run-up event

So far, the objective of this thesis has been to investigate the use of CFD for estimating wave-in-deck loads in a simplified situation where a two-dimensional deck is modelled. However, as an illustrative example to further explore and demonstrate the possibilities of the CFD software, a three-dimensional platform is also modelled. In this case, wave run-up is observed and pressure impulses around the columns of the platform are estimated and compared against experimental values. Wave run-up is of great interest where the water can reach the main deck and cause high pressure impacts. It can cause severe damages to local structural members and other necessary equipment near the columns. The difficulty with such experiments is that the impact pressures are very dependent on where the measurement sensors are placed. Generally, the pressure decreases as the distance from the columns increases and for a three-dimensional simulation, wave diffraction and reflections interfere with incoming waves. Thus the result is highly dependent on the situation and can differ a lot locally.

It should be stressed that pending three-dimensional study is not very accurate and should more or less be looked upon as an inspiration for further development.

7.1 Experimental set-up

The three-dimensional object studied in this part is the GVA 33000 semi-submersible production unit, designated for the two fields Jack and St. Malo in the Gulf of Mexico (Thor, 2010). The unit is permanently moored using a 16 line chain-polyester-chain system and intended for use in ultra-deep water (deeper than 1,500 m) and severe environmental conditions. The hull consists of a ring pontoon with four columns, supporting a boxlike upper structure, see Figure 7.2. It was commissioned in 2013 and in November 2009 a model in scale 1:60 was tested in the MARINTEK ocean basin in Trondheim. In both the reference report and in this study, all values are presented as full-scale. Several tests were executed which included slamming pressures, global and local motions, accelerations, air-gap performance and riser porch velocities for a wide variety of extreme environmental conditions. In this study, only the slamming pressures from five panels near the aft columns are considered where waves have been applied as the only load (no wind and current).

All model tests were performed in the most severe conditions with respect to platform motions, thus all environmental conditions are applied at a specific heading. The waves had a heading 13 degrees and the test was carried out during a 3 hour event with irregular waves. Waves were modelled with a JONSWAP spectrum with $T_p = 14.76$ s, $H_s = 15.47$ m and $\gamma = 2.6$. Below are the main dimensions of the platform. Due to physical limitations of the water tank, it was not possible to scale the full depth:

- Length: 99.88 m
- Breadth: 104.16 m
- Depth: 69.51 m
- Draught: 41 m
- Air gap: 19 m
- Design water depth: 2 133 m
- Model test water depth: 360 m

It is not very convenient to model a JONSWAP spectra in Fluent, since obtaining reliable results would require an extremely long simulation. Since the pressure impulses are compared against the maximum values from the test, it was decided to only model one regular wave in Fluent, based on the most probable maximum wave height encountered during 1000 waves (about 4 hours), according to below formula:

$$H_{max} = H_s\sqrt{\frac{1}{2}\cdot \ln(1000)}$$

The wave height then becomes 28.75 m (the wave length of 340.14 m is kept).

Three pressure panels are located underneath the deck, right in front of the aft SB column. The panels have a distance of 5, 10, 15 m away from the column respectively. The last two panels are placed with an angle of about 45^0 towards the centreline, with approximately 5 m in between. Figure 7.1 shows the coordinates of the panels. Origin is placed in the middle of the platform at the free water surface and x-direction is positive against the wave heading and y-direction towards port.

Panel no:	x [m]	y [m]	z [m]
8	-31.2	-24.7	19.0
9	-27.9	-21.1	19.0
11	-23.4	-40.5	19.0
12	-18.4	-40.5	19.0
13	-13.5	-40.5	19.0

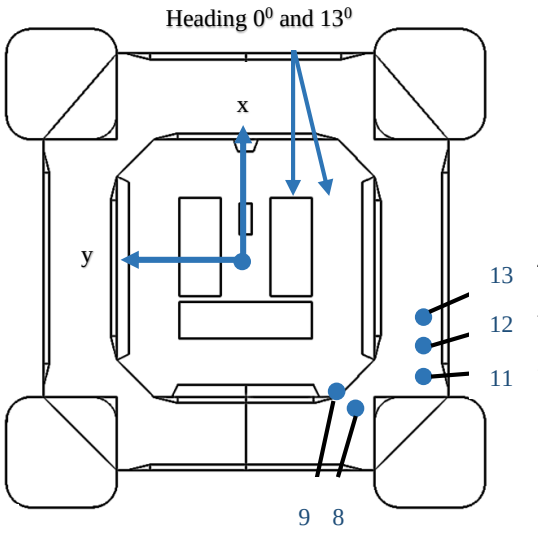

Figure 7.1 – Location and coordinates of pressure panels.

7.2 Simulation model

First step in the numerical study was to open the three-dimensional geometry in ANSYS DesignModeler and clean the model from unnecessary parts. Before continuing with meshing small equipment and piping had to be removed to make the model easier to handle. The finished geometry can be seen in Figure 7.2.

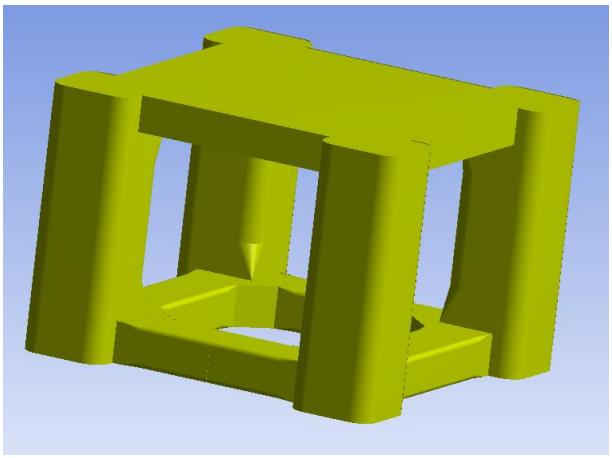

Figure 7.2 – CAD model of the GVA 33000 production semi-submersible unit.

The size of the surrounding domain had to be specified as well. A feature called "Enclosure" was used to split the platform in half to create a symmetry boundary and generate a box enclosing the platform. The enclosing volume had a distance of 10 m to the platform's sides. This feature also removed the geometry and left a space for a surface mesh. The enclosed platform can be seen in Figure 7.3.

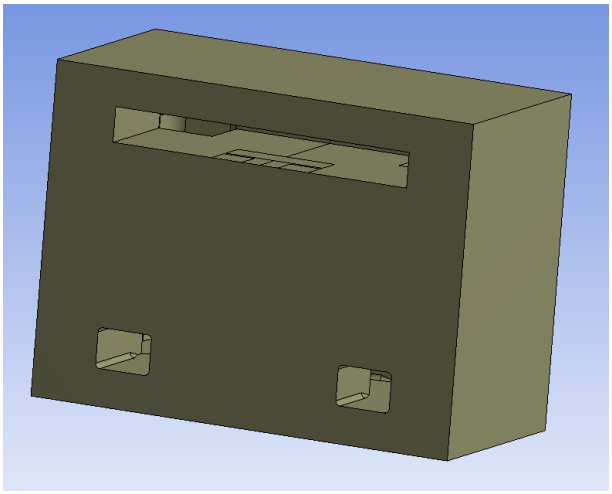

Figure 7.3 – Enclosing volume around half of the platform across the symmetry line.

To create a larger domain with a structured mesh, the domain was extended to a reasonable size. To be able to specify mesh sizing in different regions, it was favourable to divide the domain into 12 blocks, see Figure 7.4. Since wave length was specified to 340.14 m it was decided to have the domain as 400 m upstream, 150 m downstream, 150 m deep and 100 m to the side of the platform. This was actually a very small domain with these wave settings, but this domain was chosen to keep the amount of mesh cells reasonably low. Possibility of wave reflections at the outlet boundary was high, but since only the first wave impact was considered, the domain was believed to be sufficiently large. The simulation was initialized in a wavy condition, so a reflected wave would not have enough time to influence the waves near the columns.

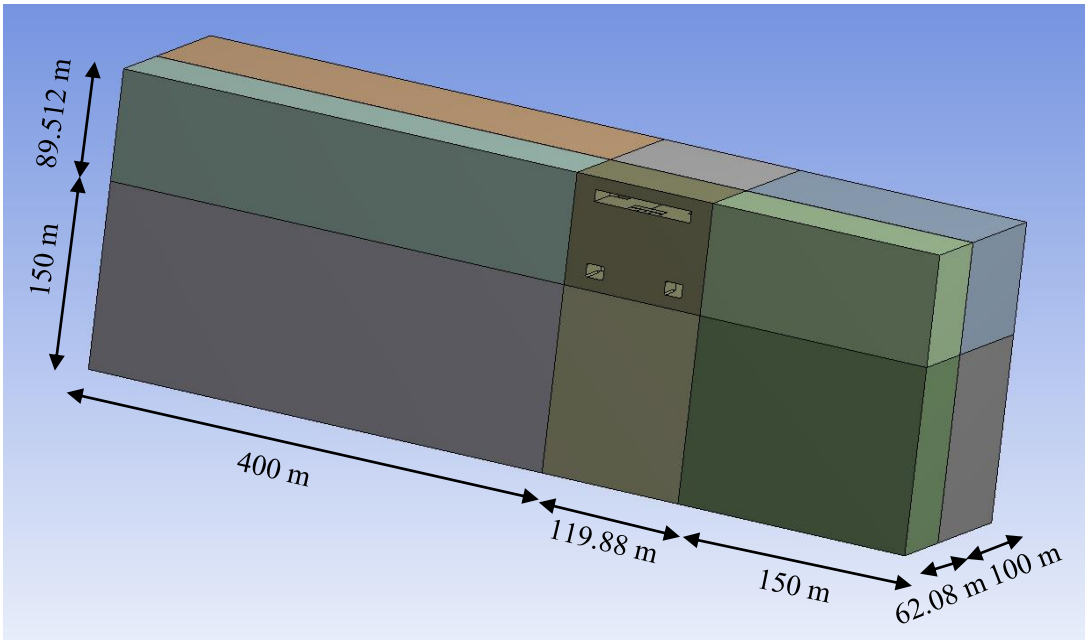

Figure 7.4 – Domain of the three-dimensional study with dimensions.

A structured mesh was generated in all 11 boxes that is adjacent to the enclosing box. In this box, a mesh consisting of tetrahedrons was used. 15 m above and under the still waterline (the wave height was 28.75 m) the mesh was refined. The cell size in this refined region was specified to 0.6 m, in order to have the same number of cells per wave height as the two-dimensional case (approximately 50 cells/wave height). This refinement was done throughout the entire width of the domain. Downstream of the platform the mesh size was increased to numerically dissipate the waves and decrease the number of computing cells. Also towards the side and bottom of the domain the mesh was smoothly increased to make the mesh more efficient. Upstream of the platform the mesh was kept quite detailed to not harm any incoming waves. The final mesh ended up with 16 864 006 elements and 8 974 683 nodes, most of them in the tetrahedrons region to obtain better and more accurate results. The side view of the mesh can be seen in Figure 7.5.

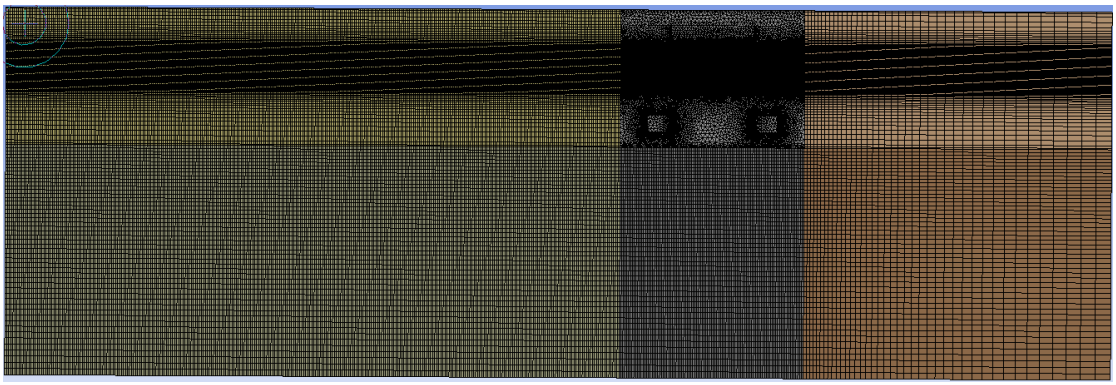

Figure 7.5 – Side view of the mesh.

Case setup and solver settings in Fluent were basically the same as in the two-dimensional case. Obviously the size of the incoming waves was changed to a wave length of 340.14 m and a wave height of 28.75 m. The time step size was specified to 0,005 s and the simulation had 6000 time steps, creating a simulation of total 30 s. The

platform was fixed in space and the simulation was started in a wavy condition to minimize reflections and decrease the simulation time. No numerical beach was activated and no wave heading was specified, since this would cause problems with the symmetry boundary. Five different pressure points were defined to represent slamming panel 5 to 9 in the model test. The simulation was calculated with pressure-velocity coupling as Coupled. Actually, PISO with the NITA (non-iterative-time-advancement) option was used first. However, divergence was detected in x-momentum and the simulation was restarted, using Coupled.

7.3 Sources of error

During the model test, irregular waves were produced from a JONSWAP wave spectrum during three hours. In the simulation the most probable maximum wave height encountered during 1000 waves was used to describe one equivalent wave. Of course there is no guarantees this equivalent wave is similar in amplitude nor period.

To save computational time and make the simulation easier, it was decided to use a symmetry through the platform's centreline. In the model test, waves had a heading of 13^0 but this was not possible in the simulation without considering the entire domain due to asymmetry. Another assumption which greatly affects the quality of the simulation is that the platform was fixed during the CFD simulation, while in the experiments the platform was moored with motions in six degrees of freedom. Performing simulations with a moving platform would require information about weights, moments of inertia and motion characteristics. It would also require more CPU time which was a limiting factor in this project. Since the air-gap and inclination of the platform would vary, the mesh needed also to be dynamic and motion characteristics must be specified in a UDF.

The domain in the simulation was also too small for such long waves. Unfortunately, the number of elements (16 864 006) was precisely what the computer could manage to prepare the case, before sending it to the Beda cluster. The domain could therefore not be increased.

Another source of error was that the empirical test was made with a 1:60 model of the platform, but the generated results were scaled to full size using Froude's law of scaling. Scaling always produces uncertainties in the results and optimal would be to simulate the small-scale model instead.

The location of the pressure points in the simulation were placed at the same location as the pressure panels in the model tests. Since no heading was used the relative angle against the incoming waves were not the same.

7.4 Results from the wave run-up event

The visual results from the VOF plots look satisfactory. The simulation starts with a wave crest near the upstream edge of the platform and continues until the second wave trough is right underneath the platform, see Appendix D. Wave run-up can be noticed on all four columns and when the second wave reaches the platform, diffraction and reflection effects is clearly visible and influences the second wave.

The maximum positive pressure occurs when the wave crest is just underneath the platform's centre, see Figure 7.6. Time instant for this occurrence is 16 s.

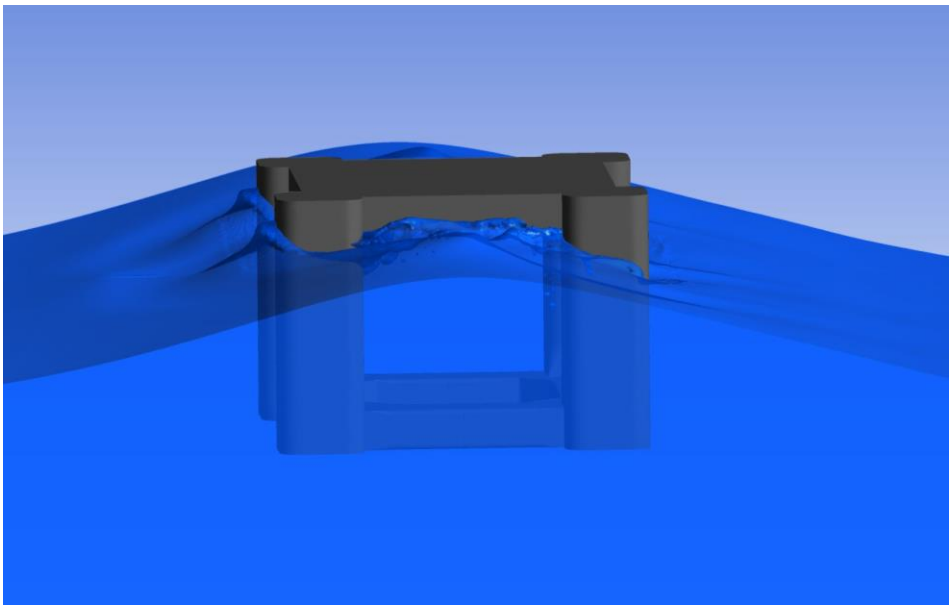

Figure 7.6 – VOF plot for the highest peak pressures.

Table 7.1 compares the measured maximum pressures from both the CFD simulation and the model test. As can be seen, the results differ extensively with an error factor between 0.8 and 3.79. These results are not particularly satisfying, but as mentioned earlier there are a lot of error sources. However, some conclusions can be made. Since the jet mainly shoots along the deck, vertical pressures on deck are likely to decrease rapidly away from the column, which can be seen from panel 11 – 13. They are directed towards the incoming wave with a spacing of 5 m in between. The same behaviour can be noticed on Panel 8 and 9, where Panel 9 is further away from the column. At least the CFD simulation shows this behaviour, but unfortunately not the model test. It can also be noticed that the pressure decreases non-linearly away from the columns.

Panel no:	Pressure [kPa] (Beda)	Pressure [kPa] (model test)	Difference (factor)
8	877.4	706	0.80
9	640.5	972	1.52
11	1 554.5	5 897	3.79
12	608.3	1 877	3.09
13	351.9	1 321	3.75

Table 7.1 – Comparison of maximum pressures on the three-dimensional object.

In Figure 7.7 – 7.9 the pressure signals from the 3 hour long model test are displayed. As can be seen, only a few of the generated waves from the spectrum have an amplitude large enough to cause wave run-up and impact the underside of the deck. Notice that the largest impact takes place at the same time, or for the same wave, for panel 9, 11, 12 and 13. For panel 8 the maximum pressure occurs earlier. Figure 7.9 b, shows the pressure signal on panel 9 in the region around the most severe impact. The horizontal axis is adjusted to show the time corresponding to one wave length, with the pressure peak in the middle. It can also be noticed that noise exists in the data.

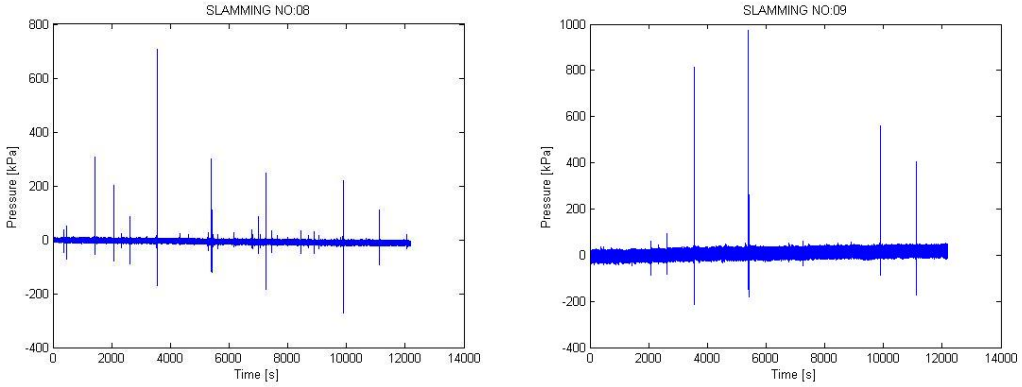

Figure 7.7 – Experimental pressure signal on Panel 8 and Panel 9.

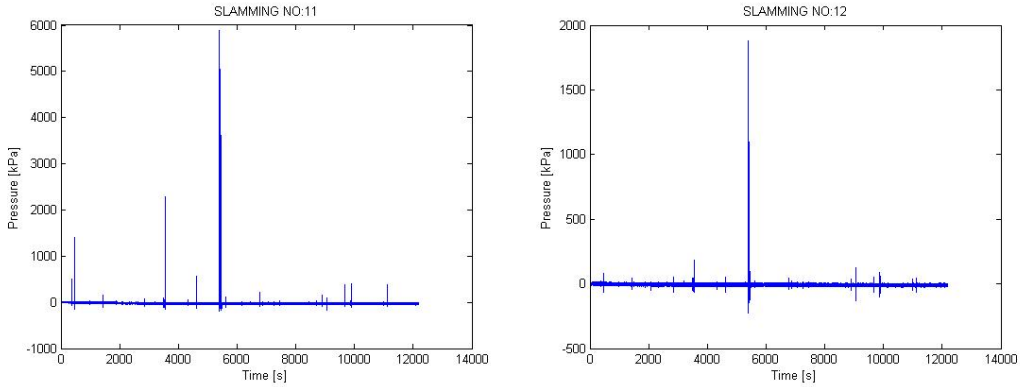

Figure 7.8 - Experimental pressure signal on Panel 11 and Panel 12.

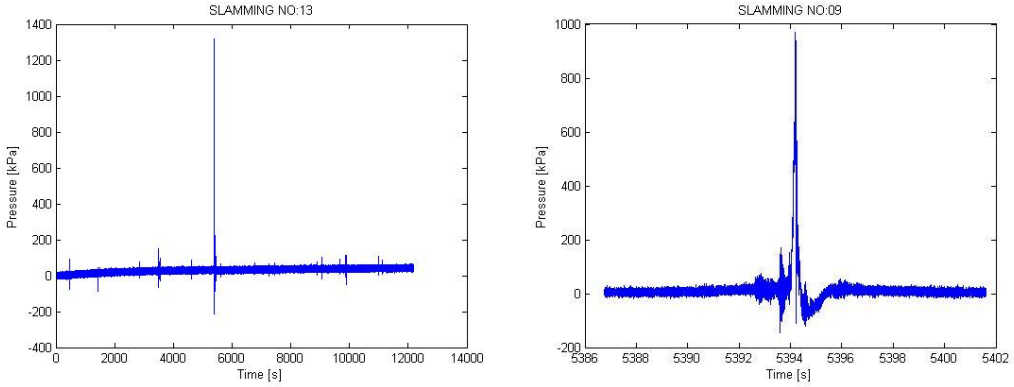

Figure 7.9 – Experimental pressure signal on Panel 13. The right picture shows the pressure impulse from the highest peak of Panel 9. It is zoomed to show the time corresponding to one wave length.

8 Conclusions

The objective of this thesis has been to investigate the use of CFD for estimating wave-in-deck loads in simplified situations. Two-dimensional regular waves have been used to model a wave impact event on a rigid horizontal deck with fixed air-gap. A three-dimensional case has also been simulated to study the outcome of a more complex situation. The results from the simulations have been verified against reference experiments in order to assess the CFD working procedure. To fulfil such analysis, the total vertical force acting on the platform deck has been designated as the evaluation criteria in the two-dimensional case. In the three-dimensional case the pressures at a certain number of panels have been considered. Using this method of analysis, a study was conducted with the aim of learning more about the physics behind wave impact loads and the possibilities of the CFD software.

In addressing the objective of the thesis, a CFD methodology is proposed. The work of this thesis has illustrated the complex nature of wave impact events and shown that, if executed correctly, CFD simulations can be a useful tool for such assessments. Modelling of two-dimensional regular waves can provide good results that correlates to test data. Simulation results in this project agree very well with the empirical test data used as reference and especially case 1 shows very satisfying results. On the other hand, this case had the smallest wave amplitude and wave length, thus it was the calmest condition. Performing a three-dimensional case turned out to be more complex. The results do not correlate as good as in the two-dimensional study and due to the many error sources it is hard to draw any general conclusions.

Key properties of an impact event have been presented. Initially, the structure experiences a positive slamming dominated lifting force during the water entry phase, followed by a negative force during the water exit phase. The force in the latter phase is dominated by negative added mass due to negative fluid particle accelerations. Its magnitude is larger than the positive force peak in all tested two-dimensional cases. The water exit phase has a duration longer than if the wave would have propagated undisturbed and longer than the water entry phase. The water seems to "stick" to the bottom plate, which results in a wave profile with much higher curvature close to the body. When the minimum force peak occurs almost the whole deck is wetted, while half of the deck is wetted for the maximum force peak. Hence, the water exit phase is important for global structural effects and the water entry phase is more critical for local structural responses due to the highest average pressures. The lifting force magnitude is highly dependent on wave amplitude and wave period. For the three-dimensional case the total vertical force has not been considered since no experimental data was provided.

Conclusions drawn from the study are that quality of the mesh and time step size clearly influence the results. For the two-dimensional study, two parallel studies were compared; one with coarse mesh and larger time step and another with much finer resolution, referred as the Beda simulation. Best results were obtained when the time step was at least 0.001 s. Since the highest wave celerity among the tests was 1.952 m/s, it means that in the Beda simulation the flow travel almost one element length per time step in a region near the water surface. It should be noted that using smaller time steps cause longer runtime for the simulations. If data is collected frequently, the storage capacity might be a limiting factor.

The coarse mesh had a mesh size of 5 mm near the waterline and with this configuration, a small noticeable numerical diffusion occurred after a while. The waves lost their

amplitude, but since the simulations were performed in a wavy start condition and only the first impact was of interest, this numerical diffusion was negligible for the first wave. For the smallest wave (case 1) this corresponded to 20 elements per wave height and 384 elements per wave length.

Best results were obtained in the Beda simulations, where the mesh had an edge size of 2 mm near the waterline. With this configuration no numerical diffusion was noticed. For the smallest wave, number of elements was 50 per wave height and 960 elements per wave length.

During the study, difficulties arose when modelling turbulence. When turbulence intensity constants (k and ε) were increased, the wave amplitude flattened out due to numerical diffusion. No remedy for this effect was found, but if the turbulence constants are set to be extremely small, the solution coincides with the inviscid solution in the water entry phase, while in the water exit phase the curve tends to go more towards experimental values.

Generally, the magnitude of the positive force peak increases as the wave height and wave length increases. The negative force peak is harder to interpret since a very sudden and sharp force peak can be noticed in the CFD simulations. An increase in wave height seems to increase the magnitude of the negative force peak, while a larger wave period decreases the absolute value of the negative force.

The sharp and sudden negative peak can be noticed in all four two-dimensional cases. The experimental results do have similar tendency, but not as pronounced and significant. It appears this effect comes from some unphysical cause, but no relationship could be seen based on figures of volume fraction, velocity, pressure or turbulence. A theory was that the large negative force occurred when the water surface started to release from the upstream edge of the deck, but no such conclusions could be drawn from further tests. At the interface between the water and body, a thin layer of water/air mixture was visible (VOF constant ≈ 0.7). Another theory was that it could have been something to do with this interface mixture layer, but tests showed that this layer was present a long time before and after the negative peak occurred.

Using a free water surface generates reflections at the downstream boundary which could influence the undisturbed waves and the force measurements. Using an appropriate size of the domain together with a numerical beach near the outlet boundary could minimize these effects. At the same time, it is important to be careful when deciding damping resistance so the numerical dampening not affects a non-damping zone. However, in these simulations no numerical beach was used because of the short simulation time. Numerical reflections did not have sufficient time to travel upstream and influence the undisturbed waves near the deck.

It is important not to forget that the empirical tests surely contain errors and uncertainties as well. The same problems are present here, with wave reflections in the wave flume and the accuracy of performing two-dimensional test in a three-dimensional environment. It is important to bear in mind that both computational and experimental tests represent only a simplified model of the reality.

9 Future work

The main focus in this project has been to investigate the vertical lifting force affecting the two-dimensional block. The block has been fixed in space with no substructure in the water. A more realistic situation might be a moored floating platform with submerged columns and pontoons. A step in that direction was done by simulating a three-dimensional platform, fixed in space. However, going further with more realistic three-dimensional simulations would be interesting. The motions of the platform will then be important as well as buoyancy and moments of inertia of the model. Since the air-gap and inclination of the platform will vary, the mesh needs to be dynamic. ANSYS Fluent can treat above mentioned issues by using User Defined Functions (UDF's). In short, more realistic simulations would be interesting to perform subject to reliable experimental data for comparison.

In experiments done by Baarholm, the wetted length and wetting velocity of the platform were measured during the wave impact event and used in the analysis. The wetting velocity depends on wave steepness and generally higher wetting velocity implies higher forces. Finding relationships of these parameters would be very interesting, but was excluded in this thesis. The reason was mainly due to the difficulty of predicting the wetted length in Fluent, since the outcome is very dependent on the VOF value. For instance, a VOF limit of 0.7 resulted in a wetted length near zero, while 0.9 led to the whole deck being wetted.

A more detailed mesh study is also of interest for future work, since the results of this project concluded that the simulation outcome is highly dependent on the quality of the mesh. The reason why no extensive mesh dependency study was executed was because of time limitations. A single simulation could take up to a week and the Beda cluster was usually occupied with other projects during this period, causing the simulations to be placed in a queue.

The most common procedure of analysing a floating object's response to waves is based on the measurements of its motions in irregular waves of a given spectrum. Reference data for these kind of tests is much easier to find, but unfortunately CFD simulations with irregular waves take a lot of time and generates enormous amount of data. The object must be exposed to the waves in a long time to obtain reliable results. Also, controlling the correctness of the irregular wave generation is much more complex. In this project only the first wave impact is considered and therefore only regular waves have been used.

Settings regarding turbulence models can be discussed as well. In this thesis, the results from the simulations coincided better with the experimental results if a viscous *k-ε realizable model* together with *Enhanced Wall Treatment* was adopted. The k and ε constants were extremely small, 10^{-5}, otherwise the wave lost its shape and amplitude due to diffusion. It would however be interesting to investigate this further and see if this behaviour can be changed with different turbulence settings.

Lastly, only the first incoming wave has been considered in the tests, but it was noticed in the two-dimensional case that the second and third waves yielded much higher peak forces. From a structural point of view, knowledge about these peak forces is substantial for a complete ultimate limit state assessment and would be interesting to investigate further.

10 References

American Petroleum Institute. (2002). *Recommended Practice for Planning, Designing and Constructing Fixed Offshore Platforms - Working Stress Design, API RP 2A-WSD.*

ANSYS. (2015). Retrieved from ANSYS: http://www.ansys.com/Products

ANSYS Inc. (2013, November). ANSYS Fluent User's Guide R. 15.0. Canonsburg.

ANSYS Inc. (2014, November). ANSYS Fluent Theory Guide R 15.0. Canonsburg.

Baarholm, R. (2001). *Theoretical and Experimental Studies of Wave Impact underneath Decks of Offshore Platforms.* Institute for marine hydrodynamics. Trondheim: NTNU.

Baarholm, R. (2009). Experimental and theoretical study of three-dimensional effects on vertical wave-in-deck forces, OMAE2009-79560. *ASME 2009 28th International Conference on Ocean, Offshore and Arctic Engineering.* Honolulu: OMAE2009.

Baarholm, R., & Faltinsen, O. M. (2004). Wave impact underneath horizontal decks. *Marine Science and Technology*(9), 9:1-13.

Baarholm, R., & Stansberg, C. T. (2004). *Extreme Vertical Wave Impact on the Deck of a Gravity-Based Structure (GBS) Platform.* Trondheim: MARINTEK.

Bellezi, C. A., & Cheng, L. Y. (2014). Study of wave impact onto a semi-submersible platform using moving particles semi-implicit (MPS) method. *10th World Congress on Computational Mechanics. 1.* Sao Paulo: Blucher Mechanical Engineering Proceedings.

Daily Mail. (2015, January 15). *News*. Retrieved 2015, from Mail Online: http://www.dailymail.co.uk/news/article-2911847/North-Sea-oil-rig-stays-afloat-despite-massive-storm-swells-coast-Scotland.html

DNV. (2010, October). Environmental Conditions and Environmental Loads. *Recommended Practice DNV-RP-C205*. Det Norske Veritas.

Frei, W. (2013, 9 16). Retrieved from Comsol: http://cn.comsol.com/blogs/which-turbulence-model-should-choose-cfd-application-cn/

GVA. (2013). Retrieved 2015, from GVA A KBR Company: http://www.gvac.se/

GVA. (2013). *Drilling Units*. Retrieved from GVA - A KBR Company: http://gvac.se/Products/Semisubmersibles/Drilling-Units/

Henry, A. M. (2011). *Wave forces on bridge decks and damping techniques to reduce damages.* Master's Thesis, B.S., University of Tennessee at Chattanooga, Department of Civil and Environmental engineering, Chattanooga.

Hirt, C. W., & Nichols, B. D. (1981). Volume of fluid (VOF) method for the Dynamics of free boundaries. *Computational Physics*, 201-225.

Huijs et al., F. (2011). Calculation of wave forces and internal loads on a semi-submersible at shallow draft using an IVOF method, OMAE2011-49236. *ASME 2011 30th International Conference on Ocean, Offshore and Arctic Engineering.* Rotterdam: OMAE2011.

ITTC. (n.d.). The Specialist Committee on Waves. *23rd International Towing Tank Conference, 2*, pp. 505-736.

Iwanowski et al., B. (2009). CFD simulation of wave run-up on a semi-submersible and comparison with experiment, OMAE2009-79052. *ASME 28th International Conference on Ocean, Offshore and Arctic Engineering.* Honolulu.

Janson, C.-E. (2014). *Waves, Motions and Manoeuvring.* Gothenburg, Sweden: Chalmers University of Technology.

Journée, J. M., & Massie, W. W. (2001). *Offshore Hydromechanics* (1st Edition ed.). Delft University of Technology.

Kisacik et al., D. (n.d.). *Experimental results of breaking wave impact on a vertical wall with an overhanging horizontal cantilever slab.* Ghent University, Department of Civil Engineering.

Kraskowski, M. (2012). Application of the rans flow model for the analysis of the motion of floating objects in waves. *KONES Powertrain and Transport, 19*(1), 199-206.

MARINTEK. (2009). *MARINTEK Wave Impact Loads JIP: Task 2B - Global Wave in Deck Small Scale Testa.* Trondheim.

MarnetCFD. (n.d.). *Best practice guidlines for marine applications of computational fluid dynamics.*

Matsumoto et al., F. T. (2013). Wave Run-Up and Air Gap Prediction for a Large-Volume Semi-Submersible Platform, 011302. *Offshore Mechanics and Arctic Engineering, 135*.

Petroluem Safety Authority Norway. (2014, December). Retrieved January 2015, from Petroleumstilsynet: www.ptil.no/getfile.php/Regelverket/Innretningsforskriften_e.pdf

Stansberg et al., C. T. (2005). Extreme Wave Amplification and Impact Loads on Ofshore Structures, OTC 17487. *Offshore Technology Conference.* Houston.

Stoehr, L. P. (2013). *Development of CFD Models for the Purposes of Exploring Free Surface Wave Phenomena, 4-1-2013.* Western Michigan University.

Thor, M. (2010). *Jack & St. Malo Project - Wave Basin Model Test Evaluation Report.* Chevron.

Veldman, A. E., & Huijsmans, R. H. (2008). *Extreme wave impact on offshore platforms and coastal structures.* University of Groningen, Institute for Mathematics and Computing Science.

Wellens et al., P. R. (2009). CFD simulations of a semi-submersible with absorbing boundary conditions, OMAE2009-79342. *ASME 28th International Conference on Ocean, Offshore and Arctic Engineering.* Honolulu: OMAE2009.

Versteeg, H. K., & Malalasekera, W. (2007). *An Introduction to Computational Fluid Dynamics - The Finite Volume Method* (2nd Edition ed.). Harlow, Essex, England: Pearson Education Limited.

Vestbostad, T. M. (2009). *A numerical study of wave-in-deck impact using a two-dimensional constrained interpolation profile method.* Norwegian University of

Science and Technology, Department of Marine Technology. Trondheim: NTNU.

White, F. M. (2011). *Fluid Mechanics* (7th Edition ed.). McGraw-Hill.

APPENDIX A

Input parameters Case 5

```
Fluent
Version: 2d, dp, pbns, vof, rke, transient (2d, double precision,
pressure-based, VOF, realizable k-epsilon, transient)
Release: 16.0.0
Title:

  Model                         Settings
   ------------------------------------------------------------
   Space                         2D
   Time                          Unsteady, 1st-Order Implicit
   Viscous                       Realizable k-epsilon turbulence
   Wall Treatment                Enhanced Wall Treatment
   Heat Transfer                 Disabled
   Solidification and Melting    Disabled
   Species                       Disabled
   Coupled Dispersed Phase       Disabled
   NOx Pollutants                Disabled
   SOx Pollutants                Disabled
   Soot                          Disabled
   Mercury Pollutants            Disabled

Material Properties
-------------------
   Material: water-liquid (fluid)
      Property                          Units      Method  Value(s)
      ------------------------------------------------------------
      Density                           kg/m3      constant   998.2
      Cp (Specific Heat)                j/kg-k     constant   4182
      Thermal Conductivity              w/m-k      constant   0.6
      Viscosity                         kg/m-s    constant 0.001003
      Molecular Weight                  kg/kgmol   constant 18.0152
      Thermal Expansion Coefficient     1/k        constant   0
      Speed of Sound                    m/s        none       #f

   Material: air (fluid)
      Property                          Units      Method  Value(s)
      ------------------------------------------------------------
      Density                           kg/m3      constant   1.225
      Cp (Specific Heat)                j/kg-k     constant 1006.43
      Thermal Conductivity              w/m-k      constant  0.0242
      Viscosity                         kg/m-s  constant 1.7894e-05
      Molecular Weight                  kg/kgmol   constant  28.966
      Thermal Expansion Coefficient     1/k        constant   0
      Speed of Sound                    m/s        none       #f

   Material: aluminum (solid)
      Property               Units    Method     Value(s)
      ------------------------------------------------------
      Density                kg/m3    constant   2719
      Cp (Specific Heat)     j/kg-k   constant   871
      Thermal Conductivity   w/m-k    constant   202.4

Cell Zone Conditions
   Zones
```

```
      name                        id   type
      ------------------------------------
      fluid-part-surface_body     3    fluid

   Setup Conditions

      fluid-part-surface_body

         Condition                                          Value

         Material Name                                water-liquid
         Specify source terms?                                no
         Source Terms
((x-momentum) (y-momentum) (k) (epsilon))
         Specify fixed values?                                no

         Fixed Values
((x-velocity (inactive . #f) (constant . 0) (profile  )) (y-
velocity (inactive . #f) (constant . 0) (profile  )) (k (inactive
. #f) (constant . 0) (profile  )) (epsilon (inactive . #f)
(constant . 0) (profile  )))
         Frame Motion?                                        no
         Relative To Cell Zone                                -1
         Reference Frame Rotation Speed (rad/s)                0
         Reference Frame X-Velocity Of Zone (m/s)              0
         Reference Frame Y-Velocity Of Zone (m/s)              0
         Reference Frame X-Origin of Rotation-Axis (m)         0
         Reference Frame Y-Origin of Rotation-Axis (m)         0
         Reference Frame User Defined Zone Motion Function   none
         Mesh Motion?                                         no
         Relative To Cell Zone                                -1
         Moving Mesh Rotation Speed (rad/s)                    0
         Moving Mesh X-Velocity Of Zone (m/s)                  0
         Moving Mesh Y-Velocity Of Zone (m/s)                  0
         Moving Mesh X-Origin of Rotation-Axis (m)             0
         Moving Mesh Y-Origin of Rotation-Axis (m)             0
         Moving Mesh User Defined Zone Motion Function       none
         Deactivated Thread                                   no
         Laminar zone?                                        no
         Set Turbulent Viscosity to zero within laminar zone? yes
         Embedded Subgrid-Scale Model                          1
         Momentum Spatial Discretization                       0
         Cwale                                             0.325
         Cs                                                  0.1
         Porous zone?                                         no
         Porosity                                              1
         Two-Phase Corey's Model?                             no
         Reference Relative Permeability                     0.4
         Residual Saturation                                0.27
         Corey Exponent                                        3
         Reference Relative Permeability                     0.1
         Residual Saturation                                0.16
         Corey Exponent                                        2
         Interfacial Area Density (1/m)                        1
         Heat Transfer Coefficient (w/m2-k)                    1
         Numerical Beach                                      no
         Beach Group ID                                        1
```

```
         Damping Type                                          0
         Compute from Inlet Boundary                           0
         Free Surface Level (m)                                1
         Bottom Level (m)                                      0
         X-Component of Flow Direction                         1
         Y-Component of Flow Direction                         0
         Damping Length Specification                          0
         Wave Length (m)                                    1.92
         Number of Wave Lengths                                1
         Start Point (m)                                    10.8
         End Point (m)                                      13.5
         Relative Velocity Resistance Formulation            yes
         Linear Damping Resistance (1/s)                       7
         Quadratic Damping Resistance (1/m)                   62

Boundary Conditions
-------------------
   Zones

      name            id   type
      ----------------------------------
      inlet           6    velocity-inlet
      outlet          7    pressure-outlet
      wall            8    wall
      wall_platform   9    wall
      symmetry        10   symmetry

   Setup Conditions
      inlet

         Condition                                   Value

         Open Channel Wave BC                        yes
         Secondary Phase for Inlet                   0
         Wave BC Options                             0
         Free Surface Level (m)                      1
         Bottom Level (m)                            0
         Reference Wave Direction                    2
         X-Component of Reference Direction          1
         Y-Component of Reference Direction          0
         Wave Modeling Options                       0
         Wave Group Inputs                           (((theory .
4) (wave-ht (constant . 0.1) (profile  )) (wave-len (constant .
2.41) (profile  )) (phase-diff (constant . -1.5707961) (profile
)) (heading-angle (constant . 0) (profile  ))))
         Shallow Wave Inputs                         (((theory .
0) (wave-ht (constant . 1) (profile  )) (wave-len (constant . 1)
(profile  )) (offset (constant . 0) (profile  )) (heading-angle
(constant . 0) (profile  ))))
         Frequency Spectrum Method                   0
         Peak Shape Parameter                        3.3
         Significant Wave Height (m)                 1
         Peak Frequency (rad/s)                      1
         Minimum Frequency (rad/s)                   0.66
         Maximum Frequency (rad/s)                   1.66
         Number of frequency components              10
         Directional Spreading Method                0
         Frequency Independent Cosine Exponent       1
```

Mean Wave Heading Angle (deg)	0
Angular Deviation (deg)	90
Number of Angular components	4
Averaged Flow Specification Method	1
Velocity Specification Method	2
Reference Frame	0
Averaged Flow Velocity Magnitude (m/s)	0
Averaged Flow X-Velocity (m/s)	0
Averaged Flow Y-Velocity (m/s)	0
Velocity Magnitude (m/s)	0
Supersonic/Initial Gauge Pressure (pascal)	0
X-Velocity (m/s)	0
Y-Velocity (m/s)	0
X-Component of Flow Direction	1
Y-Component of Flow Direction	0
X-Component of Axis Direction	1
Y-Component of Axis Direction	0
Z-Component of Axis Direction	0
X-Coordinate of Axis Origin (m)	0
Y-Coordinate of Axis Origin (m)	0
Z-Coordinate of Axis Origin (m)	0
Angular velocity (rad/s)	0
Turbulent Specification Method	0
Turbulent Kinetic Energy (m2/s2)	1e-05
Turbulent Dissipation Rate (m2/s3)	1e-05
Turbulent Intensity (%)	5
Turbulent Length Scale (m)	1
Hydraulic Diameter (m)	1
Turbulent Viscosity Ratio	10
is zone used in mixing-plane model?	no

outlet

Condition	Value
Open Channel	yes
Outlet Group ID	1
Pressure Specification Method	0
Pressure Specification Method	0
Free Surface Level (m)	1
Gauge Pressure (pascal)	0
Bottom Level (m)	0
Density Interpolation Method	0
Backflow Direction Specification Method	1
X-Component of Flow Direction	1
Y-Component of Flow Direction	0
X-Component of Axis Direction	1
Y-Component of Axis Direction	0
Z-Component of Axis Direction	0
X-Coordinate of Axis Origin (m)	0
Y-Coordinate of Axis Origin (m)	0
Z-Coordinate of Axis Origin (m)	0
Turbulent Specification Method	2
Backflow Turbulent Kinetic Energy (m2/s2)	1
Backflow Turbulent Dissipation Rate (m2/s3)	1
Backflow Turbulent Intensity (%)	9.9999998e-06
Backflow Turbulent Length Scale (m)	1
Backflow Hydraulic Diameter (m)	1

```
   Backflow Turbulent Viscosity Ratio            1e-05
   is zone used in mixing-plane model?           no

wall

   Condition                                              Value
   -------------------------------------------------------------
   Wall Motion                                              0
   Shear Boundary Condition                                 0
   Define wall motion relative to adjacent cell zone?     yes
   Apply a rotational velocity to this wall?               no
   Velocity Magnitude (m/s)                                 0
   X-Component of Wall Translation                          1
   Y-Component of Wall Translation                          0
   Define wall velocity components?                        no
   X-Component of Wall Translation (m/s)                    0
   Y-Component of Wall Translation (m/s)                    0
   Rotation Speed (rad/s)                                   0
   X-Position of Rotation-Axis Origin (m)                   0
   Y-Position of Rotation-Axis Origin (m)                   0
   X-component of shear stress (pascal)                     0
   Y-component of shear stress (pascal)                     0
   Fslip constant                                           0
   Eslip constant                                           0
   Specularity Coefficient                                  0

wall_platform

   Condition                                              Value
   -------------------------------------------------------------
   Wall Motion                                              0
   Shear Boundary Condition                                 0
   Define wall motion relative to adjacent cell zone?     yes
   Apply a rotational velocity to this wall?               no
   Velocity Magnitude (m/s)                                 0
   X-Component of Wall Translation                          1
   Y-Component of Wall Translation                          0
   Define wall velocity components?                        no
   X-Component of Wall Translation (m/s)                    0
   Y-Component of Wall Translation (m/s)                    0
   Rotation Speed (rad/s)                                   0
   X-Position of Rotation-Axis Origin (m)                   0
   Y-Position of Rotation-Axis Origin (m)                   0
   X-component of shear stress (pascal)                     0
   Y-component of shear stress (pascal)                     0
   Fslip constant                                           0
   Eslip constant                                           0
   Specularity Coefficient                                  0

symmetry
   Condition   Value
   -----------------
Solver Settings
---------------
   Equation          Solved
   ------------------------
   Flow              yes
   Volume Fraction   yes
```

```
   Turbulence        yes

 Numerics
   Numeric                           Enabled
   ------------------------------------------
   Absolute Velocity Formulation     yes

 Unsteady Calculation Parameters
   ------------------------------------
   Time Step (s)                     0.001
   Max. Iterations Per Time Step     20

 Relaxation
   Variable                      Relaxation Factor
   ----------------------------------------------
   Density                       1
   Body Forces                   1
   Volume Fraction               0.5
   Turbulent Kinetic Energy      0.8
   Turbulent Dissipation Rate    0.8
   Turbulent Viscosity           1

Variable                      Type       Criterion     Tolerance
   ------------------------------------------------------------
   Flow                       F-Cycle    0.1
   Volume Fraction            Flexible   0.1           0.7
   Turbulent Kinetic Energy   Flexible   0.1           0.7
   Turbulent Dissipation Rate Flexible   0.1           0.7

 Pressure-Velocity Coupling
   Parameter                                 Value
   ------------------------------------------------
   Type                                      Coupled
   Pseudo Transient                          no
   Flow Courant Number                       200
   Explicit momentum under-relaxation        0.75
   Explicit pressure under-relaxation        0.75

 Discretization Scheme
   Variable                      Scheme
   ---------------------------------------------
   Pressure                      PRESTO!
   Momentum                      Second Order Upwind
   Volume Fraction               Compressive
   Turbulent Kinetic Energy      Second Order Upwind
   Turbulent Dissipation Rate    Second Order Upwind

 Solution Limits
   Quantity                          Limit
   ---------------------------------------
   Minimum Absolute Pressure         1
   Maximum Absolute Pressure         5e+10
   Minimum Temperature               1
   Maximum Temperature               5000
   Minimum Turb. Kinetic Energy      1e-14
   Minimum Turb. Dissipation Rate    1e-20
   Maximum Turb. Viscosity Ratio     100000
```

APPENDIX B

ANSYS FLUENT - Input parameters				
Start	Double precision	(Recommended for Multiphase)		
General	Solver	Type	Pressure-based	
		Velocity formulation	Absolute	
		Time	Transient	
		2D space	Planar	
		Gravity	-9,81	X
Models	Multiphase VOF	No. Eulerian phases	2	
		Formulation	Implicit	
		Coupled level set	Level set	
		Body force formulation	Implicit body force	X
		VOF submodels	Open channel flow	X
		VOF submodels	Open channel wave BC	X
		Interface modeling	Sharp	
		Interface modeling	Interfacial Anti-diffusion	X
	Viscous	Viscous / SST K-omega		
Phases	Primary	Air		
	Secondary	Water		
	Interaction	None..		
Cell zone	Edit mixture	Numerical beach	Numerical beach	
conditions		Damping type	1D / 2D	
		Compute from inlet	Inlet	
		No. Wave lengths	2	
		Damping restistance (1/s)	0,67	
		Damping restistance (1/m)	0,55	
	Operating conditions	Operating pressure	101325	
		Insert ref. point for air		
		Specified operating density	1,225	X
Boundary condition	Inlet - Velocitiy - Mixture	Open channel wave BC	Open channel wave BC	X
		Averaged flow m/s	2	
		(Turbulent intensity	5)	
		(Turbulent viscosity	5)	
	Multiphase	Secondary phase for inlet	Water	
		Wave BC options	Shallow/Intermediate waves	
		Free surface + Bottom level		
		Wave	First order Airy	
		Wave height	3,15	
		Wave length	20	
		Phase diff/Heading	0/0	

	Outlet - Pressure - Mixture	Backflow direction method	Normal to boundary	
		(Turbulent intensity	5)	
		(Turbulent viscosity	5)	
	Multiphase	Pressure specification method	Free surface level	
		Phase diff/Heading	0/0	
		Density Interpolation	From Neighboring cell	
Dynamic mesh		None...		
Solution	Scheme	PISO/Coupled	PISO/Coupled	
	Spatial descretization	Gradient	Least square cell based	
		Pressure	PRESTO!	
		Momentum	Second order upwind	
		Volume fraction	Compressive	
		(Turbulent	Second order upwind)	
		(Dissipation	First order upwind)	
	Transient formulation	Transient formulation	First order implicit	
		Transient formulation	Non iterative time adv.	X
		High order term relaxation	Relaxation	
Monitors		Lift monitor		
Solution initialization	Initialization	Initialization methods	Standard initialization	
		Compute from	Inlet	
		Reference frame	Relative to cell zone	
		Open channel method	Flat	
		(Double check initail values ?)		
	Initialize	Initialize		
	Patch	Press patch		
		Phase	Water	
		Variable	Volume fraction	
		VOF patch options	Volumetric smoothing	X
		Value	1	
		Registers to patch	hexahedron-r0	
Graphics		Show contours - phases		
Calculation activities		Autosave every time step	1	
		(Automatic export ?)		
		Solution Animations		
Run calculation	Time stepping method	Step size (s)	0.02 (could be variable ?)	
	Fixed	Number of steps	1500	
	Options		Extrapolate varailbes	
			Data sampling for time	
		Max iterations/time step	15	

APPENDIX C

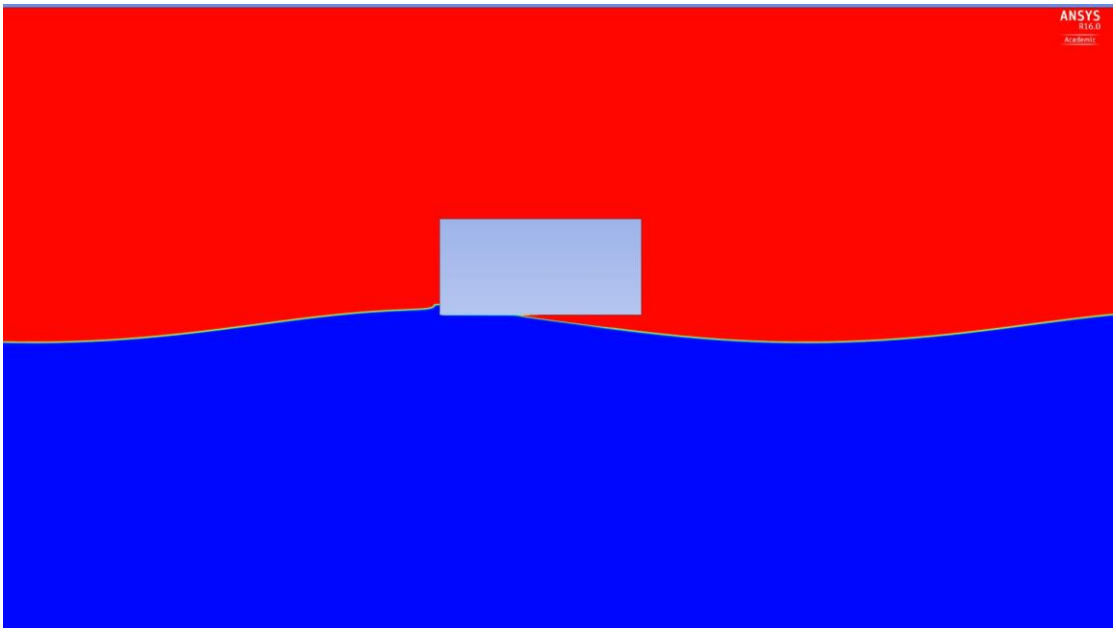

Figure C1 – TS 490. 35.61 N. Before max peak.

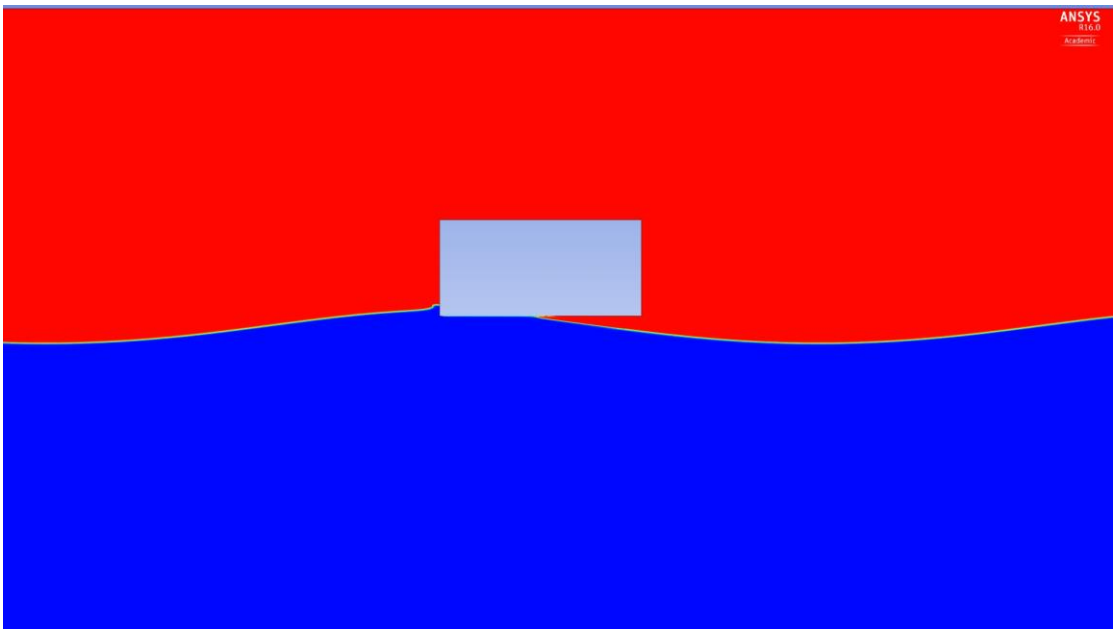

Figure C2 – TS 510. 37.66 N. Max peak.

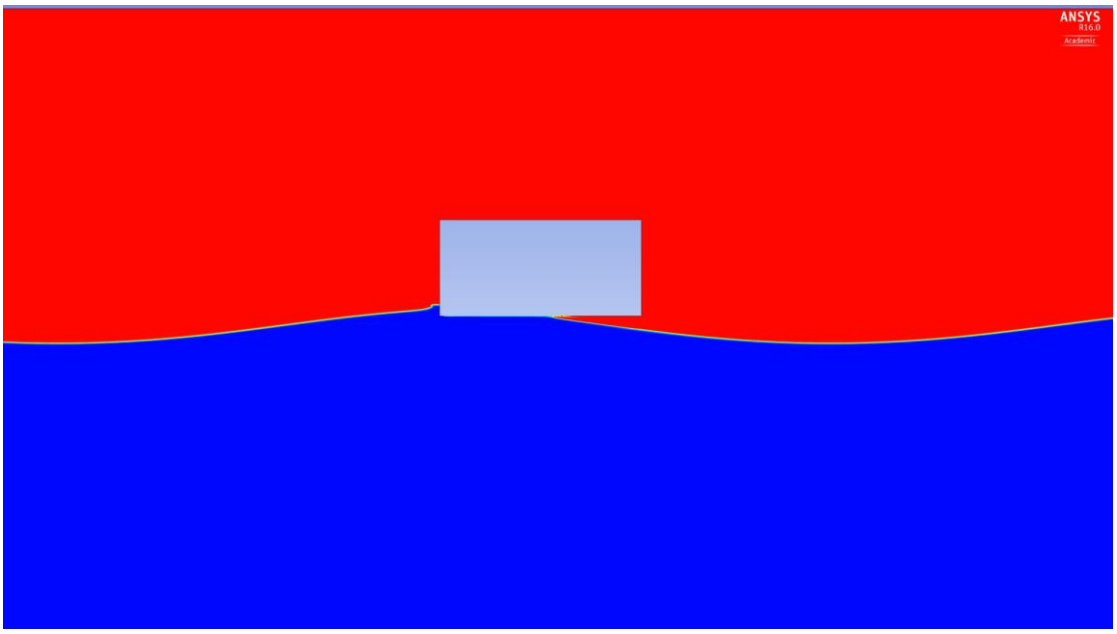

Figure C3 – TS 530. 37.27 N. After max peak.

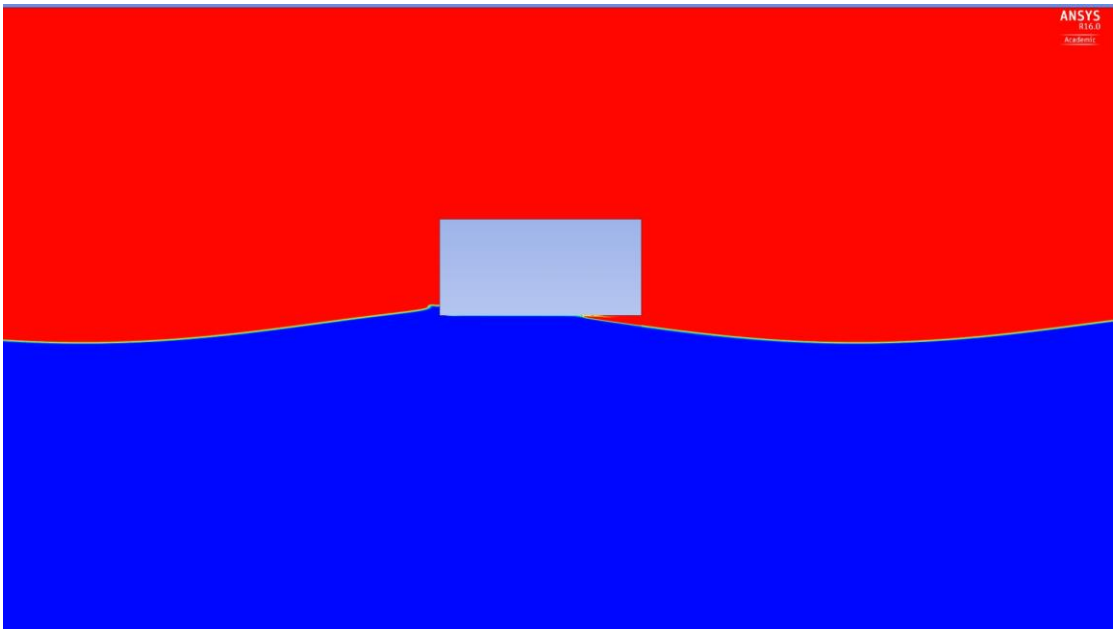

Figure C4 – TS 570. 32.27 N.

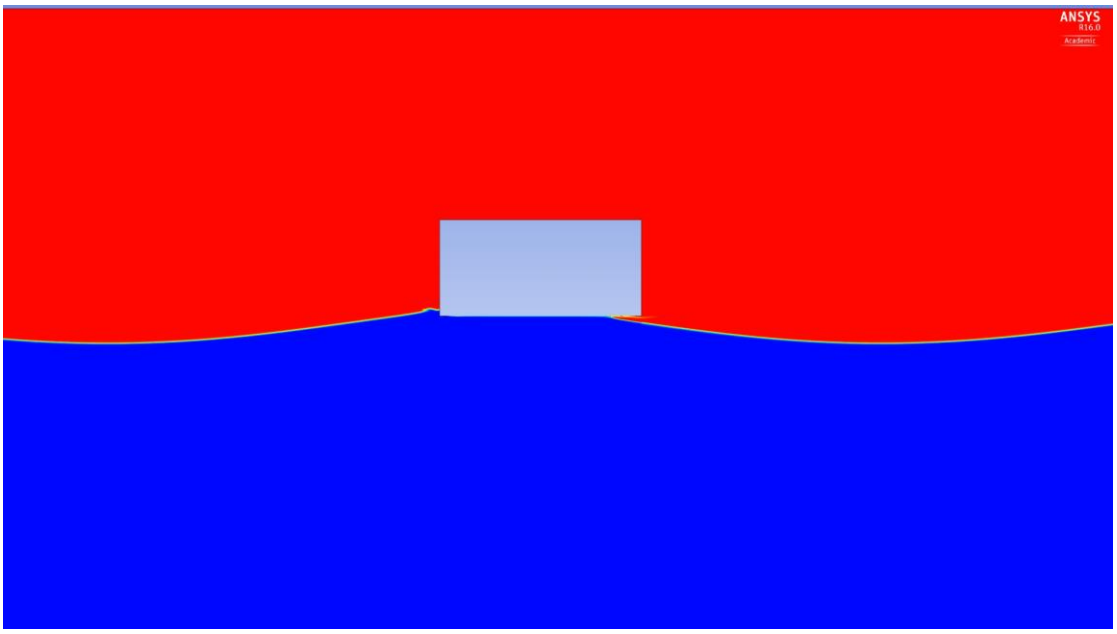

Figure C5 – TS 610. 17.97 N.

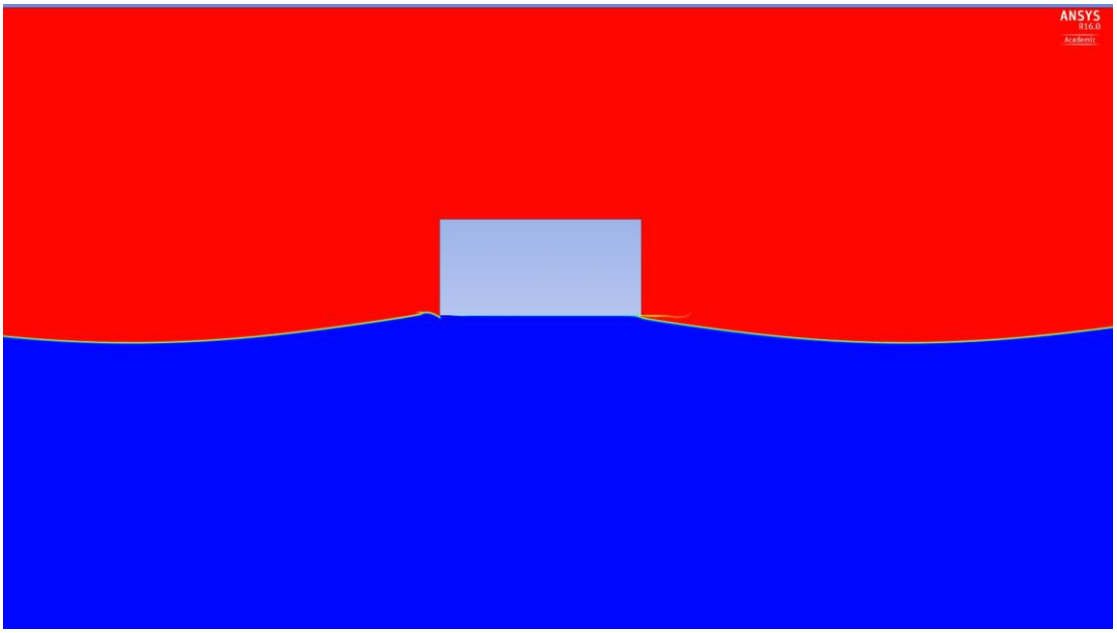

Figure C6 – TS 650. 7.24 N. Force starts to be negative.

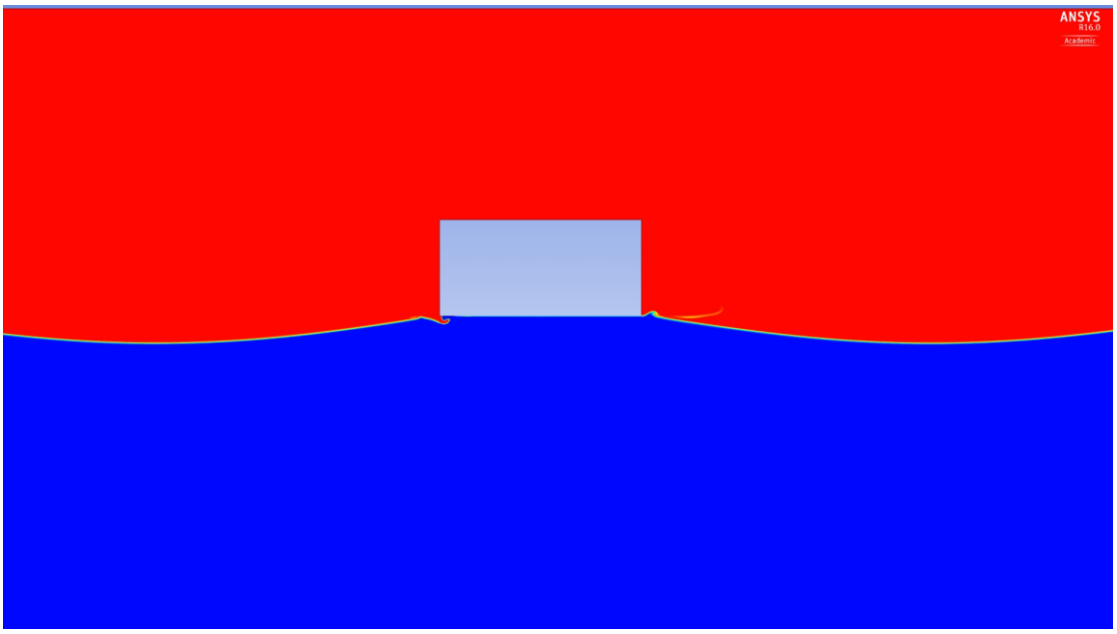

Figure C7 – TS 690. -54.16 N.

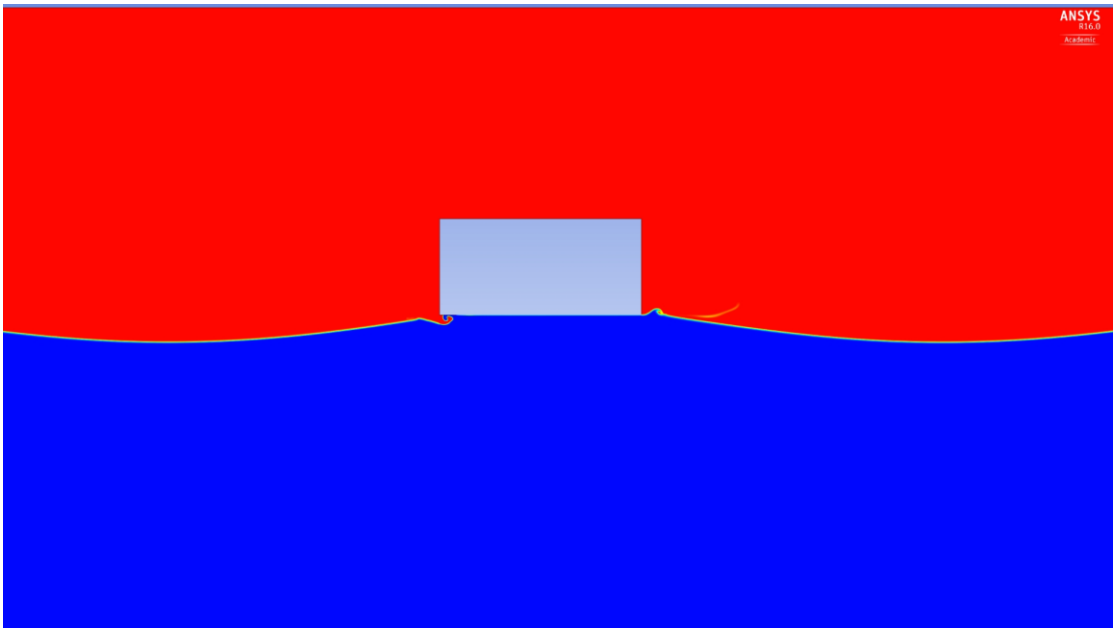

Figure C8 – TS 710. -58.80 N. Before min force peak.

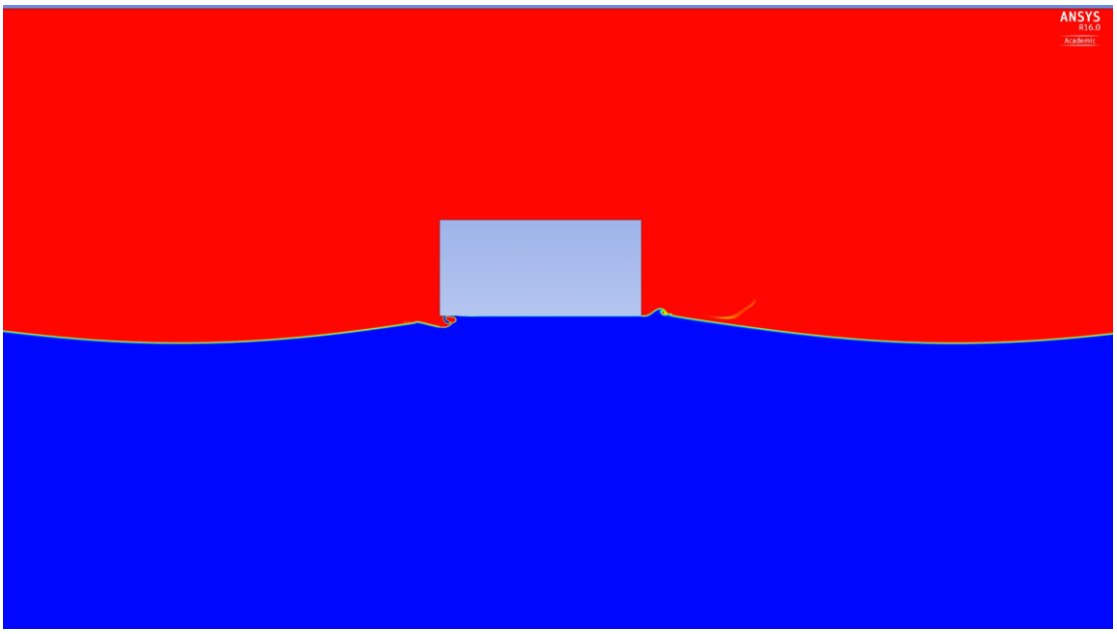

Figure C9 – TS 730. -69.94 N. Min force peak.

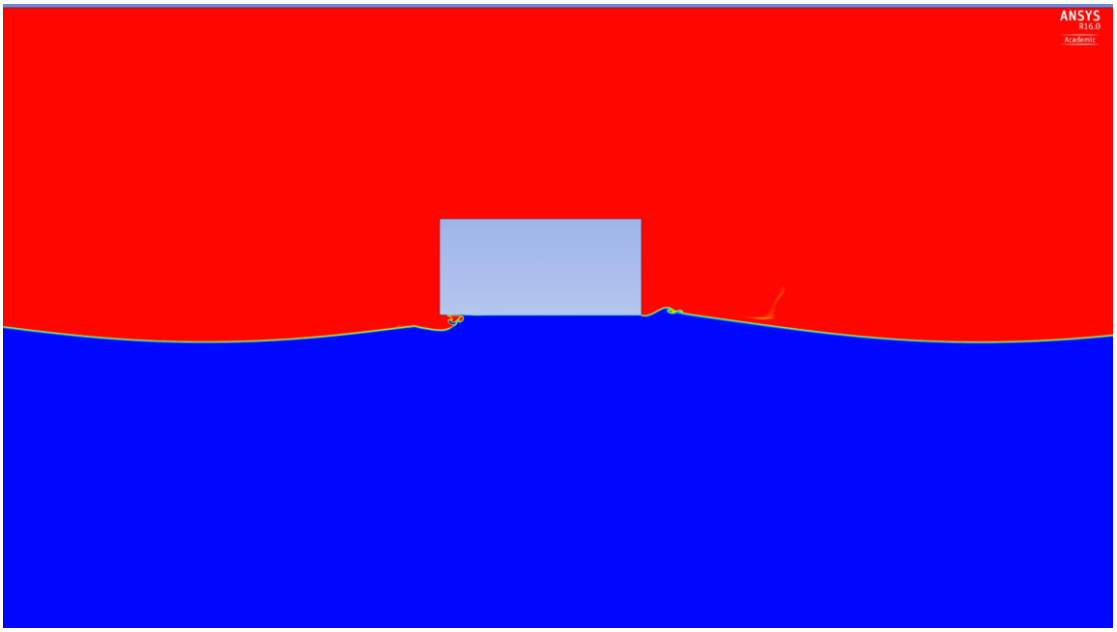

Figure C10 – TS 770. -58.38 N.

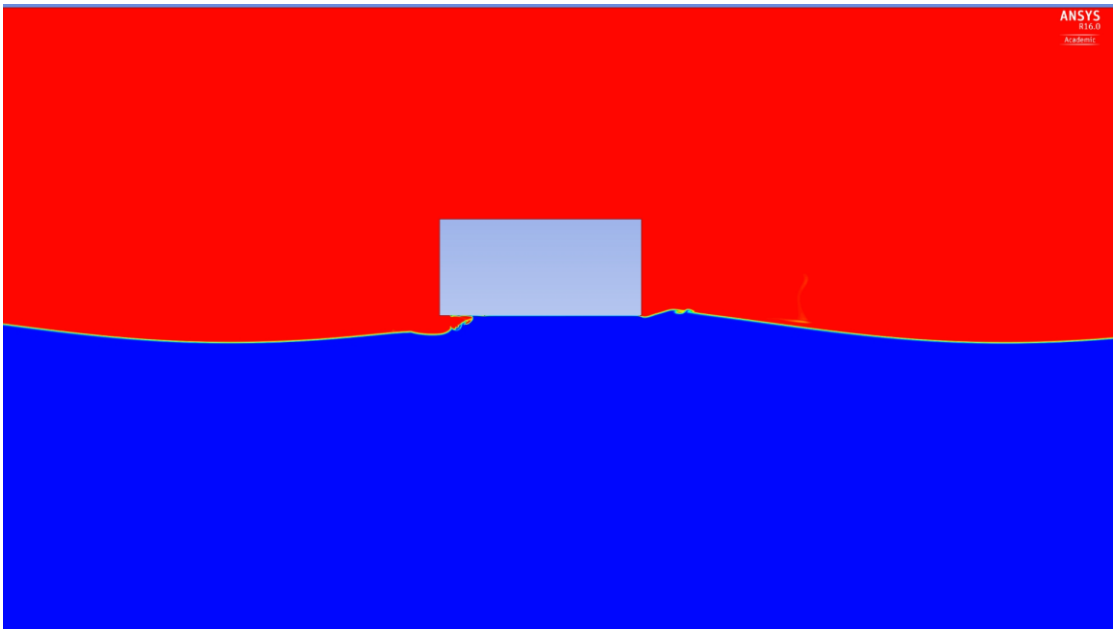

Figure C11 – TS 810. -48.77 N.

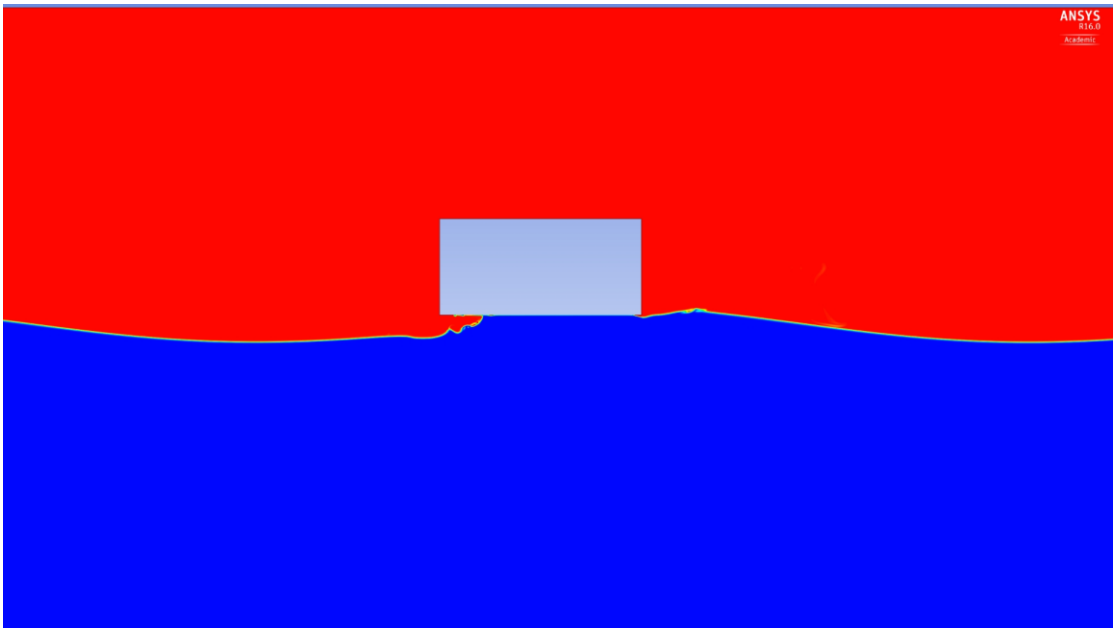

Figure C12 – TS 850. -44.10 N.

APPENDIX D

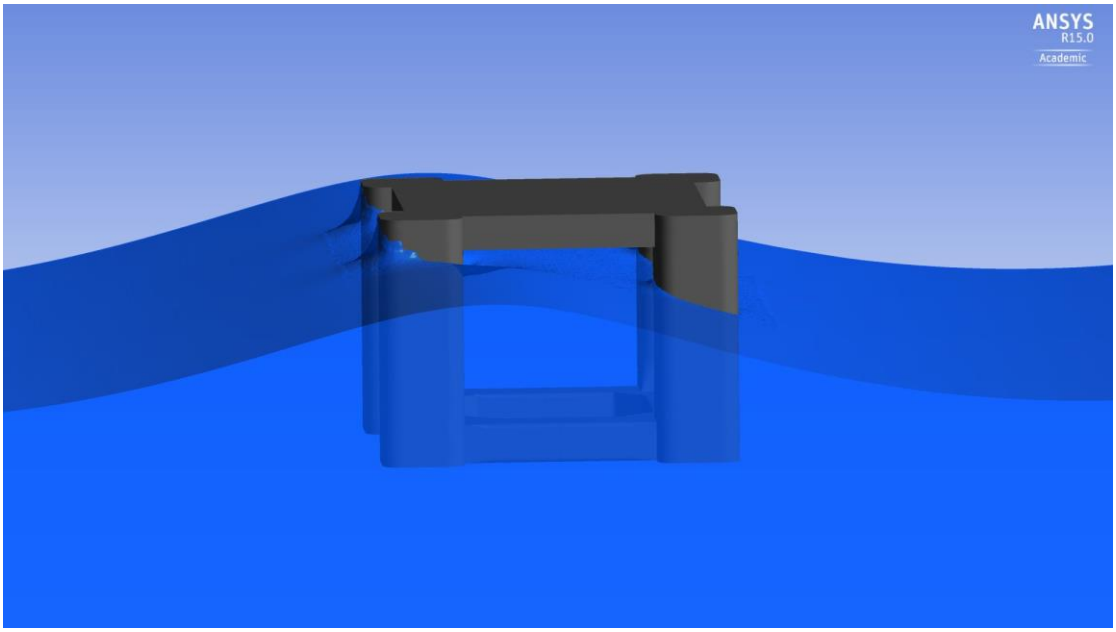

Figure D1 – 1s.

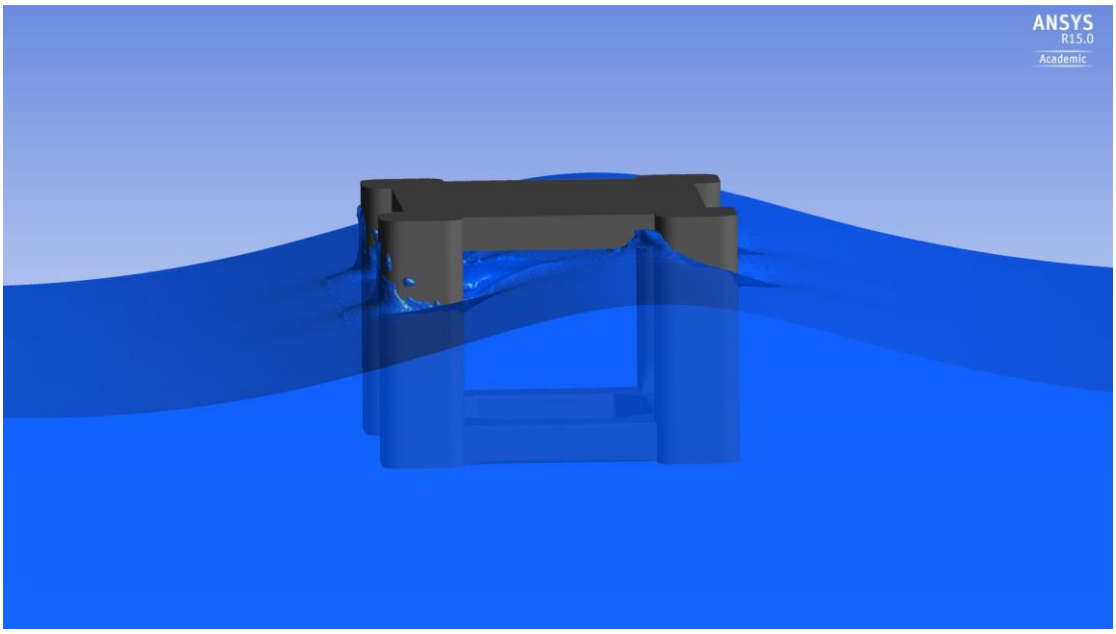

Figure D2 – 3s.

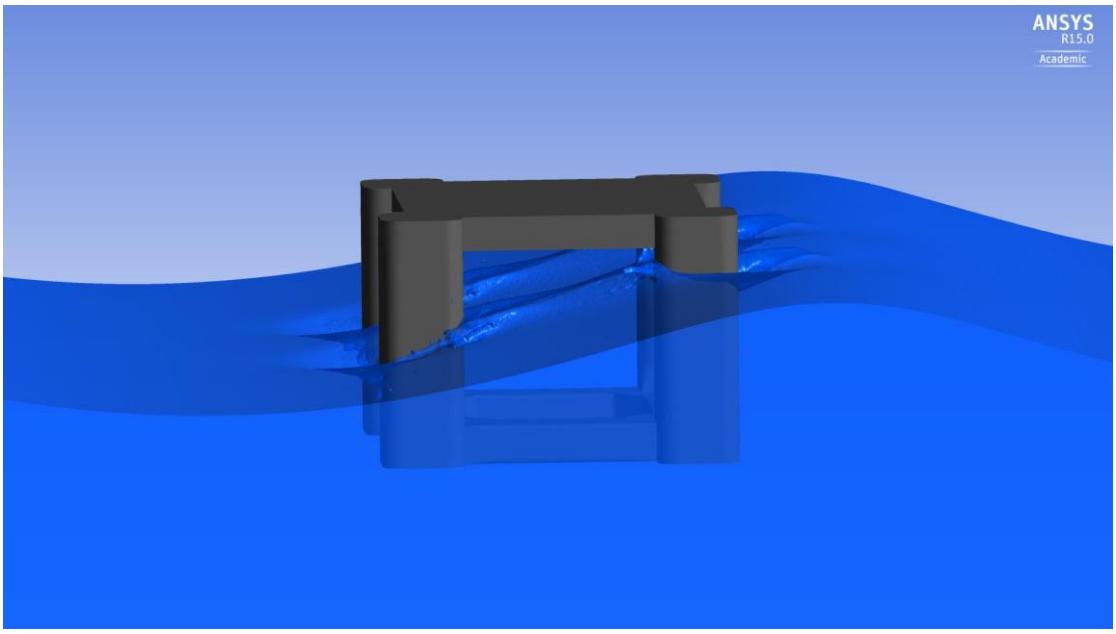

Figure D3 – 5s.

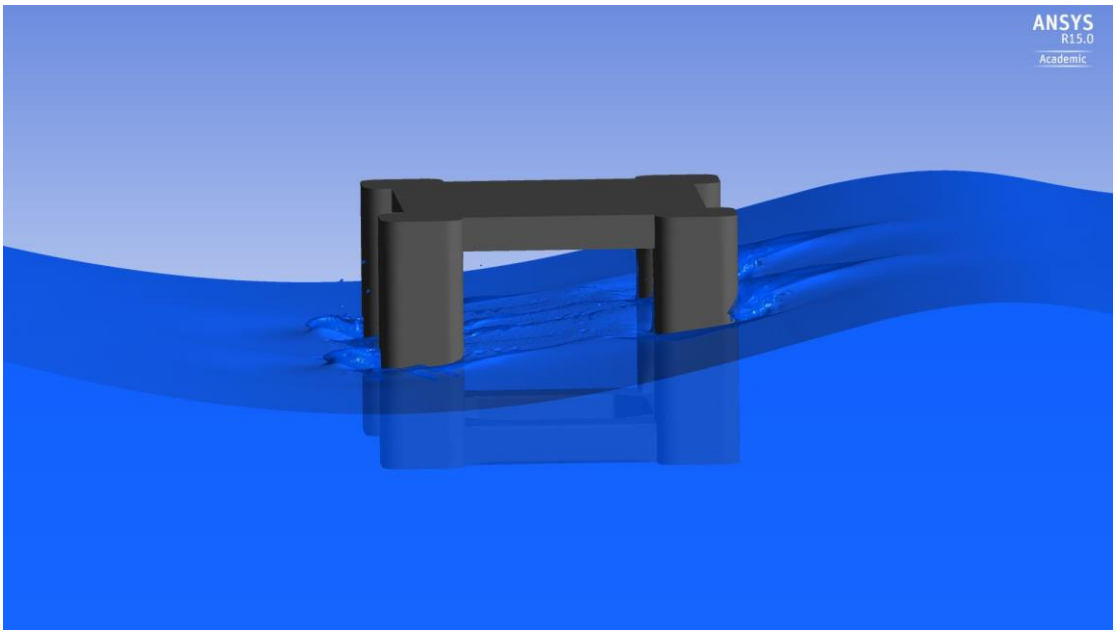

Figure D4 – 7s.

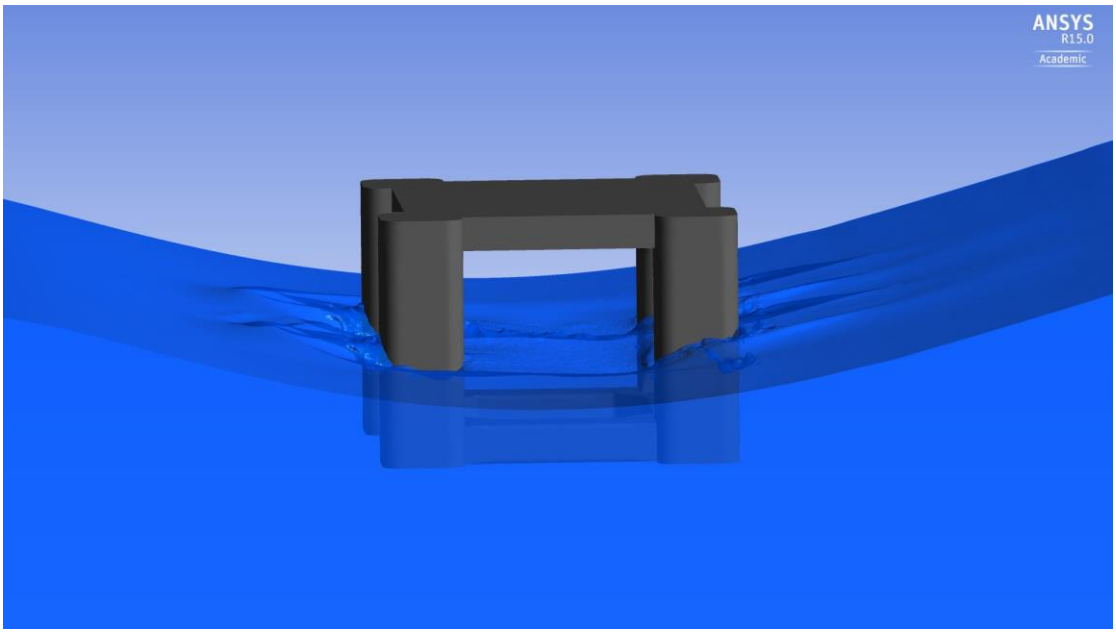

Figure D5 – 9s.

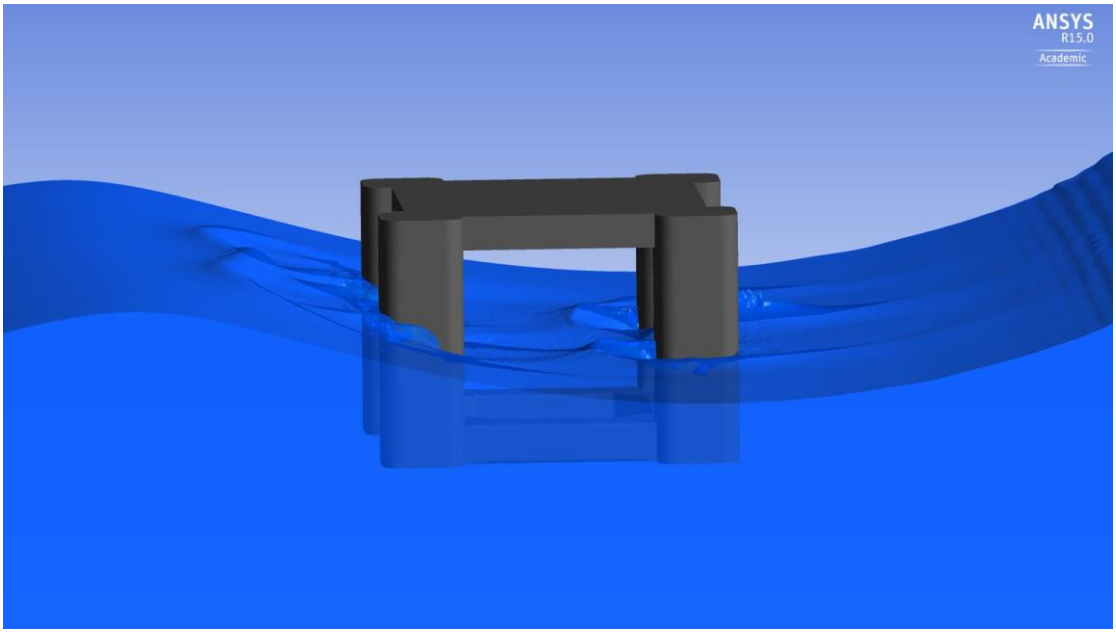

Figure D6 – 11s.

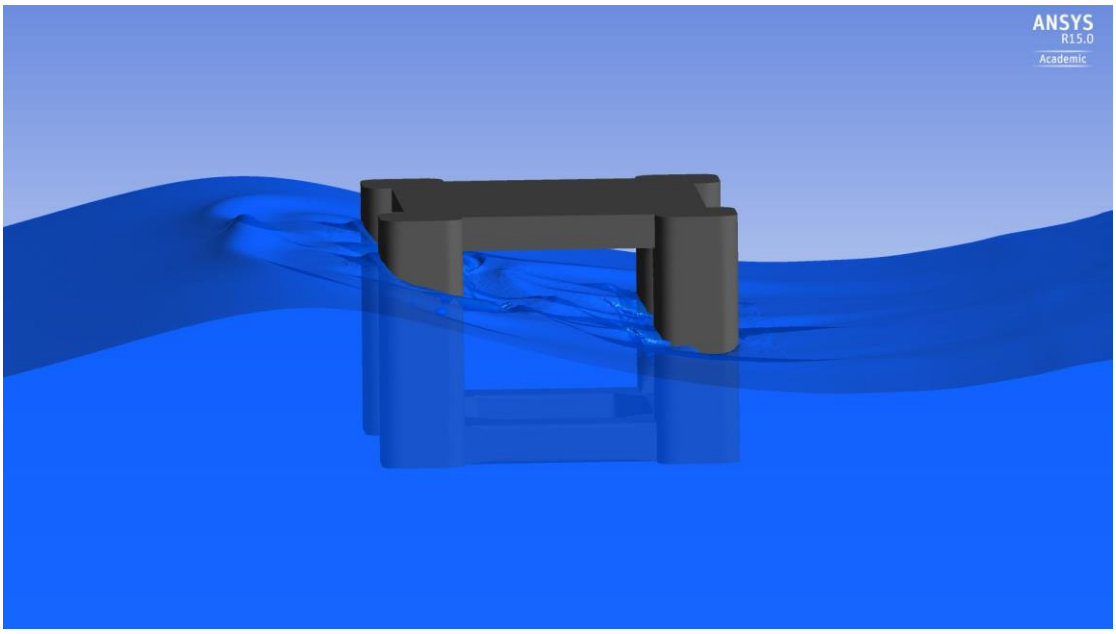

Figure D7 – 13s.

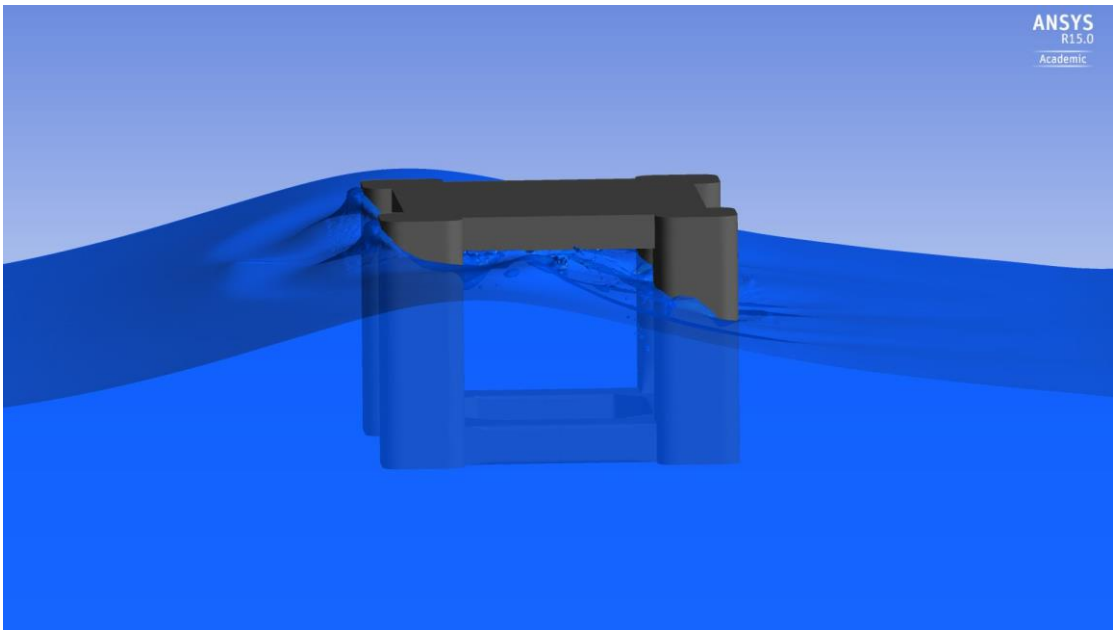

Figure D8 – 15s.

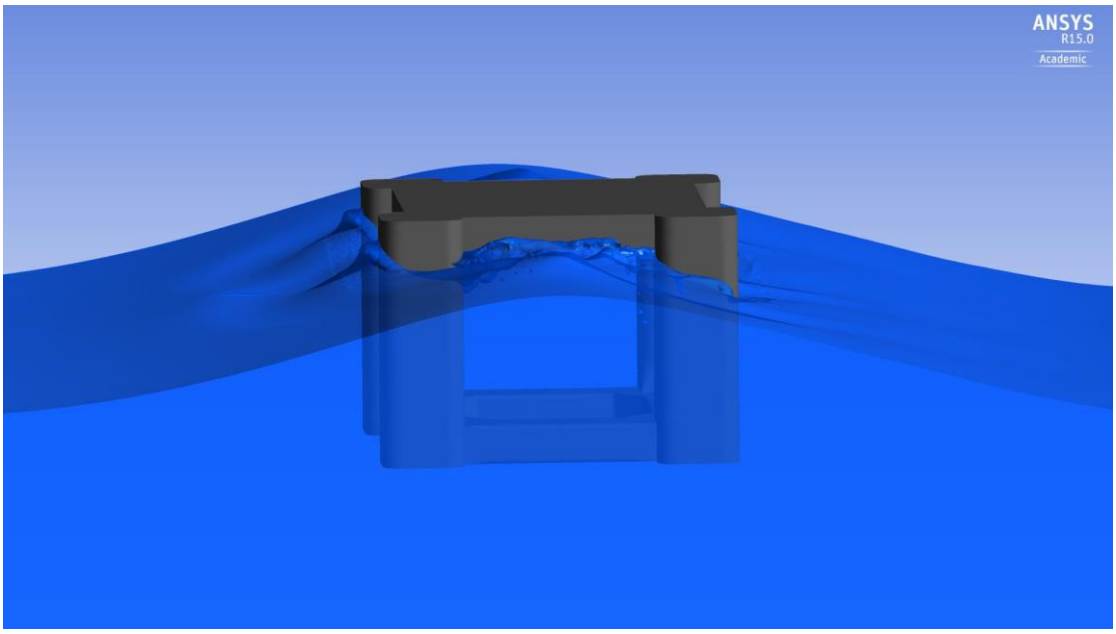

Figure D9 – 16s: Maximum lifting pressure.

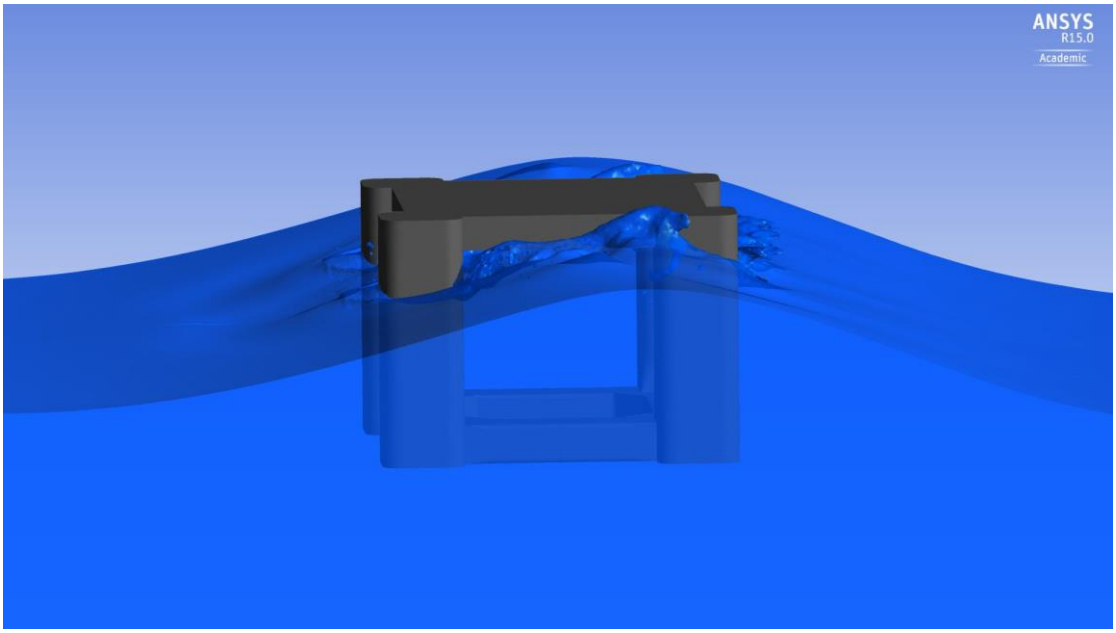

Figure D10 – 17s.

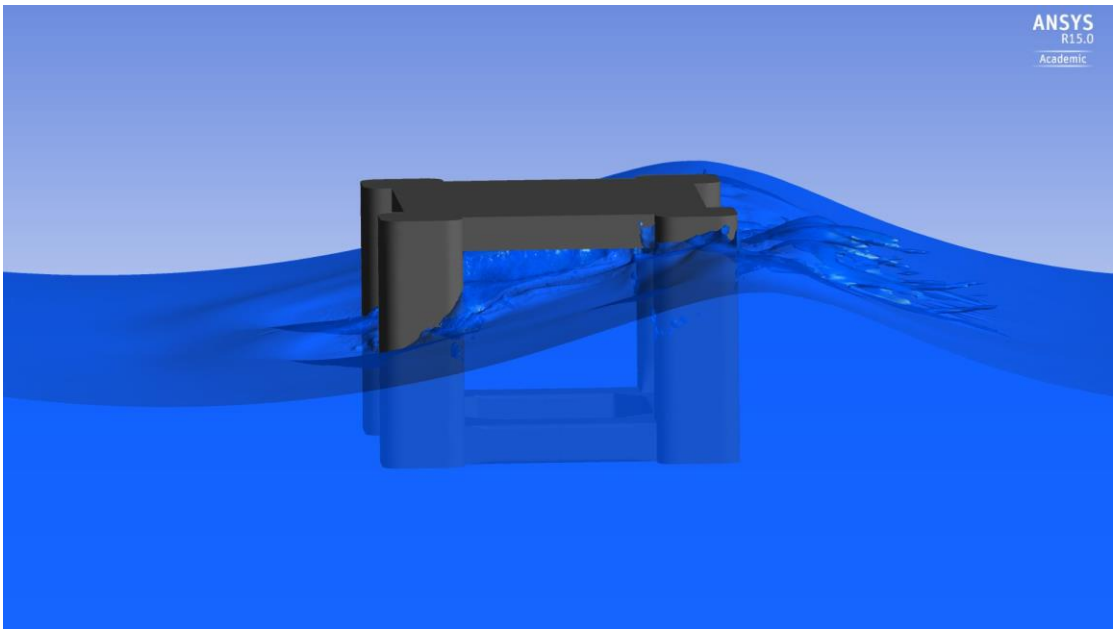

Figure D11 – 19s.

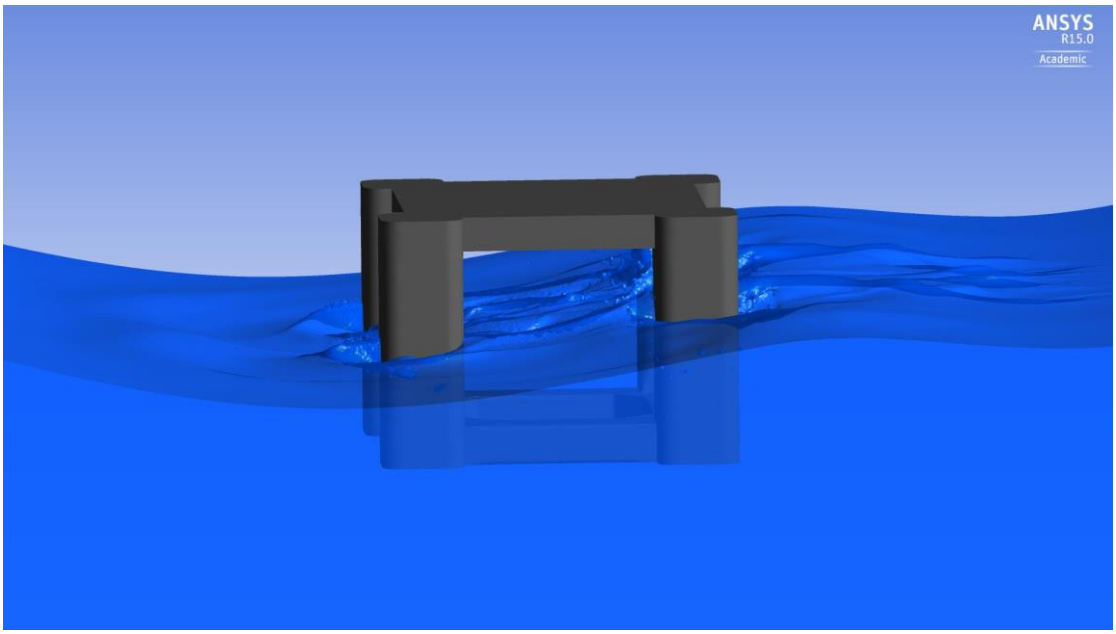

Figure D12 – 21s.